Analysis and Approximation of Coupled 1D-3D Flow Models

Ingeborg Gåseby Gjerde

Thesis for the degree of Philosophiae Doctor (PhD)
University of Bergen, Norway
2020

UNIVERSITY OF BERGEN

Analysis and Approximation of Coupled 1D-3D Flow Models

Ingeborg Gåseby Gjerde

Thesis for the degree of Philosophiae Doctor (PhD)
at the University of Bergen

Date of defense: 18.03.2020

Year: 2020

Title: Analysis and Approximation of Coupled 1D-3D Flow Models

Name: Ingeborg Gåseby Gjerde

Print: Skipnes Kommunikasjon / University of Bergen

Preface

This dissertation is submitted as a partial fulfillment of the requirements for the degree of Doctor Philosophy (PhD) at the University of Bergen. The advisory committee has consisted Kundan Kumar (University of Karlstad) and Jan M. Nordbotten (University of Bergen).

The PhD project has been financially supported by Norwegian Research Council grant 250223 as a part of the TheMSES project: https://themses.w.uib.no.

Acknowledgements

Det er noe fint og forstandig ved tall,
de vet hva de vil og de gjør det de skal.

Piet Hein

Many things have been said about what it's like to do a PhD. Some have likened it to doing a group project, except that the lazy one, the one who always turns things in late, the one who wasn't paying attention, and the over-achiever that actually does all the work are now the same person. Others have likened it to running orienteering without a map. At the beginning of the PhD, you only have a vague idea of where you are and an even vaguer idea of where you're going. Progress is made in leaps and bursts in between the countless wrong turns. Before you know it, however, you find yourself at the finish line, asking yourself "how was this so hard? All I had to do was run from here to there."

This dissertation would not have seen daylight without the competent guidance of my supervisors, so my first thanks goes to Kundan Kumar and Jan Martin Nordbotten. First, I want to thank Kundan, who has a natural gift for answering every question in a way that is both clear and easy to understand. His patient nature and passion for mathematics have truly been invaluable. Second, I want to thank Jan, whose enthusiasm, knowledge and writing skills have been indispensable when it came to finishing this PhD. I could not have asked for a better advisory committee.

For the Porous Media Group, including professors, postdocs and all the PhD students, thank you for being such an amazing group of people. I am especially grateful to Max and Eren for their invaluable friendships. Special thanks also go to David Seus, Wietse, Alessio, Michael, Manuel, Ivar, Runar, Davide and Ana. For the entire group, I feel so incredibly lucky to have worked with you and experienced so many memorable times with you. You've truly made this PhD a great experience.

I would also like to thank Paolo Zunino for hosting me during a three-month stay at Politecnico Milano. I hope we have many more opportunities to collaborate in the future. Lastly, I would like to thank Barbara Wohlmuth for sharing her considerable mathematical knowledge and giving us the idea behind this PhD.

En siste takk går til familie og venner. Jeg er heldig som har så mange bra mennesker i livet mitt. Takk Mamma og Pappa for at dere alltid er der for meg. Takk til Force Marsjør (norges ledende juzzband) for å ha gjort torsdag til ukens hyggeligste dag. Takk til Silje, Thea, Siri, Caroline, Sigrid, Christel, Marte og Monika for at dere er så flotte og gode venninner.

Abstract

In this thesis, we consider a specific instance of mixed-dimensional partial differential equations (PDEs) commonly referred to as the coupled 1D-3D flow model. The model itself consists of the Poisson equation defined on two different domains, the first being three-dimensional (3D) and the second being a one-dimensional (1D) subdomain of the first. The two equations are coupled by the use of an averaging operator and a generalized Dirac line source.

Physically, the coupled 1D-3D flow model can be used to describe fluid flow in a 3D porous domain embedded with cylindrical channels of radius R. This radius is further assumed negligible compared to the size of the 3D domain. We consider herein two main applications of this model, namely (i) water flow between a well and a reservoir and (ii) blood flow through vascularized tissue. From a computational perspective, these applications are highly challenging to simulate due to the scale disparity between the flow domains. A reservoir, for example, might extend several kilometres in the horizontal plane. Reservoir flow simulations therefore use meshes on the order of tens or hundreds of meters. The well, having a radius of only ~ 10cm, will therefore not be resolved in the reservoir mesh. Instead, the well is represented in the reservoir equations as a generalized Dirac line source. Critically, the Dirac line source will cause the solution of the reservoir equation to be *singular*. I.e., the solution diverges to infinity on the line. As we will see, this complicates both the analysis and approximation of the coupled 1D-3D flow problem.

To better understand the impact of these solution singularities, we first restrict our attention to the Poisson equation posed in a 3D domain when the right-hand side is a Dirac line source. We refer to this more simply as the *line source problem*. This problem has previously been studied using its primal formulation; we extend this work to its mixed formulation. The analysis is carried out using weighted Sobolev spaces. These quantify regularity of the solution, and can thus be used to estimate its approximation properties. We consider herein the mixed finite element method, for which our analysis shows that the solution singularities causes the approximation to fail to converge in the standard sense.

We then formulate a singularity removal method for the line source problem. The method is based on a solution splitting into higher and lower regularity terms. The lower regularity terms are here given explicitly and capture the solution singularity. The higher regularity term, referred to as the *remainder term*, is defined as the solution of its own elliptic equation. The right-hand side of this equation belongs to L^2; thus, its analysis and approximation follow from standard elliptic theory. In the singularity removal method, only the remainder term is approximated, and the full solution reconstructed by the solution splitting. This approach is found to enjoy significantly improved approximation properties compared to the straightforward approximation of the full solution. In particular, it is found to retrieve optimal convergence rates for the lowest-order standard and mixed finite element methods.

Finally, we consider suitable approximation methods for the coupled 1D-3D flow problem. The line source makes this problem particularly difficult to approximate numerically, as the coupling condition in this model is formulated precisely in the region where the solution degenerates. As the coupling condition also constitutes the driving force of the model, this can further pollute the entire numerical approximation.

To deal with this, we return to the solution splitting and decompose the solution into singular and regular terms. Next, via algebraic manipulations, we then reformulate the coupled 1D-3D flow problem so that it posed solely with respect to the high regularity terms. The solution can then be approximated via its higher regularity terms, and the full solution reconstructed by the solution splitting. We refer to this reformulation as a *singularity removal method for the coupled 1D-3D flow problem*. This method was found to retrieve optimal convergence rates for the lowest-order standard finite element method. Moreover, it was found to make the approximation robust with respect to having a small channel radius R. This makes the method especially attractive for applications where the channel radius is negligible compared to the total size of the simulation domain.

Outline

This dissertation consists of two parts. The scientific background is introduced in Part I followed by the scientific results in Part II.

Part I consists of seven chapters. Chapter 1 serves as an introduction to the topic of coupled 1D-3D flow models. Two applications are also presented that serve as the motivation for this study. Chapter 2 gives a brief description of the mathematical methodology we will use. In particular, we outline the different steps involved in the analysis and approximation of PDEs; this will later serve as a roadmap for the thesis itself. Chapter 3 introduces the governing physical laws and gives a derivation of the coupled 1D-3D flow problem. In Chapter 4, we provide the background theory of partial differential equations.

Chapters 5 and 6 summarize the scientific contributions of this thesis and put it into context with earlier research on the same topic. Chapter 5 treats the analysis and approximation of elliptic equations with a line source. Chapter 6 treats the analysis and approximation of the coupled 1D-3D flow model. The main result of this chapter is the formulation of a singularity removal method that can be used to obtain robust approximation methods. Finally, Chapter 7 summarizes the scientific contributions of the articles included in Part II and presents an outlook on future research.

Part II contains the scientific results, which consists of the following three articles and one conference proceeding:

Paper A: Ingeborg G. Gjerde, Kundan Kumar, Jan M. Nordbotten, Barbara Wohlmuth
Splitting Method for Elliptic Equations with Line Sources
ESAIM: M2AN 53 (2019) 1715–1739

Paper B: Ingeborg G. Gjerde, Kundan Kumar, Jan M. Nordbotten
A Mixed Approach to the Poisson Problem with Line Sources
SIAM Journal of Numerical Analysis, submitted
arXiv:1910.11785 [math.NA]

Paper C: Ingeborg G. Gjerde, Kundan Kumar, Jan M. Nordbotten (2018),
Well Modelling by Means of Coupled 1D-3D Flow Models
ECMOR XVI - 16th European Conference on the Mathematics of Oil Recovery, doi:10.3997/2214-4609.201802117

Paper D: Ingeborg G. Gjerde, Kundan Kumar, Jan M. Nordbotten,
A Singularity Removal Method for Coupled 1D-3D Flow Models
Computational Geosciences, in press
doi:10.3997/2214-4609.201802117

Contents

Part I:

Scientific Background

Chapter 1

Introduction

Let us start by considering the following question: What does fluid flow in a geological reservoir have in common with blood flow in the human circulatory system? To begin with, both topics have been and will be of huge importance to the world:

- In the context of flow in reservoirs, petroleum and natural gas currently make up more than half of the primary energy consumption of the world [37]. In the future, carbon capture and sequestration in geological formations is hoped to mitigate the industrial contributions to global warming [26]. As energy production shifts to renewable energy, there will be an increased need for energy storage; this has sparked an interest in e.g. aquifer thermal energy storage. Finally, the earth itself generates thermal energy; this energy can be harvested through geothermal energy production [16].

- In the context of medicine, diseases of the vascular system account for a significant portion of the global disease burden. In a report from the World Health Organization, ischaemic heart disease, stroke and chronic obstructive pulmonary disease are listed as the top three causes of death in 2016 [67]. Alzheimer's disease and other dementias, listed in [67] as the fifth largest cause of death, are currently hypothesized to be caused by vascular changes in the brain. As the population of the world is ageing, Alzheimer's disease can only be expected to take an increasing toll. Despite intense research on the disease, treatment remains elusive, with several drug trials recently abandoned because they were seen unlikely to work [60].

From the view of mathematics, the problems mentioned above share a common structure, in the sense that their mechanisms can be described by the same type of mathematical model. At first, this observation may seem of interest only to mathematicians. It can, however, serve a higher purpose, as mathematical models form the cornerstone of numerical simulation. Nmerical simulations can further be used to understand, predict and forecast physical processes. An excellent example of this principle is found in meteorology, where numerical weather prediction is successfully used to produce weather forecasts. Numerical simulation has also been extensively used in the context of geological systems, where they are used to answer questions related to safety, efficiency and economic gain [55; 63]. In the context of medicine, perfusion (i.e. the blood volume flow through tissue) is a valuable indicator for the physiological condition of the tissue. Clinical measurements of perfusion therefore provide valuable indicators in a wide range of medical conditions such as Alzheimer's disease [19; 38], stroke [58] and cancer [33]. For this reason, a lot of research effort is currently

committed to formulating mathematical models of microcirculation. In the future, numerical simulation of microcirculation will hopefully contribute to the understanding of mechanisms behind vascular disease and the evaluation of possible interventions.

In this work, we consider a specific type of mixed-dimensional PDE that can be used to describe (i) the interaction between a well and reservoir and (ii) flow through vascularized tissue. Both of these flow problems are multiscale in nature due to the scale disparity between the flow domains. I.e, a well typically has a negligible radius compared to a reservoir; similarly, the capillaries have negligible radius compared to e.g. an organ. For this reason, an upscaling technique will be necessary to reduce the computational complexity of the problem.

The upscaling technique considered in this work is a dimensional reduction of the model, where the equations describing flow in either well or blood vessel are reduced to 1D. This equation is then coupled to the 3D flow equation describing flow in either reservoir or biological tissue. The coupling uses an averaging operator as well as a generalized Dirac delta concentrated on the 1D domain. The major drawback of this approach is that the line source causes the solution to become singular. This complicates both the analysis and the approximation of the coupled 1D-3D flow model.

The main contributions of this thesis are as follows:

1. **The rigorous analysis of the Poisson equation with line sources**

   Earlier research on the coupled 1D-3D flow models identified the line source as the main cause of the challenges associated with this model. To better understand the influence of the line source, it is common first to study simply the Poisson equation (posed in a 3D domain) with a line source in the right-hand side. We refer to this as the *line source problem*.

   Previous research studied the line source problem using its primal formulation [23; 22]. In Paper B, we extend this work to its mixed formulation. In this paper, the existence of a solution is proven using weighted Sobolev spaces. For the approximation, we consider the mixed finite element method. An advantage of this method is that it provides locally mass conservative approximations. However, it was found that due to the singular nature of the solution, the mixed finite element fails to converge in the standard sense.

2. **The formulation of a solution splitting method**

   The line source induces a particular mathematical structure in the solution. In Papers A and B, this structure was uncovered by the use of a solution splitting. There it was shown that, under certain restrictions on the parameters, the solution of the line source problem admits a splitting into higher and lower-regularity terms. Centrally, the lower-regularity terms can be given explicitly with respect to the endpoints of the line. The higher-regularity term, denoted the *remainder*, is defined as the solution of its own Poisson equation with a right-hand side belonging to L^2. Thus, its regularity and approximation properties follow from standard elliptic theory.

   With the solution splitting in hand, one can define an improved numerical approach where the solution is approximated via its remainder term. Suitable discretization methods can then be found in the standard literature. Papers A and B studied the primal and mixed finite element methods for this problem, respectively. In both cases, it was

found that the singularity removal restored optimal convergence rates for lowest-order elements.

3. **The development of a singularity removal method for the coupled 1D-3D flow model**

   Returning to the coupled 1D-3D flow model, the singular behaviour of the solution is now of particular trouble, as the coupling condition is formulated in the same region that the solution degenerates. Papers C and D considered the primal finite element approximation of this problem. Therein, numerical evidence was provided showing that this approximation may fail to converge if the channel radius R is smaller than the mesh size. This is problematic as the coupled 1D-3D flow problem was formulated for applications where the channel radius is negligible.

   With this as motivation, Papers C and D consider an extension of the solution splitting method to the coupled 1D-3D flow model. There, the 3D solution is split into a lower-regularity term capturing the solution singularity and a higher-regularity remainder term. Via algebraic manipulation, the coupled 1D-3D flow model can then be reformulated so that it is given with respect to the higher-regularity terms. The result is a new set of governing equations for the problem in which the singularities have been removed. The solution can then be approximated via the reformulated equations, and the full solution reconstructed using the solution splitting. This was referred to as the *singularity removal method for the coupled 1D-3D flow problem*. In Paper D, this method was implemented using a standard finite element method to approximate the reformulated equations. The singularity removal method was found to yield optimal convergence for lowest-order elements. Centrally, it was further found to restore convergence when the channel radius R is negligible compared to the mesh size.

1.1 Motivation

Elliptic equations with line sources are used in a variety of applications. In civil engineering, for example, this type of equation has been used to model the effect of 1D steel components to reinforce concrete structures [57]. In geophysics, line sources have been used to model the interference of metallic pipelines and bore-casings in electromagnetic modelling of reservoirs [84]. In biology, line sources are used to model water flow through a root system [39; 43]. In this thesis, we will focus on two main applications of the coupled 1D-3D flow problems, namely, (i) water flow between a well and reservoir and (ii) blood flow through vascularized tissue. The purpose of this section is to describe in more detail the physical processes governing these two scenarios.

1.1.1 Interaction between a well and reservoir

In general, the subsurface consists of more or less permeable rock or sediment types. If the permeability of this rock or sediment is large enough, fluids (e.g. water, oil or gas) may flow through it. In applications such as oil or gas production, geothermal energy production, carbon storage and aquifer thermal energy storage, wells are drilled into the reservoir

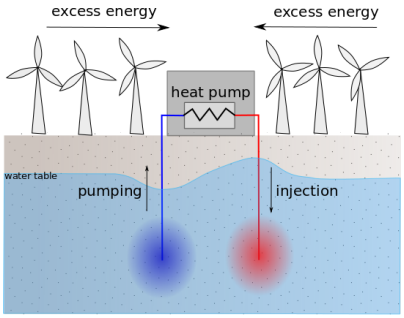

Figure 1.1: An illustration showing how aquifer thermal energy works. First, water is heated using excess energy and injected into the aquifer. As the rock making up the aquifer has a lower heat capacity than water, it acts as a thermos, with only small amounts of heat dissipating to the surrounding rock. The energy can then be retrieved by producing hot water back to the surface.

and connected to it in high-permeability regions. This facilitates the extraction of natural resources such as groundwater, natural gas or petroleum, or in the case of geothermal energy and carbon storage, the injection of water or CO_2.

In the future, renewable energy is projected to provide an increasing share of the worlds energy demands. Renewable energy is by nature intermittent; thus, there is a need to develop large-scale storage methods for excess energy. Thermo-Mechanical Subsurface Energy Storage (TheMSES) has been proposed as one such storage method. The idea is that in times of overproduction of energy, excess energy can be used to heat water. This hot water can then be injected into the subsurface. As rock has lower thermal capacity than water, only minimal amounts of heat are expected to dissipate into the surrounding rock. When needed, the hot water can then be produced back to the surface and converted to electricity using a heat pump.

In the context of TheMSES, the quantity of interest would be the temperature of the water being either injected and produced at the surface. This naturally depends on the heat and fluid flow in the aquifer. As rocks are porous, fluid flow therein is typically modelled using Darcy's law combined with mass conservation [63]. The well, contrarily, allows for a free flow of fluids. Assuming that the flow therein is laminar and the well sufficiently long, this flow is typically modelled using the Hagen-Poiseuille equation. Heat flow occurs as a result of both conduction and convection processes, the latter being the heat transferred by fluid flow through the rock. This is modelled mathematically using a transport equation [54]. The well typically has a negligible radius compared to the size of the simulation domain. To avoid having to resolve the well in the mesh, the heat and fluid flow therein is assumed axisymmetric so that it can be described by a 1D equations [5]. Finally, the connection flow between well and aquifer is typically modelled by Starling's law of filtration, which states that the mass flux between well and aquifer will be proportional to their pressure difference.

The connection flow between well and aquifer is well known to be non-trivial to simulate due to the scale disparities between domains. Considering the mesh representing the aquifer, its mesh cells will necessarily be coarse, in the sense that they can extend tens or hundreds of metres in the horizontal plane. Near the well, however, the pressure varies considerably over short distances. For this reason, the numerically computed pressure will generally not be

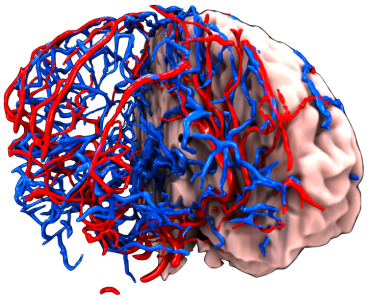

Figure 1.2: The geometry of the vascular network of a human brain, extracted from MRI images. Arterial blood vessels are indicated in red and venous blood vessels in blue. The dataset and visualization are from [36].

representative of the true pressure in the near well region. This can pollute the approximation of the pressure difference between well and aquifer. As this pressure difference constitutes the driving force of the fluid flow, it can further pollute the numerical approximation of the heat flow.

1.1.2 Flow through vascularized tissue

The cardiovascular system in the human body allows for the circulation of blood and with it, the transport of nutrients, oxygen, carbon dioxide, hormones and blood cells. As such, it is of critical importance in fighting disease, stabilizing temperature and pH and maintaining homoeostasis. The cardiovascular system itself is composed of the heart, blood and blood vessels. The blood circulation is divided into two distinct loops: The pulmonary and systemic loops. The first of these passes by the lungs so that the blood is oxygenated. The second of these is responsible for the circulation of oxygenated blood to organs, tissues and cells.

Blood is supplied to the systemic loop from the heart to the aorta. This is a thick-walled artery with a diameter measuring 2.0 to 3.0 cm. The blood is then transported through a branching network of arteries (measuring 100.0 µm to 2.0 cm in diameter), into another branching network of arterioles (measuring 10.0 to 100.0 µm in diameter) and finally into the capillaries (measuring 5.0 to 10.0 µm). At the capillary level, oxygen is allowed to diffuse through the vessel walls into the surrounding tissue. The capillaries then merge into venules, and again into veins, and finally into the two major veins that empty back into the heart.

The passage of blood from capillary bed to tissue is often referred to as perfusion. A large variety of severe medical conditions involve alterations in perfusion; hence, its measurements and simulation both have considerable clinical value. Mathematically, perfusion is a highly challenging process to model, as the physical processes occur on a large variety of spatial and temporal scales. The tissue itself is composed of dispersed cells separated by a connective pore space, where the pores are filled with fluids such as blood and water. For this reason, fluid flow through tissue is usually modelled by Darcy's law [40]. Mass transport within the tissue is achieved by both convection or diffusion processes within the tissue; mathematically, this is modelled by a transport equation.

The blood flow through the vascular network is well known to be non-Newtonian and pulsative in nature (and thus unsteady). A complete exposition on the mathematical models

governing blood flow is beyond the scope of this thesis. Let us only note that the governing equations for this type of flow would be particularly challenging to approximate numerically. For this reason, simplified models have been developed, that reduce the blood flow in the capillaries to the 1D Hagen-Poiseuille equation. Thus, the governing equations reduce to be on the same form as for fluid flow between aquifer and well. So far, this model has been used to describe e.g. blood and oxygen transport through the vascularized tissue of the brain [73; 34; 83; 30; 56], the efficiency of cancer treatment by hyperthermia [61], the efficiency of drug delivery through microcirculation [17; 71] and the effect of Type 2 diabetes on the the vascular system [80].

Note that one here has the same issues with scale disparity, as the capillary network has a negligible diameter ($5.0 - 10.0$ µm) compared to e.g. the length of an average human brain (~ 10 cm). Thus, the mesh representing the tissue will likely not be fine enough to capture the pressure profile around the capillaries accurately. Again, this can pollute the numerical approximation of the pressure difference between tissue and vascular network. As this pressure difference is one of the driving forces of perfusion, this can further pollute the entire numerical approximation.

Chapter 2

Methodology

In this section, we will give a short introduction to the mathematical methodology used in this thesis. This introduction also serves as a roadmap for how the thesis is structured. The methodology itself is schematically illustrated in Figure 2.1.

Recall from the previous section that we want to be able to simulate (i) the interaction between a well and aquifer and (ii) flow through vascularized tissue. To do so, the first step is to get an understanding of the physical background of the problem. Once this is done, one can use this understanding to formulate a mathematical model for the problem. In our case, this will result in a set of PDEs which we take as the *governing equations* of the problem.

The second step involves using concepts from functional analysis to formulate the governing equations as a *variational formulation*. This allows for one to search for generalized solutions in Hilbert spaces. We consider in this work the primal and mixed variational formulations of the problem. Both formulations first require one to identify the appropriate function spaces for the solution. As we will see, once these spaces are in hand, it in many cases becomes straightforward to prove the existence of a solution. Moreover, the solution spaces provide information about the smoothness of the problem. This will later be used to inform the numerical methodology used for its approximation.

The third step involves formulating a numerical approximation of the problem. To do so, one may discretize the variational formulation, by assuming the solution belongs to some finite-dimensional function space. In this thesis, we consider discretization by the use of finite elements. For the primal formulation, this results in the *primal finite element method*. For the dual formulation, this results in the *mixed finite element method*.

Given a discretization of the variational formulation, it can then be formulated as a matrix equation. The fourth step involves using linear algebra to solve for the *solution approximation*. Finally, the numerical method should undergo *validation* to test whether it provides a sensible approximation of the solution. To do so, one can use the method of manufactured solutions to generate test problems. The approximation quality can then be measured quantitatively by checking its convergence rate and comparing these to theoretical estimates.

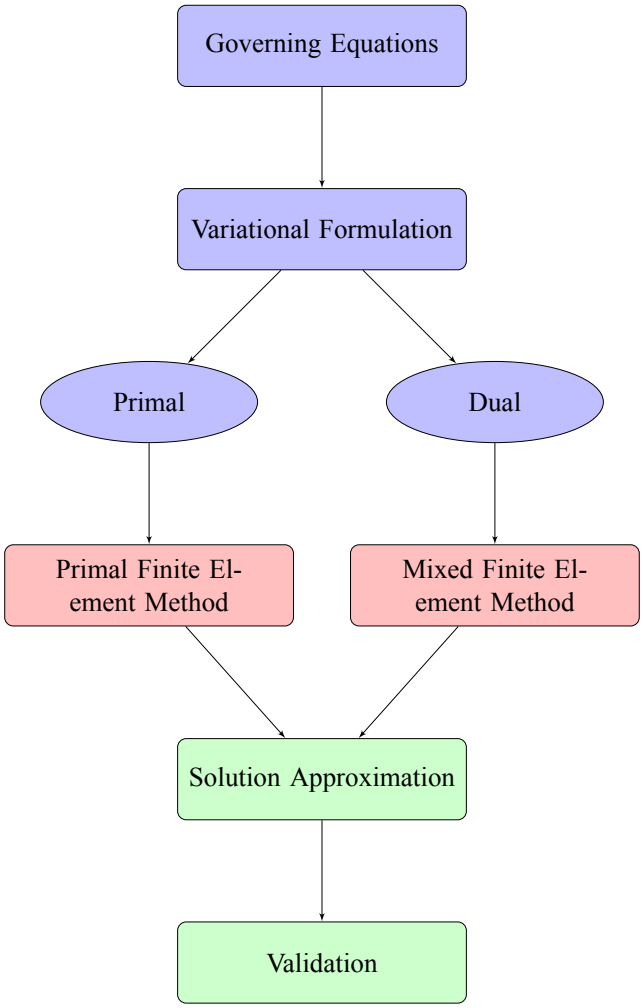

Figure 2.1: The conceptual path we follow in order to model, analyse and approximate coupled 1D-3D flow models.

Chapter 3

Governing Equations

In this section, we introduce the governing equations for the coupled 1D-3D flow problem. To do so, we consider the physical processes behind the applications introduced in Section 1, and show how they can be expressed as a mathematical system of equations.

The derivation is given using the following steps: First, we specify in more detail the geometrical setting of the problem. This will involve two distinct flow domains: A 3D domain $\Omega \subset \mathbb{R}^3$ representing a porous media, embedded with a network of channels $\Sigma \subset \Omega$. The channels are assumed to have negligible radius so that the domain Σ can be shrunk onto its centreline Λ. Next, we introduce the governing equations of the problem. The first of these is mass conservation, followed by associated constitutive laws and boundary conditions to close the system. As Ω represents a porous media, we there apply Darcy's law. Next, Λ represents a network of thin channels, and we there apply Hagen-Poiseuille's law. Finally, Starling's law of filtration is used to couple the flow equations on Ω and Λ. The resulting is a mixed-dimensional system of elliptic PDEs, commonly referred to as the *coupled 1D-3D flow model.*

Figure 3.1: (Left) The domain Ω embedded with a generalized cylinder Σ_ϵ. The cylinder Σ is described by a centreline Λ and has a radius R. (Right) A generalized cylinder Σ with centreline Λ and radius R. The curve Λ is associated with a Frenet-Serret frame $\mathbf{T}, \mathbf{N}, \mathbf{B}$; here, $\mathbf{T}$ denotes its unit tangent vector, $\mathbf{N}$ its unit normal vector, and $\mathbf{B}$ its unit binormal vector.

3.1 Geometrical Setting

Consider a given open domain $\Omega \subset \mathbb{R}^3$, assumed bounded and convex with smooth boundary $\partial\Omega$. Embedded in this domain we have a collection of disjoint generalized cylinders $\Sigma = \cup_{i=1}^{n}\Sigma_i$, meaning that each cylinder Σ_i is the swept volume of a circle of radius R_i along a curve Λ_i. To be more precise, the cylinders Σ_i each have a C^2-regular centreline Λ_i, parametrized by $\boldsymbol{\lambda}_i(s_i) = [\lambda_i^1(s_i), \lambda_i^2(s_i), \lambda_i^3(s_i)]$ so that $\Lambda_i = \{\boldsymbol{\lambda}_i(s_i),\ s_i \in (0, L_i)\}$. Here, we assumed $\|\boldsymbol{\lambda_i}'(s_i)\| = 1$ so that s_i coincides with the arc-length. We further assume Σ is completely embedded into Ω, such that the distance between $\partial\Omega$ and $\partial\Sigma$ is strictly positive.

Let now s denote a global parametrization parameter so that $\Lambda = \{\boldsymbol{\lambda}(s),\ s \in (0, L)\}$ with $L = \sum_{i=1}^{n} L_i$. Using notation as in [32], take $\mathbf{T}, \mathbf{N}, \mathbf{B}$ be the Frenet-Serret frame of Λ. Let X and Y denote the axes along the vectors $\mathbf{N}, \mathbf{B}$ of the Frenet-Serret frame. The coordinate axes X, Y then form a local coordinate system having origin on Λ, and the domain Σ can now be described as

$$\Sigma = \{\boldsymbol{\lambda}(s) + r\cos(\theta)\mathbf{N}(s) + r\sin(\theta)\mathbf{B}(s),\ 0 < s < L,\ 0 < \theta \leq 2\pi,\ 0 < r \leq R(s)\}, \tag{3.1}$$

where $r = r(s)$ and $\theta = \theta(s)$ are the cylindrical coordinates of X, Y. Its boundary Γ can be parametrized by

$$\Gamma = \{\boldsymbol{\lambda}(s) + R(s)\cos(\theta)\mathbf{N}(s) + R(s)\sin(\theta)\mathbf{B}(s),\ 0 < s < L,\ 0 < \theta \leq 2\pi\}. \tag{3.2}$$

Let $\tilde{\Omega} = \Omega \setminus \Sigma$. In the context of subsurface flow, the domain $\tilde{\Omega}$ might represent an aquifer and Σ one or more wells that have been drilled into it. In the context of vascularized flow, $\tilde{\Omega}$ might represent e.g. an organ, while Σ would represent the blood vessels forming its vascular network. In both of these cases, there will be a scale disparity between $\tilde{\Omega}$ and Σ, in the sense that $R(s) \ll \text{size}(\Omega)$. A mesh representing Ω would then have to be exceedingly fine in order to resolve the cylinder boundaries Γ. With this in mind, we make now our first simplifying assumption:

(A1) We assume the porous media flow domain $\tilde{\Omega}$ can be identified with the entirety of Ω, i.e., we set $\tilde{\Omega} = \Omega$.

3.2 Conservation of Mass

The concept of conservation forms a cornerstone in all physical models. Conservation laws arise in several different fields of physics and include conservation of energy, conservation of electric charge and conservation of linear and angular momentum. In this work, we take as our starting point the conservation of mass, which will be applied on both domains Ω and Σ.

In order to describe mass conservation mathematically, let for now U denote some arbitrary domain filled by an incompressible fluid. At each point in the domain, we assume there is a given mass m per unit volume and a given flux $\mathbf{q}$, where the latter is a vector function representing the discharge of a fluid per unit area. Lastly, take f to be a source or sink of mass. Formally, we have the relation that

$$\begin{pmatrix}\text{mass change}\\ \text{in time}\end{pmatrix} = \begin{pmatrix}\text{mass entering or leaving}\\ \text{through the boundary}\end{pmatrix} + \begin{pmatrix}\text{mass entering or leaving}\\ \text{due to the sink}\end{pmatrix},$$

which can be expressed mathematically as

$$\int_U \dot{m}\,\mathrm{d}U = -\int_{\partial U} \mathbf{q}\cdot\mathbf{n}\,\mathrm{d}s + \int_U f\,\mathrm{d}U. \tag{3.3}$$

Here, ∂U denotes the boundary of the domain, $\dot{m}$ denotes the total change in mass over time and $\dot{m}$, $\mathbf{n}$ the outward normal vector to ∂U with unit length. Using then the divergence theorem on the first term on the right-hand side of (3.3), we find the relation

$$\int_U \dot{m} + \nabla\cdot\mathbf{q} - f\,\mathrm{d}x = 0,$$

where $\nabla\cdot$ denotes the divergence operator. We restrict ourselves in this work to consider steady state solutions, in which case $\dot{m} = 0$. Note now that this equation holds in any given, stationary domain U. Consequently, one has the following law of conservation:

$$\nabla\cdot\mathbf{q} = f \quad \text{in } U. \tag{3.4}$$

Let us now return to the geometrical setting introduced in Section 3.1. Mass conservation in the sense of (3.4) can then be applied to both domains Ω and Σ. In the case of Σ, this domain is assumed to have a negligible radius $R(s)$. With this in mind, we make the following simplifying assumption:

(A2) The flow in Σ is assumed axisymmetric, i.e, invariant across each cross section of Σ.

The flux $\mathbf{q}$ therein can then be described in terms of a single scalar parameter, $\mathbf{q} = \hat{q}(s)\mathbf{T}$, where the hat indicates that this is a 1D function defined on Λ. Mass conservation (3.4) in Σ then reduces to a ordinary differential equation:

$$\frac{\mathrm{d}\hat{q}}{\mathrm{d}s} = \hat{f} \quad \text{on } \Lambda, \tag{3.5}$$

where $\mathrm{d}\hat{q}/\mathrm{d}s = \hat{q}(\nabla\cdot\mathbf{T})$.

3.3 Constitutive Laws

In this section, we give the constitutive laws and boundary conditions used in each flow domain Ω and Σ. As the domain Ω is assumed porous, we apply there Darcy's law. The domain Σ is assumed to consist of a collection of thin channels; for this reason, we apply there Hagen-Poiseuille's law.

3.3.1 Darcy's law

In this section, we will introduce Darcy's law for fluid flow in porous domains. A porous media is defined as a material volume containing in an interconnected void space. The latter is more commonly referred to as the pore space and is typically filled with a fluid. Several constitutive relationships exist that describe the fluid flow through the media, the most famous of which being Darcy's law. Darcy's law which considers two driving forces for fluid flow through porous media, the first being gravity and the second originating from pressure differences within the fluid. Mathematically, this is described by the relationship

$$\mathbf{q} = -\kappa(\nabla p - \rho\mathbf{g}), \tag{3.6}$$

where ρ denotes the density of the fluid, $\mathbf{g}$ the gravitational force, κ the permeability tensor, and ∇p denotes the pressure gradient. The minus sign in front of it accounts for the fact that fluid will flow from high to low-pressure regions. Darcy's law was first formulated by Henry Darcy after a series of experiments on water flow through sand [63]. Later, it has been derived rigorously through homogenisation of the Navier-Stokes equations under the assumption of creeping flow [85].

The permeability tensor κ depends on the properties of the porous media; physically, it can be interpreted as representing the resistance the porous media gives to fluid flow. This naturally depends on the porosity of the domain, and also the spatial configuration of the pore space. For example, a pore space forming long and tortuous flow paths will give more resistance to the traversing fluid. Thus, it can be expected to have lower permeability. In this work, we restrict κ to be a strictly positive scalar. The extension to tensor-valued κ will in most cases be straightforward. As a notable exception, we note the splitting method defined in Section 5.4; this will be further addressed in Remark 5.4.1.

With Darcy's law at our disposal, we are now ready to state the governing equations on the domain Ω. For simplicity, we neglect gravitational forces, so that $\mathbf{q} = -\kappa\nabla p$. Additionally, we assume the fluid to be incompressible, so that mass conservation holds in the sense of (3.4). This yields the following set of equations:

$$\mathbf{q} = -\kappa\nabla p \qquad \text{in } \Omega, \tag{3.7a}$$
$$\nabla \cdot \mathbf{q} = f \qquad \text{in } \Omega, \tag{3.7b}$$
$$p = 0 \qquad \text{on } \partial\Omega_D, \tag{3.7c}$$
$$\mathbf{q} \cdot \mathbf{n} = 0 \qquad \text{on } \partial\Omega_N. \tag{3.7d}$$

Here, (3.7c)-(3.7d) are the boundary conditions that close the system. The domain Ω is assumed decomposed disjointly so that $\partial\Omega = \partial\Omega_D \cup \partial\Omega_N$; equations (3.7c)-(3.7d) will give the Dirichlet and Neumann-type boundary conditions of the problem, respectively. In order for the solution to be unique, we further assume $\partial\Omega_D$ to have positive measure.

3.3.2 Hagen-Poiseuille flow

In the previous section, we introduced the governing equations taken in the domain Ω. In this section, we will introduce the corresponding constitutive law for the domain Σ. This domain is assumed to consist of a network of thin channels, each with a given radius R_i. Letting L_i be the length of the channel, we assume $R_i \ll L_i$. As in the previous section, we neglect the influence of gravity. Consider first a single channel. Assuming then that the fluid is Newtonian, and the fluid flow laminar, the pressure decay across the channel will be approximately linear. For steady-state flow, this is formalized by the Hagen-Poiseuille equation

$$Q = -\frac{\rho\pi R^4}{8\mu L}(\hat{p}_{\text{out}} - \hat{p}_{\text{in}}), \tag{3.8}$$

where Q denotes the volumetric flow rate and $\hat{p}_{\text{out}} - \hat{p}_{\text{in}}$ the pressure difference between the endpoints of the channel. The variable μ denotes the dynamic viscosity of the fluid. In the context of TheMSES, the viscosity μ will generally depend in a non-linear manner on the fluid temperature. In the case of blood, the viscosity is, in general, non-linear and complicated

to describe; we refer the interested reader to [72]. For the sake of simplicity, we set μ to be constant in this work.

Before proceeding, let us note that several of the assumptions behind the Hagen-Poiseuille equation are not valid for blood flow. Firstly, blood is a non-Newtonian fluid. Secondly, blood flow through the vascular system is pulsatile in nature, and thus unsteady. This suggests that we should consider the three-dimensional Navier-Stokes equations. Considering the complex structure of a vascular network, this would be prohibitively expensive to resolve numerically. We are, however, concerned with modelling the exchange of mass between the circulatory system and the surrounding tissue. This exchange happens at the level of microcirculation, at which the effect of blood pulsation is almost negligible [70; 31]. With this in mind, the flow is assumed laminar and steady. Next, as the pressure pulsations are negligible, the blood vessels can be assumed rigid in the sense that they have a fixed radius. Lastly, the non-Newtonian flow behaviour of blood is modelled in a simplified manner using an algebraic relationship. With these assumptions, the one-dimensional Navier-Stokes equation can be reduced to the Hagen-Poiseuille equation (3.8) [21; 66].

Assume now for the sake of simplicity $\mu = \rho = 1$. Proceeding as in [85, Appendix C], (3.8) can be related to an intrinsic phase average form of Darcy's law by

$$\hat{\mathbf{q}} = -\frac{R^2}{8}\nabla p(s), \tag{3.9}$$

where $\hat{p} = \hat{p}(s)$, $\hat{\mathbf{q}} = \hat{\mathbf{q}}(s)$ and $\hat{\kappa} = \hat{\kappa}(s)$ are defined along the centreline Λ. We are now ready to state the governing equations on Σ. Recall first that $\hat{\mathbf{q}} = \hat{q}\mathbf{T}$ due to (A2). Multiplying both sides of (3.8) by $\mathbf{T}$, and combining it with mass conservation in the channel, one has

$$\hat{q} = \hat{\kappa}\frac{\mathrm{d}\hat{p}}{\mathrm{d}s} \qquad \text{in } \Lambda, \tag{3.10a}$$

$$\frac{\mathrm{d}\hat{q}}{\mathrm{d}s} = \hat{f} \qquad \text{in } \Lambda, \tag{3.10b}$$

$$\hat{p} = 0 \qquad \text{on } \partial\Lambda_D, \tag{3.10c}$$

$$\hat{q} = 0 \qquad \text{on } \partial\Lambda_N, \tag{3.10d}$$

where $\hat{\kappa} = R^2/8$. Here, differentiation along Λ is defined by $\mathrm{d}p/\mathrm{d}s = \nabla\hat{p}\cdot\mathbf{T}$. Equations (3.10c)-(3.10d) give the Dirichlet and Neumann boundary conditions, respectively. The latter condition is a no-flow condition on the Neumann boundary of Σ simplified by the relation $\mathbf{q}\cdot\mathbf{n} = \hat{q}\mathbf{T}\cdot\mathbf{n} = 0$. As in the previous section, the domain Λ is assumed decomposed disjointly so that $\partial\Lambda = \partial\Lambda_D \cup \partial\Lambda_N$. In order for the solution to be unique, we again assume $\partial\Lambda_D$ to have positive measure.

3.4 The Coupled 1D-3D Flow Model

In the two preceding sections, we formulated the governing equations for fluid flow in the domains Ω and Σ. In this section, we will couple these two systems via an exchange term f that describes the mass exchange between the two domains.

As our coupling condition we use the linear filtration law stating that the connection flow f between domains Ω and Λ will be proportional to their pressure difference:

$$f(s) = 2\pi R L_p(\hat{p}(s) - \bar{p}(s)) \quad \text{ on } \Gamma. \tag{3.11}$$

Here L_p denotes the transmural hydraulic conductivity of either well or blood vessel. The variable $\bar{p}$ is defined as $\bar{p} = \Pi p$, where Π denotes the averaging operator

$$\Pi p = \frac{1}{2\pi} \int_0^{2\pi} p(\boldsymbol{\lambda}(s) + R(s)\cos(\theta)\mathbf{N}(s) + R(s)\sin(\theta)\mathbf{B}(s))\,\mathrm{d}\theta. \tag{3.12}$$

Thus, the variable $\bar{p}(s)$ then denotes the average of p along the circle with center $\boldsymbol{\lambda}(s)$ and radius $R(s)$ lying parallel to Λ. From this point on, this will be denoted more simply as

$$\bar{p}(s) = \frac{1}{2\pi} \int_0^{2\pi} p(s, R, \theta)\,\mathrm{d}\theta. \tag{3.13}$$

In the context of flow through vascularized tissue, (3.11) is known as Stirling's law of filtration [77]. In the context of reservoir simulation, (3.11) is known as a inflow-performance relation, with L_p referred to as the well index.

To insert this source term in the three-dimensional flow equation (that is defined on Ω), we introduce a generalized Dirac delta function δ_Λ, defined as a sequence of nascent Dirac functions:

$$\delta_\Lambda = \lim_{\epsilon \to 0} \delta_\Lambda^\epsilon, \quad \delta_\Lambda^\epsilon = \begin{cases} \frac{1}{\pi\epsilon^2} & \text{for } r \leq \epsilon, \\ 0 & \text{otherwise,} \end{cases} \tag{3.14}$$

where $r(\mathbf{x}) = \mathrm{dist}(\mathbf{x}, \Lambda)$. For smooth test functions ϕ, one has the property

$$\int_\Omega \delta_\Lambda \phi \,\mathrm{d}\Omega = \int_\Lambda \phi \,\mathrm{d}\Lambda \quad \text{for all } \phi \in C^0(\bar{\Omega}). \tag{3.15}$$

The coupled 1D-3D flow model can then be stated as

$$\mathbf{q} = -\kappa \nabla p \qquad \text{in } \Omega, \tag{3.16a}$$

$$\nabla \cdot \mathbf{q} = \beta(\hat{p} - \bar{p})\delta_\Lambda \qquad \text{in } \Omega, \tag{3.16b}$$

$$\hat{q} = -\hat{\kappa}\frac{\mathrm{d}\hat{p}}{\mathrm{d}s} \qquad \text{in } \Lambda, \tag{3.16c}$$

$$\frac{\mathrm{d}\hat{q}}{\mathrm{d}s} = -\beta(\hat{p} - \bar{p}) \qquad \text{in } \Lambda, \tag{3.16d}$$

with boundary conditions

$$p = 0 \qquad \text{on } \partial\Omega_D, \tag{3.17a}$$

$$\mathbf{q} \cdot \mathbf{n} = 0 \qquad \text{on } \partial\Omega_N, \tag{3.17b}$$

$$\hat{p} = 0 \qquad \text{on } \partial\Lambda_D, \tag{3.17c}$$

$$\hat{q} \cdot n = 0 \qquad \text{on } \partial\Lambda_N. \tag{3.17d}$$

Chapter 4

Mathematical Background

In this section we will introduce the classical variational framework of PDEs, and show how it can be used to

1. prove the existence of weak solutions,
2. define suitable discretization methods.

To do so, we consider the Poisson equation

$$\mathbf{q} + \kappa \nabla p = 0 \qquad \text{in } \Omega, \tag{4.1a}$$
$$\nabla \cdot \mathbf{q} = f \qquad \text{in } \Omega, \tag{4.1b}$$
$$p = 0 \qquad \text{on } \partial\Omega_D, \tag{4.1c}$$
$$\mathbf{q} \cdot \mathbf{n} = 0 \qquad \text{on } \partial\Omega_N, \tag{4.1d}$$

in a bounded convex domain $\Omega \subset \mathbb{R}^d$ with smooth boundary $\partial\Omega$, with right-hand side $f \in L^2(\Omega)$ and a strictly positive permeability $\kappa \in L^\infty(\Omega)$. Let us remark that the purpose of this section is didactic. The theory presented here is standard and can be found in most textbooks treating PDEs and finite element methods. In the next chapter, we will show how this theory can be extended to treat elliptic equations with line sources.

The section will proceed as follows. We begin in Section 4.1 by defining and giving some central properties of Sobolev spaces. With this in hand, we next show how one can prove the existence of a weak solution belonging to some suitable Sobolev space. We do this in two parts, considering first its primal formulation in Section 4.2.1 and then its mixed formulation in Section 4.2.2. Lastly, we show in Section 4.3 how the solution can be discretized to obtain approximation methods for the solution. We consider in this thesis two different finite element methods for the approximation: the primal finite element method, introduced in Section 4.3.1, and the mixed finite element method, introduced in Section 4.3.2.

4.1 Sobolev Spaces

Let $\Omega \subset \mathbb{R}^d$ denote a bounded convex domain with smooth boundary $\partial\Omega$, $\mathrm{d}x$ the Lebesgue measure on this space, σ the σ-algebra of measurable sets on Ω, and (Ω, σ, dx) the standard Lebesgue measure space. For a function $u : \Omega \to \mathbb{R}$ and $1 \leq p < \infty$, we further define

$$\|u\|_{L^p(\Omega)} := \left(\int_\Omega |u|^p \, \mathrm{d}x \right)^{\frac{1}{p}}, \tag{4.2}$$

and for $p = \infty$,

$$\|u\|_{L^p(\Omega)} := \text{ess sup}\{|u|^p\}. \tag{4.3}$$

The L^p-spaces on (Ω, σ, dx) can then be defined as

$$L^p(\Omega) = \{u : \Omega \to \mathbb{R} \text{ such that } \|u\|_{L^p(\Omega)} < \infty\}. \tag{4.4}$$

Here, the notation $L^p(\Omega)$ tacitly assumes that this is the L^p-space with respect to the (standard) Lebesgue measure space. The space $L^p(\Omega)$ is Banach for $1 \leq p \leq \infty$. For $p = 2$, it is also a Hilbert space with inner product

$$(u, v)_{L^2(\Omega)} = \int_\Omega uv \, \mathrm{d}x.$$

As such, $u, v \in L^2(\Omega)$ will satisfy the following Cauchy-Schwarz inequality:

$$|(u, v)_{L^2(\Omega)}| \leq \|u\|_{L^2(\Omega)} \|v\|_{L^2(\Omega)}. \tag{4.5}$$

Let us now define the concept of weak derivatives. Let $L^1_{\text{loc}}(\Omega)$ be the space of locally integrable functions

$$L^1_{\text{loc}}(\Omega) = \{u : \Omega \to \mathbb{R} \text{ such that } \|u\|_{L^1(K)} < \infty \text{ for all } K \subset \Omega \text{ compact}\}, \tag{4.6}$$

and take $\gamma = (\gamma_1, ..., \gamma_d)$ to be a multi-index of order $|\gamma| = \gamma_1 + ... + \gamma_d$, where each component γ_i is a non-negative integer. The γth weak derivative of a function u, denoted $D^\gamma u := v \in L^1_{\text{loc}}(\Omega)$, is defined as the function satisfying

$$\int_\Omega u D^\gamma \phi \, \mathrm{d}x = (-1)^{|\gamma|} \int_\Omega v\phi \, \mathrm{d}x \quad \text{for all } \phi \in C_c^\infty(\Omega), \tag{4.7}$$

where $C_c^\infty(\Omega)$ denotes the set of infinitely differentiable test functions with compact support in Ω.

Let now $k \geq 0$ be an integer. The Sobolev space $W^{k,p}(\Omega)$ can then be defined as

$$W^{k,p}(\Omega) = \{u \in L^p(\Omega) \text{ such that } D^\gamma u \in L^p(\Omega) \text{ for } |\gamma| \leq k\},$$

where $D^\gamma u \in L^1_{\text{loc}}(\Omega)$ denotes the weak derivative of u. This is a Banach space endowed with the norm

$$\|u\|^p_{W^{k,p}(\Omega)} = \sum_{|\gamma| \leq k} \|D^\gamma u\|^p_{L^p(\Omega)}.$$

The Sobolev space $W^{k,p}(\Omega)$ admits the following highly useful property known as *density of smooth functions*:

Theorem 4.1.1. *Given $u \in W^{k,p}(\Omega)$, there exists functions $u_m \in W^{k,p}(\Omega) \cap C^\infty(\Omega)$ such that*

$$u_m \to u \quad \textit{in } W^{k,p}(\Omega). \tag{4.8}$$

As the functions belonging to a Sobolev space are only defined in a weak sense, we need to redefine the way we take its boundary value.

Definition 4.1.2 (Trace operator)**.** The *trace operator* $T : W^{1,p}(\Omega) \to L^2(\partial\Omega)$ is a bounded linear operator satisfying

$$\|Tu\|_{L^2(\partial\Omega)} \leq C_T \|u\|_{W^{1,p}(\Omega)} \qquad \text{for each } u \in W^{1,p}(\Omega), \tag{4.9a}$$

$$Tu = u|_{\partial\Omega} \qquad \text{for each } u \in W^{1,p}(\Omega) \cap C^0(\bar{\Omega}), \tag{4.9b}$$

for some constant $C_T > 0$.

Here, $C^0(\bar{\Omega})$ denotes the set of continuous functions in the closure of Ω. (4.9b) then guarantees that for continuous functions, the trace will agree with the boundary data. We use a subscript zero to indicate the subspace of $W^{k,p}(\Omega)$ with zero trace on the Dirichlet boundary $\partial\Omega_D$:

$$W_0^{k,p}(\Omega) = \{u \in W^{k,p}(\Omega) \text{ such that } Tu = 0 \text{ on } \partial\Omega_D\}. \tag{4.10}$$

Functions in $W_0^{1,p}(\Omega)$ admit the following useful property:

Lemma 4.1.3 (Poincaré inequality)**.** *For $u \in W_0^{1,p}(\Omega)$ there exists a constant C_P, depending only on p and Ω, such that*

$$\|u\|_{L^p(\Omega)} \leq C_P \|\nabla u\|_{L^p(\Omega)}. \tag{4.11}$$

For $p = 2$, the space $W^{1,p}(\Omega)$ is also a Hilbert space, customarily denoted $H^k(\Omega) = W^{k,2}(\Omega)$. This space has the inner product

$$(u, v)^2_{H^k(\Omega)} = \sum_{|\gamma| \leq k} (D^\gamma u \, D^\gamma v)^2_{L^2(\Omega)}.$$

We again use a subscript zero to indicate the subspace of $H^1(\Omega)$ with zero trace on $\partial\Omega_D$:

$$H_0^1(\Omega) = \{u \in H^1(\Omega) \text{ such that } Tu = 0 \text{ on } \partial\Omega_D\}. \tag{4.12}$$

Next, let us introduce the H-div Sobolev spaces,

$$H(\text{div}; \Omega) = \{\mathbf{u} \in (L^2(\Omega))^d \text{ such that } \nabla \cdot \mathbf{u} \in L^2(\Omega)\}.$$

This is a Hilbert space with inner product

$$(\mathbf{u}, \mathbf{v})^2_{H(\text{div};\Omega)} = (\mathbf{u}, \mathbf{v})^2_{L^2(\Omega)} + (\nabla \cdot \mathbf{u}, \nabla \cdot \mathbf{v})^2_{L^2(\Omega)}.$$

We denote by $H_0(\text{div}; \Omega)$ the subspace of $H(\text{div}; \Omega)$ with zero normal trace:

$$H_0(\text{div}; \Omega) = \{\mathbf{u} \in H(\text{div}; \Omega) \text{ such that } \mathbf{u} \cdot \mathbf{n} = 0\}, \tag{4.13}$$

where $\mathbf{u} \cdot \mathbf{n}$ is taken in the trace sense.

Remark 4.1.4. A word of caution is in order with respect to the trace of functions in $H(\text{div}; \Omega)$. The norm induced by this space is weaker than that of $H^1(\Omega)$. For this reason, the space $\mathbf{u} \in H(\text{div}; \Omega)$ does not admit traces in the sense Definition 4.1.2. Instead, the space admits a normal trace $\mathbf{u} \cdot \mathbf{n}|_{\partial\Omega}$. The normal trace does not generally belong to $L^2(\partial\Omega)$; instead, it belongs to the dual of the fractional-order Sobolev space $H^{\frac{1}{2}}(\partial\Omega)$ [13, Lemma 2.1.1]. In the subsequent chapters, this will not be a problem as we assume homogeneous boundary conditions.

Finally, let us introduce the concept of a dual space. For a given function space V, we define its dual space V^* as the space of linear, continuous functionals acting on V. This is a normed space, with its norm given by

$$\|u\|_{V^*} = \sup_{v \in V \setminus \{0\}} \frac{\langle u, v \rangle_{V^* \times V}}{\|v\|_V}, \tag{4.14}$$

with angled brackets denoting the duality pairing.

4.2 Weak Solutions of the Poisson Equation

With the Sobolev spaces defined, we are now ready to formulate two different variational formulations of the Poisson equation. The section is structured as follows. We begin by deriving its primal variational formulation in Section 4.2.1. With the help of the Lax-Milgram Lemma, we are then able to prove the existence of a solution belonging to $p \in H^1(\Omega)$. Next, we derive the mixed variational formulation of the problem in Section 4.3.2. Using the Ladyzhenskaya–Babuška–Brezzi (LBB) theorem, we then prove the existence of a solution in the space $(p, \mathbf{q}) \in L^2(\Omega) \times H(\mathrm{div}; \Omega)$.

4.2.1 Primal formulation

Let us first consider the primal variational formulation of (4.1a)-(4.1d). In this formulation, we use the fact that $\mathbf{q} = -\kappa \nabla p$ to eliminate the flux from the system, so that it is formulated solely with respect to p. This yields the following set of equations:

$$\nabla \cdot (-\kappa \nabla p) = f \qquad \text{in } \Omega, \tag{4.15a}$$

$$p = 0 \qquad \text{on } \partial\Omega_D, \tag{4.15b}$$

$$\kappa \nabla p \cdot \mathbf{n} = 0 \qquad \text{on } \partial\Omega_N. \tag{4.15c}$$

Next, we multiply (4.15a) with a test function $v \in H_0^1(\Omega)$ and integrate by parts on the left-hand side. Using the notation $(\cdot, \cdot)_\Omega = (\cdot, \cdot)_{L^2(\Omega)}$, this yields

$$(\nabla \cdot (-\kappa \nabla p), v)_\Omega = (\kappa \nabla p, \nabla v)_\Omega - (\kappa \nabla p \cdot \mathbf{n}, v)_{\partial\Omega_D} - (\kappa \nabla p \cdot \mathbf{n}, v)_{\partial\Omega_N}. \tag{4.16}$$

Using then that $v = 0$ on $\partial\Omega_D$ and $\kappa \nabla p \cdot \mathbf{n} = 0$ on $\partial\Omega_N$, the last two terms on the right-hand side of (4.16) vanish, yielding simply

$$(\kappa \nabla p, \nabla v)_\Omega = (f, v)_\Omega. \tag{4.17}$$

Let now $a(p, v) = (\kappa \nabla p, \nabla v)$ and $L(v) = (f, v)_\Omega$. The primal variational formulation of (4.1a)-(4.1d) then reads:

Find $p \in H_0^1(\Omega)$ such that

$$a(p, v) = L(v) \qquad \text{for all } v \in H_0^1(\Omega). \tag{4.18}$$

The solution p of (4.18) is referred to as a weak solution of (4.1a)-(4.1d) as it only solves this problem in the variational sense. The Neumann boundary condition $\kappa \nabla p \cdot \mathbf{n} = 0$ on

$\partial\Omega_N$ enters as a *natural boundary condition*, in the sense that it appears in the variational formulation and is therefore naturally included in the system of equations. The Dirichlet boundary condition $p = 0$ on $\partial\Omega_D$, contrarily, enters as an *essential boundary condition* that has to be explicitly prescribed to the function space $H_0^1(\Omega)$.

The variational formulation (4.18) makes it possible to prove, in a straightforward manner, the existence of a weak solution p. The proof is based on an application of the famous Lax-Milgram Lemma:

Lemma 4.2.1 (Lax-Milgram)**.** *Let V be a Hilbert space, $a : V \times V \to \mathbb{R}$ a continuous and coercive bilinear form, and $L : V \to \mathbb{R}$ a continuous linear form. Then there exists $p \in V$ solving the variational problem*

$$a(p, v) = L(v) \quad \text{for all } v \in V. \tag{4.19}$$

Theorem 4.2.2. *Let $f \in L^2(\Omega)$ and $\kappa \in L^\infty(\Omega)$ be strictly positive. Then there exists $p \in H_0^1(\Omega)$ solving* (4.18)*.*

Proof. Let $V = H_0^1(\Omega)$, $a(p, v) = (\nabla p, \nabla v)$ and $L(v) = (\kappa\nabla p, \nabla v)_\Omega$. The proof consists of verifying the assumptions of the Lax-Milgram Lemma. By the linearity of the gradient, a is clearly bilinear. By Cauchy-Schwarz (4.5), we know that

$$\begin{aligned} a(p, v) &= (\kappa\nabla p, \nabla v)_\Omega \\ &\leq \|\kappa\|_{L^\infty(\Omega)} \|\nabla p\|_{L^2(\Omega)} \|\nabla v\|_{L^2(\Omega)} \\ &\leq \|\kappa\|_{L^\infty(\Omega)} \|p\|_{H_0^1(\Omega)} \|v\|_{H_0^1(\Omega)}, \end{aligned} \tag{4.20}$$

and

$$\begin{aligned} L(v) &= (f, v)_\Omega \\ &\leq \|f\|_{L^2(\Omega)} \|v\|_{L^2(\Omega)} \\ &\leq \|f\|_{L^2(\Omega)} \|v\|_{H_0^1(\Omega)}. \end{aligned} \tag{4.21}$$

Thus, a and L are continuous. By the Poincaré inequality (4.11),

$$\begin{aligned} a(p, p) &= (\nabla p, \nabla p)_\Omega \\ &= \frac{1}{2}\|\nabla p\|_{L^2(\Omega)}^2 + \frac{1}{2}\|\nabla p\|_{L^2(\Omega)}^2 \\ &\geq \frac{1}{2C_P}\|p\|_{L^2(\Omega)}^2 + \frac{1}{2}\|\nabla p\|_{L^2(\Omega)}^2 \\ &\geq \frac{1}{2}\min(1, \frac{1}{C_P})\|p\|_{H_0^1(\Omega)}^2 \end{aligned} \tag{4.22}$$

and a is coercive. □

Finally, let us note that in some cases, the solution p enjoys higher regularity than what was found in the previous theorem. For the sake of simplicity, we assume here that $\partial\Omega_N = \emptyset$ to avoid having mixed boundary conditions. From [28, Section 6.3, Theorem 5], we have the following result:

Theorem 4.2.3 (Lifting theorem)**.** *Let $\partial\Omega_N = \emptyset$. For $f \in L^2(\Omega)$ and $\kappa \in W^{1,\infty}(\Omega)$, there then exists $p \in H_0^2(\Omega)$ solving* (4.18) *satisfying*

$$\|p\|_{H_0^2(\Omega)} \leq C_L \|f\|_{L^2(\Omega)} \tag{4.23}$$

for some constant $C_L > 0$.

4.2.2 Mixed formulation

Next, let us consider the mixed variational formulation of (4.1a)-(4.1d), where the name mixed refers to the fact that we keep the flux $\mathbf{q}$ as a variable. First, let us multiply (4.1a) with a test function $\mathbf{v} \in H_0(\mathrm{div};\Omega)$ and (4.1b) with a test function $\theta \in L^2(\Omega)$:

$$(\kappa^{-1}\mathbf{q},\mathbf{v})_\Omega - (\nabla\cdot\mathbf{v},p)_\Omega = -(p,\mathbf{v}\cdot\mathbf{n})_{\partial\Omega} \qquad \text{for all } \mathbf{v}\in H_0(\mathrm{div};\Omega), \tag{4.24a}$$

$$(\nabla\cdot\mathbf{q},\theta)_\Omega = (f,\theta)_\Omega \qquad \text{for all } \theta\in L^2(\Omega). \tag{4.24b}$$

Note now that $p=0$ on $\partial\Omega_D$ and $\mathbf{v}\cdot\mathbf{n}=0$ on $\partial\Omega_N$, meaning that $(p,\mathbf{v}\cdot\mathbf{n})_{\partial\Omega}=0$. Setting then $a(\mathbf{q},\mathbf{v})=(\mathbf{q},\mathbf{v})_\Omega$, $b(\mathbf{q},\theta)=-(\nabla\cdot\mathbf{q},\theta)_\Omega$ and $L(\theta)=(f,\theta)_\Omega$, we arrive at the following mixed variational formulation of (4.1a)-(4.1d):

Find $(p,\mathbf{q})\in L^2(\Omega)\times H_0(\mathrm{div};\Omega)$ such that

$$a(\mathbf{q},\mathbf{v}) + b(\mathbf{v},p) = 0 \qquad \text{for all } \mathbf{v}\in H_0(\mathrm{div};\Omega), \tag{4.25a}$$

$$b(\mathbf{q},\theta) = L(\theta) \qquad \text{for all } \theta\in L^2(\Omega). \tag{4.25b}$$

Note that contrary to the variational formulation (4.18), the boundary condition on the pressure enters as a *natural boundary condition*, while the boundary condition on the flux enters as an *essential boundary condition*. It thus has to be prescribed in the function space.

As in the previous section, the variational formulation makes it straightforward to prove the existence of a solution. This time, the proof relies on the LBB Theorem for saddle point problems:

Theorem 4.2.4 (LBB Theorem)**.** *Let X and M be Hilbert spaces, and assume we are given the two continuous bilinear forms $a : X\times X\to\mathbb{R}$ and $b : X\times M\to\mathbb{R}$, and the two continuous linear forms $F : X\to\mathbb{R}$ and $L : M\to\mathbb{R}$. Let K denote the kernel space of b, defined as*

$$K = \{v\in X : b(v,p) = 0 \text{ for all } p\in M\}.$$

Then there exists $(\mathbf{q},p)\in X\times M$ solving the following saddle point problem

$$a(q,v) + b(p,v) = F(v) \text{ for all } v\in X, \tag{4.26a}$$

$$b(q,\theta) = L(\theta) \text{ for all } \theta\in M, \tag{4.26b}$$

given that a is continuous on the kernel of b, i.e. there exists $C>0$ such that

$$a(v,v)\geq C\|v\|_X^2 \text{ for all } v\in K, \tag{4.27}$$

and b satisfies the following inf-sup condition: There exists $C>0$

$$\sup_{v\in X\setminus\{0\}} \frac{b(v,p)}{\|v\|_X} \geq C\|p\|_M \text{ for all } p\in M. \tag{4.28}$$

Here, the inf-sup condition is often referred to as a *compatibility condition* for the spaces X and M.

The following theorem guarantees the existence of a solution to the mixed problem. The proof relies on an application of Theorem 4.2.3. To avoid the case of mixed boundary conditions, we therefore restrict our attention to the case $\partial\Omega_N=\emptyset$.

Theorem 4.2.5. *Let $\partial\Omega_N = \emptyset$. Let $f \in L^2(\Omega)$ and $\kappa \in L^\infty(\Omega)$ be strictly positive. Then there exists $(p, \mathbf{q}) \in L^2(\Omega) \times H(div; \Omega)$ solving* (4.26a)-(4.26b).

Proof. Take $X = H(\mathrm{div}; \Omega)$ and $M = L^2(\Omega)$, and $a(\mathbf{q}, \mathbf{v}) = (\mathbf{q}, \mathbf{v})_\Omega$, $b(\mathbf{v}, p) = -(\nabla \cdot \mathbf{v}, p)_\Omega$, $F(\mathbf{v}) = 0$ and $L(\theta) = (f, \theta)_\Omega$. The proof then consists of verifying the assumptions of the LBB Theorem. As in the proof of Theorem 4.2.2, the continuity of a, b and L follow by straightforward application of Cauchy-Schwarz (4.5).

To show that a is also coercive on the kernel of b, consider a fixed $\mathbf{v} \in K$. Setting $p = \nabla \cdot \mathbf{v} \in L^2(\Omega)$, we have

$$b(\mathbf{v}, p) = -(\nabla \cdot \mathbf{v}, \nabla \cdot \mathbf{v})_\Omega = -\|\nabla \cdot \mathbf{v}\|^2_{L^2(\Omega)}, \tag{4.29}$$

meaning that $\nabla \cdot \mathbf{v} = 0$ for all $\mathbf{v} \in K$. Thus,

$$a(\mathbf{q}, \mathbf{q}) = (\mathbf{q}, \mathbf{q})_\Omega = \|\mathbf{q}\|^2_{L^2(\Omega)} = \|\mathbf{q}\|^2_{L^2(\Omega)} + \|\nabla \cdot \mathbf{q}\|^2_{L^2(\Omega)} = \|\mathbf{q}\|^2_{H(\mathrm{div};\Omega)}, \tag{4.30}$$

and coercivity thus holds with $C = 1$.

Finally, let us show that the inf-sup condition holds. The proof works by fixing p in M and then finding $\mathbf{v}_p \in H(\mathrm{div}; \Omega)$ solving $\nabla \cdot \mathbf{v}_p = p$. Letting $\mathbf{v}_p = \nabla\xi$, we see that this reduces to solving $\Delta\xi = p$. As $p \in L^2(\Omega)$, by Theorem 4.2.3, a solution $\xi \in H^2(\Omega)$ exists satisfying

$$\|\xi\|^2_{H^2(\Omega)} = \|\xi\|^2_{L^2(\Omega)} + \|\mathbf{v}_p\|^2_{L^2(\Omega)} + \|\nabla \cdot \mathbf{v}_p\|^2_{L^2(\Omega)} \leq C_L \|p\|^2_{L^2(\Omega)} \tag{4.31}$$

for some $C_L > 0$. It follows that

$$\|\mathbf{v}_p\|^2_{H(\mathrm{div};\Omega)} = \|\mathbf{v}_p\|^2_{L^2(\Omega)} + \|\nabla \cdot \mathbf{v}_p\|^2_{L^2(\Omega)} \leq C_L^2 \|p\|^2_{L^2(\Omega)}. \tag{4.32}$$

Moreover, $b(\mathbf{v}_p, p) = (p, p)_\Omega = \|p\|^2_{L^2(\Omega)}$. Thus, we have

$$\sup_{\mathbf{v} \in H(\mathrm{div};\Omega)\setminus\{0\}} \frac{b(\mathbf{v}, p)}{\|\mathbf{v}\|_{H(\mathrm{div};\Omega)}} \geq \frac{b(\mathbf{v}_p, p)}{\|\mathbf{v}_p\|_{H(\mathrm{div};\Omega)}} \geq \frac{\|p\|^2_{L^2(\Omega)}}{C_L \|p\|_{L^2(\Omega)}} \geq \frac{1}{C_L} \|p\|_{L^2(\Omega)} \tag{4.33}$$

meaning that (4.28) holds with the constant $C = 1/C_L$. □

4.3 Finite Element Methods

In the previous section, we proved the existence of a solution to the primal and mixed variational formulations of the Poisson equation. In this section, we will show how these variational formulations can be discretized, and the result used to obtain an approximate solution. For the discretization method, we focus on two finite element methods. The first of these will be the primal finite element method, which is based on the primal variational formulation from Section 4.2.1. This is in many ways the classical finite element formulation of the problem. With this in mind, we will sometimes refer to it without the prefix primal. The second method we consider is the mixed finite element method, which is based on the mixed variational formulation from Section 4.2.2.

4.3.1 The primal finite element method

Assume for the sake of simplicity that Ω is polyhedral. Let $\mathcal{T}_h$ denote a conforming subdivision of this domain with mesh size h, where $h = \max_{T\in\mathcal{T}_h} h_T$ with h_T denoting the diameter of an element $T \in \mathcal{T}_h$. The mesh is taken quasi-uniform; i.e., letting ρ_T be the maximum diameter of a ball inscribed in element T, there exists a constant $C > 0$ such that

$$\frac{h_T}{\rho_T} \leq C \quad \text{for all } T \in \mathcal{T}_h.$$

For $k \geq 1$ integer-valued, let $\mathbb{CG}_h^k$ denote the continuous Lagrange finite element space:

$$\mathbb{CG}_h^k := \{v_h \in C^0(\Omega) : v_h|_T \in P^k(T) \text{ for all } T \in \mathcal{T}_h,\ v_h|_{\partial\Omega} = 0\}, \tag{4.34}$$

where $P^k(T)$ denotes the space of polynomials of degree k on T. The discrete formulation of (4.18) then reads:

Find $p_h \in \mathbb{CG}_h^k$ such that

$$a(p_h, v_h) = L(v_h) \quad \text{for all } v_h \in \mathbb{CG}_h^k. \tag{4.35}$$

We refer to (4.35) as the Galerkin finite element approximation of (4.18). For a domain Ω with smooth boundary $\partial\Omega$, an H^1-coercive form a and right-hand side satisfying $f \in H^k(\Omega)$ for some k, this approximation exhibits optimal order convergence [15, Theorem 5.4.4]

Theorem 4.3.1. *Let $\mathbb{CG}_h^k$ be the finite element space (4.34), $p \in H^{k+1}(\Omega)$ the weak solution of (4.15a)-(4.15c) and p_h the Galerkin finite element approximation defined by (4.35). The approximation error can then be bounded by*

$$\|p - p_h\|_{H^1(\Omega)} \leq Ch^k \|p - p_h\|_{H^{k+1}(\Omega)}. \tag{4.36}$$

If $p \in H^2(\Omega)$, we further have the estimate

$$\|p - p_h\|_{L^2(\Omega)} \leq Ch^2 \|p - p_h\|_{H^2(\Omega)}. \tag{4.37}$$

4.3.2 The mixed finite element method

Next, let us define the mixed finite element method. Recall that P^k denotes the space of polynomials of degree k. For $k \geq 1$, the solution to (4.25a)-(4.25b) is approximated using discontinuous piecewise-polynomial finite elements for the pressure and $\mathbf{H}^{\text{div}}$-conforming Raviart-Thomas elements for the velocity, i.e.

$$\mathbb{DG}_h^k := \{w_h \in L^2(\Omega) : w_h|_K \in P^{k-1}(T) \quad \forall T \in \mathcal{T}_h\}, \tag{4.38a}$$
$$\mathbb{RT}_h^k := \{\mathbf{w}_h \in L^2(\Omega) : \mathbf{w}_h|_T \in (P^{k-1}(T))^d \oplus \mathbf{x}P^{k-1}(T) \quad \forall T \in \mathcal{T}_h\}. \tag{4.38b}$$

The discrete formulation of (4.25a)-(4.25b) then consists of finding $(\mathbf{q}_h, p_h) \in \mathbb{RT}_h^k \times \mathbb{DG}_h^k$ s.t.

$$(\kappa^{-1}\mathbf{q}_h, \mathbf{v}_h)_\Omega - (\nabla \cdot \mathbf{v}_h, p_h)_\Omega = 0 \tag{4.39a}$$
$$(\nabla \cdot \mathbf{q}_h, \theta_h) = (f, \theta_h)_\Omega \tag{4.39b}$$

for all $(\mathbf{v}, \theta_h) \in \mathbb{RT}_h^k \times \mathbb{DG}_h^k$. We refer to (4.39a)-(4.39b) as the mixed finite element approximation of (4.25a)-(4.25b).

From [15, Chapter 12.4], we have the following convergence rates for the mixed finite element method:

Theorem 4.3.2. *Let $\mathbb{DG}_h^k$ and $\mathbb{RT}_h^k$ be the spaces defined in (4.38a)-(4.38b), $(p, \mathbf{q}) \in H^k(\Omega) \times (H^k(\Omega))^d$ the weak solution of (4.25a)-(4.25b) and $(p_h, \mathbf{q}_h)$ the solution of (4.39a)-(4.39b). For $1 \leq k \leq 3$, the error of the mixed finite element approximation can be bounded by*

$$\|p - p_h\|_{L^2(\Omega)} + \|\mathbf{q} - \mathbf{q}_h\|_{H(\mathrm{div};\Omega)} \leq Ch^k \left(\|p\|_{H^k(\Omega)} + \|\mathbf{q}\|_{(H^{k+1}(\Omega))^d} \right). \tag{4.40}$$

For lowest-order elements $\mathbb{DG}_h^1 \times \mathbb{RT}_h^1$, one further has [14, Chapter 3.5]

$$\|p_r - p_h\|_{L^2(\Omega)} + \|\mathbf{q} - \mathbf{q}_h\|_{H(\mathrm{div};\Omega)} \leq Ch \left(\|p\|_{H^1(\Omega)} + \|\mathbf{q}\|_{(H^1(\Omega))^d} \right). \tag{4.41}$$

Chapter 5

Elliptic Equations with Line Sources

In the previous section, we considered the Poisson equation with a right-hand side belonging to $L^2(\Omega)$, and showed how the variational framework for PDEs can be used to

1. prove the existence of weak solutions,
2. define suitable discretization methods.

In this section, we will show this same framework can be extended to the case where the right-hand side is concentrated on a line source.

Recall first the geometrical setting of Section 3.1; let $\Omega \subset \mathbb{R}^3$ denote a bounded convex 3D domain with smooth boundary $\partial\Omega$, and Λ be a smooth 1D curve with the parametrization $\boldsymbol{\lambda} = [\xi(s), \tau(s), \zeta(s)]$. We consider then the following Poisson equation:

$$\mathbf{q} + \kappa \nabla p = 0 \qquad \text{in } \Omega, \tag{5.1a}$$

$$\nabla \cdot \mathbf{q} = f\, \delta_\Lambda \qquad \text{in } \Omega, \tag{5.1b}$$

$$p = 0 \qquad \text{on } \partial\Omega, \tag{5.1c}$$

where the right-hand side is a Dirac line source δ_Λ of intensity $f \in C^0(\bar{\Omega})$, and $\kappa \in L^\infty(\Omega)$ is a strictly positive permeability. For the sake of notational simplicity, we consider here only the homogeneous Dirichlet boundary conditions (5.1c). More general boundary conditions can be handled as was presented in Chapter 4.

The section is structured as follows. We begin in Section 5.1 by defining the weighted Sobolev spaces in which one can look for solutions to (5.1a)-(5.1c). Next, we consider the variational formulation of the problem. In Section 5.2.1, we summarize D'Angelo and Quarteroni's work regarding its primal formulation [23; 22]. In Section 5.2.2, we then summarize the results from Paper B regarding the mixed formulation.

The finite element discretization of the problem is discussed in Section 5.3. The standard finite element approximation is given in Section 5.3.1, together with weighted and unweighted error estimates derived by D'Angelo in [22]. The mixed finite element approximation of the problem is given in Section 5.3.2, together with weighted and unweighted error estimates obtained numerically in Paper B. In particular, we show how this approximation fails to converge in the standard sense.

With the failure of convergence in mind, we proceed in Section 5.4 to present the solution splitting and singularity removal method proposed in Papers A and B. The solution splitting recasts (5.1a)-(5.1c) as an elliptic problem with right-hand side belonging to $L^2(\Omega)$. As such, its regularity and approximation properties follow from the theory introduced in Chapter 4.

5.1 Weighted Sobolev Spaces

As we will see, the line source in (5.1b) induces a logarithmic type singularity in p; it therefore, fails to belong to $H^1(\Omega)$. To deal with this, we now introduce the concept of a weighted Sobolev space.

Let $r(\mathbf{x}) := \text{dist}(\mathbf{x}, \Lambda)$ denote the Euclidean distance between a point $\mathbf{x} \in \Omega$ and Λ. Next, let $\alpha \in \mathbb{R}$, and define the measure $d\mu_\alpha(\mathbf{x}) = r^{2\alpha} dx$. Letting σ denote the σ-algebra of measurable sets on Ω, the triplet $(\Omega, \sigma, \mu_\alpha)$ then defines an abstract measure space. Next, we define $L^2(\Omega; d\mu_\alpha)$ as the space of square-integrable functions on $(\Omega, \sigma, \mu_\alpha)$, i.e.,

$$L^2(\Omega, d\mu_\alpha) := \left\{ u : \Omega \to \mathbb{R} \text{ such that } \int_\Omega u(\mathbf{x})^2 \mathrm{d}\mu_\alpha < \infty \right\}. \tag{5.2}$$

Equivalently, this space can be defined using the standard Lebesgue measure as

$$L^2(\Omega, d\mu_\alpha) := L^2_\alpha(\Omega) = \{ u : \Omega \to \mathbb{R} \text{ such that } r^\alpha u \in L^2(\Omega) \}. \tag{5.3}$$

The space $L^2_\alpha(\Omega)$ is a Hilbert space [59] equipped with the inner product

$$(u, v)_{L^2_\alpha(\Omega)} := \int_\Omega uv \, \mathrm{d}\mu_\alpha = \int_\Omega r^\alpha u \, r^\alpha v \, \mathrm{d}x.$$

The value of α controls how singular a function $u \in L^2_\alpha(\Omega)$ is allowed to be. For $\alpha_1 < \alpha_2$, one has $L^2_{\alpha_1}(\Omega) \subset L^2_{\alpha_2}(\Omega)$; i.e., a larger value for α results in a larger space $L^2_\alpha(\Omega)$. By an application of Cauchy-Schwarz, we obtain

$$|(u, v)| = |(r^\alpha u, r^{-\alpha} v)| \leq \|u\|_{L^2_\alpha(\Omega)} \|v\|_{L^2_{-\alpha}(\Omega)} \quad \forall\, u \in L^2_\alpha(\Omega),\, v \in L^2_{-\alpha}(\Omega), \tag{5.4}$$

meaning that the spaces $L^2_\alpha(\Omega)$ and $L^2_{-\alpha}(\Omega)$ are dual to each other.

With the space $L^2_\alpha(\Omega)$ defined, a weighted Sobolev space $H^k_\alpha(\Omega; dx) = H^k(\Omega; d\mu_\alpha)$ can now be constructed as [52; 10]

$$H^k_\alpha(\Omega) = \{ u \in L^2_\alpha(\Omega) : D^\gamma u \in L^2_\alpha(\Omega) \text{ for } |\gamma| \leq k \}, \tag{5.5}$$

where the weak derivative $D^\gamma u$ is from now on interpreted in the sense of distributions:

$$\int_\Omega u D^\gamma \phi \, \mathrm{d}x = (-1)^{|\gamma|} \int_\Omega D^\gamma u \phi \, \mathrm{d}x \quad \text{for all } \phi \in C^\infty_c(\Omega). \tag{5.6}$$

This is a Hilbert space equipped with the inner product

$$(u, v)^2_{H^k_\alpha(\Omega)} = \sum_{|\gamma| \leq k} (D^\gamma u, D^\gamma v)^2_{L^2_\alpha(\Omega)},$$

which generates the norm

$$\|u\|^2_{H^k_\alpha(\Omega)} = \sum_{|\gamma| \leq k} \|D^\gamma u\|^2_{L^2_\alpha(\Omega)}.$$

In this thesis, we will use mainly the space $H^1_\alpha(\Omega)$; the norm can then be stated more simply as

$$\|u\|^2_{H^1_\alpha(\Omega)} = \|u\|^2_{L^2_\alpha(\Omega)} + \|\nabla u\|^2_{L^2_\alpha(\Omega)}. \tag{5.7}$$

The properties of $H^k_\alpha(\Omega)$ naturally depend on the choice of weight. For $\alpha \in (-1, 1)$, the weight r^α belongs to the *Muckenhoupt* class of weights. One then has the imbedding $L^2_\alpha(\Omega) \hookrightarrow L^1(\Omega)$ [82]. In this case, the weak derivatives can be interpreted in the sense of (4.7). One further has density of smooth functions in the same sense as Theorem 4.1.1. Moreover, the space admits a weighted version of the Poincaré inequality [41]:

$$\|u\|_{L^2_{\alpha-1}(\Omega)} \leq C_\alpha \|\nabla u\|_{L^2_\alpha(\Omega)} \quad \forall\, u \in H^1_\alpha(\Omega),\, u_{|\partial\Omega} = 0,\, \alpha \in (-1, 1), \tag{5.8}$$

with the constant C_α depending on α.

The space $H^k_\alpha(\Omega)$ is often referred to as non-homogeneous weighted Sobolev space, as the weight r^α is not adjusted to account for the regularity loss associated with taking a derivative. In this work, we shall work mainly with homogeneous weighted Sobolev spaces of the type [50; 45]

$$V^k_\alpha(\Omega) = \{D^\gamma u \in L^2_{\alpha+|\gamma|-k}(\Omega), |\gamma| \leq k\}. \tag{5.9}$$

Notice that the weighting-factor is here increased together with the order of the derivative. The space $V^k_\alpha(\Omega)$ is a Hilbert space equipped with the inner product

$$(u, v)_{V^k_\alpha(\Omega)} = \sum_{|\gamma|\leq k} (D^\gamma u, D^\gamma v)_{L^2_{\alpha+|\gamma|-k}(\Omega)},$$

which generates the norm

$$\|u\|^2_{V^k_\alpha(\Omega)} = \sum_{|\gamma|\leq k} \|D^\gamma u\|^2_{L^2_{\alpha+|\gamma|-k}(\Omega)}.$$

For the case $k = 1$, this can be more simply stated as

$$\|u\|^2_{V^2_\alpha(\Omega)} = \|u\|^2_{L^2_{\alpha-1}(\Omega)} + \|\nabla u\|^2_{L^2_\alpha(\Omega)}.$$

The $H^1_\alpha(\Omega)$ and $V^1_\alpha(\Omega)$ norms are equivalent; this follows from the following inequality [10]:

$$\|u\|_{L^2_{\alpha-1}(\Omega)} \leq C_\alpha \|u\|_{H^1_\alpha(\Omega)}. \tag{5.10}$$

Finally, let us define the weighted H-div type space $V_{\alpha+1}(\mathrm{div}; \Omega)$:

$$V_{\alpha+1}(\mathrm{div}; \Omega) = \{\mathbf{q} \in (L^2_\alpha(\Omega))^3 : \nabla \cdot \mathbf{q} \in L^2_{\alpha+1}(\Omega)\}.$$

This is a Hilbert space equipped with the inner product

$$(\mathbf{q}, \mathbf{v})_{V_{\alpha+1}(\Omega;\mathrm{div})} = (\mathbf{q}, \mathbf{v})_{L^2_\alpha(\Omega)} + (\nabla \cdot \mathbf{q}, \nabla \cdot \mathbf{v})_{L^2_{\alpha+1}(\Omega)}.$$

Note that elements of this space have a weak divergence $\nabla \cdot \mathbf{q} \in L_{\alpha+1}(\Omega)$, which is non-Muckenhoupt for $\alpha > 0$. Consequently, the weak divergence of functions in $V_{\alpha+1}(\mathrm{div}; \Omega)$ may not belong to $L^1(\Omega)$.

Finally, let us note that the L^2 and L^2_α-norms are equivalent away from Λ. As the curve Λ is further contained in the interior of Ω, the spaces $H^k_\alpha(\Omega)$, $V^k_\alpha(\Omega)$ and $V_\alpha(\mathrm{div}; \Omega)$ admit traces in the same sense as what was defined in Definition 4.1.2.

5.2 Weak Solutions

5.2.1 Primal formulation

Let us first derive the primal variational formulation of (5.1a)-(5.1c). As in Section 4.2.1, we start by using the fact that $\mathbf{q} = -\kappa\nabla p$ to eliminate the flux from the system. With the homogeneous Dirichlet condition (5.1c) in mind, take

$$W^1_\alpha(\Omega) := \{u \in H^1_\alpha(\Omega) : Tu = 0 \text{ on } \partial\Omega\}. \tag{5.11}$$

Multiplying (5.1a) with a test function $v \in W^1_{-\alpha}$ then yields

$$(\kappa\nabla p, \nabla v)_\Omega = (f\delta_\Lambda, v)_\Omega.$$

Let $a(p,v) := (\kappa\nabla p, \nabla v)_\Omega$ and $L(v) = (f\delta_\Lambda, v)_\Omega$. Interpreting the Dirac line source in the sense of (3.15), one can equivalently set $L(v) = (f, v)_\Lambda$. This yields the following variational formulation:

Find $p \in W^1_\alpha(\Omega)$ such that

$$(\kappa\nabla p, \nabla v)_\Omega = (f, v)_\Lambda \quad \text{for all } v \in W^1_{-\alpha}(\Omega), \tag{5.12}$$

The existence of a solution $p \in W^1_\alpha(\Omega)$ was first proven in [23] using a generalized Lax-Milgram theorem [9]. Let us give a few comments on the proof. Firstly, as the spaces $L^2_\alpha(\Omega)$ and $L^2_{-\alpha}(\Omega)$ are dual to each other, the continuity of a follows by a straightforward application of Cauchy-Schwarz (4.5):

$$\begin{aligned} a(p,v) &= (\kappa r^\alpha \nabla p, r^{-\alpha}\nabla v)_\Omega && (5.13)\\ &\le \|\kappa\|_{L^\infty(\Omega)} \|\nabla p\|_{L^2_\alpha(\Omega)} \|\nabla v\|_{L^2_{-\alpha}(\Omega)}. && (5.14) \end{aligned}$$

The continuity of L follows from the following trace theorem [23, Theorem 4.2]:

Theorem 5.2.1 (Λ-trace operator)**.** *Let $0 < \alpha < 1$. There exists a unique linear continuous trace operator $T_\Lambda : H^1_{-\alpha}(\Omega) \to L^2(\Lambda)$ satisfying*

$$\|Tu\|_{L^2(\Lambda)} \le C\|u\|_{H^1_{-\alpha}(\Omega)} \qquad \textit{for each } u \in H^1_{-\alpha}(\Omega), \tag{5.15a}$$

$$Tu = u|_\Lambda \qquad \textit{for each } u \in H^1_{-\alpha}(\Omega) \cap C^\infty(\Omega). \tag{5.15b}$$

Note that this is not a trivial result, as a function $p \in H^1(\Omega)$ may not have a well defined trace on subdomains with codimension larger than 1.

Lastly, as for the mixed variational formulation considered in Section 4.3.2, the variational formulation (5.12) is formulated using two different function spaces. For this reason, the generalized Lax-Milgram lemma requires showing an inf-sup condition verifying their compatibility. As the constant C_α in (5.8) is not uniformly bounded with respect to α, the proof of this condition requires a rather technical Fourier expansion in order to get uniformly bounded constants. For this reason, an alternate proof was presented in [22], relying on the following Helmholtz decomposition:

Lemma 5.2.2 (Helmholtz decomposition)**.** *Let $\alpha \in (-1,1)$. For each $\mathbf{q} \in (L^2_\alpha(\Omega))^d$, there exists a unique couple $(\boldsymbol{\sigma}, z) \in (L^2_\alpha(\Omega))^d \times W^1_\alpha(\Omega)$ such that*

$$\mathbf{q} = \nabla z + \boldsymbol{\sigma} \quad \text{where } (\boldsymbol{\sigma}, \nabla w) = 0 \quad \text{for all } w \in W^1_\alpha(\Omega) \tag{5.16}$$

with $\|\nabla z\|_{L^2_\alpha(\Omega)} \leq 2\|\mathbf{q}\|_{L^2_\alpha(\Omega)}$ and $\|\boldsymbol{\sigma}\|_{L^2_\alpha(\Omega)} \leq \|\mathbf{q}\|_{L^2_\alpha(\Omega)}$.

Letting $a(\boldsymbol{\sigma}, \boldsymbol{\tau}) = (\boldsymbol{\sigma}, \boldsymbol{\tau})_\Omega$, $b(z, \boldsymbol{\tau}) = (\nabla z, \boldsymbol{\tau})_\Omega$ and $F(\boldsymbol{\tau}) = (\mathbf{q}, \boldsymbol{\tau})_\Omega$, the decomposition (5.16) can be written as: Find $(\boldsymbol{\sigma}, z) \in (L^2_\alpha(\Omega))^d \times W^1_\alpha(\Omega)$

$$a(\boldsymbol{\sigma}, \boldsymbol{\tau}) + b(z, \boldsymbol{\tau}) = F(\boldsymbol{\tau}) \quad \text{for all } \boldsymbol{\tau} \in (L^2_{-\alpha}(\Omega))^d \tag{5.17}$$

$$b(w, \boldsymbol{\sigma}) = 0 \quad \text{for all } w \in W^1_{-\alpha}(\Omega). \tag{5.18}$$

The existence of a solution can then be proved via an application of the following Brezzi-Necas-Babuška (BNB) Theorem [11, Thm 2.6] and [62]:

Theorem 5.2.3 (BNB Theorem)**.** *Let X_i and M_i be real reflexive Banach spaces ($i = 1, 2$). Assume we are given three continuous bilinear forms: $a : X_2 \times X_1 \to \mathbb{R}$, $b_1 : X_1 \times M_1 \to \mathbb{R}$, $b_2 : X_2 \times M_2 \to \mathbb{R}$. For any given $f \in (M_2)^*$ and $g \in (X_1)^*$, we consider the following problem:*

Find $(q, u) \in X_2 \times M_1$ s.t.

$$a(q, v) + b_1(v, u) = \langle g, v \rangle, \tag{5.19a}$$

$$b_2(q, \theta) = L(\theta) \tag{5.19b}$$

for all $(v, \theta) \in X_1 \times M_2$.

Let K_i denote the kernel space of b_i:

$$K_i = \{v \in X_i : b_i(v, u) = 0 \quad \forall\, u \in M_i\}.$$

The problem (5.19a)-(5.19b) then admits a solution $(q, u) \in X_2 \times M_1$ if the following assumptions hold:

Condition (C_0): Weak coercivity of $a(\cdot, \cdot)$: There exists constants $\lambda_1, \lambda_2 > 0$ s.t.

$$\sup_{v \in K_1} \frac{a(q, v)}{\|v\|_{X_1}} \geq \lambda_1 \|q\|_{X_2} \quad \forall\, q \in K_2, \tag{5.20}$$

and

$$\sup_{q \in K_2} \frac{a(q, v)}{\|q\|_{X_1}} \geq \lambda_2 \|v\|_{X_1} \quad \forall\, v \in K_1. \tag{5.21}$$

Condition (C_i) : Inf-sup condition on $b_i(\cdot, \cdot)$ There exists $\lambda_i > 0$ s.t.

$$\sup_{v \in X_i} \frac{b_i(v, u)}{\|v\|_{X_i}} \geq \lambda_i \|u\|_{M_i} \quad \forall\, u \in M_i. \tag{5.22}$$

The same theorem was used in Paper B to prove the existence of a solution to the mixed formulation of (5.1a)-(5.1c). As the proof there uses similar techniques as the proof of 5.2.2, we omit here to give a proof of the latter. To conclude the section, let us instead show how Lemma 5.2.2 can be used to prove the following existence theorem:

Theorem 5.2.4. *Let $f \in C^0(\Omega)$ and $\kappa \in L^\infty(\Omega)$ be strictly positive. There then exists $p \in W^1_\alpha(\Omega)$ solving (5.12).*

Proof. Let $a(p,v) = (\nabla p, \nabla v)_\Omega$, $b_1(\cdot,\cdot) = b_2(\cdot,\cdot) = 0$ and $L(v) = (f,v)_\Lambda$. The proof relies on an application of the BNB Theorem using $X_2 = K_2 = W^1_\alpha(\Omega)$ and $X_1 = K_1 = W^1_{-\alpha}(\Omega)$. By Cauchy-Schwarz and Theorem 5.2.1, a and L are both continuous. It only remains to show the weak coercivity of $a(\cdot,\cdot)$.

To verify (5.20), fix $p \in W^1_\alpha(\Omega)$ and set $\mathbf{q}_p = r^{2\alpha}\nabla p \in (L^2_{-\alpha}(\Omega))^d$. There then exists $\boldsymbol{\sigma}_p \in (L^2_{-\alpha}(\Omega))^d$ and $z_p \in W^1_{-\alpha}(\Omega)$ such that $\mathbf{q}_p = \nabla z_p + \boldsymbol{\sigma}_p$. Consequently,

$$a(p,z_p) = (\nabla p, \nabla z_p)_\Omega = (\nabla p, \mathbf{q})_\Omega = (r^\alpha \nabla p, r^\alpha \nabla p)_\Omega = \|p\|^2_{W^1_\alpha(\Omega)},$$

where we used $(\boldsymbol{\sigma}, \nabla p)_\Omega = 0$ for all $p \in W^1_\alpha(\Omega)$. As $\|z_p\|_{W^1_{-\alpha}(\Omega)} \leq 2\|\mathbf{q}\|_{W^1_{-\alpha}(\Omega)} = 2\|p\|_{W^1_\alpha(\Omega)}$, it follows that

$$\sup_{v \in W^1_{-\alpha}(\Omega)} \frac{a(p,v)}{\|v\|_{W^1_{-\alpha}(\Omega)}} \geq \frac{a(p,z_p)}{\|z_p\|_{W^1_{-\alpha}(\Omega)}} = \frac{\|p\|^2_{W^1_\alpha(\Omega)}}{\|z_p\|_{W^1_{-\alpha}(\Omega)}} \geq C\|p\|_{W^1_\alpha(\Omega)}.$$

and (5.20) holds with $\lambda_1 = 1/2$. (5.21) can be shown by switching the sign of α and repeating the argument with $(p,\mathbf{q})$ switched with $(\theta,\mathbf{v})$. □

5.2.2 Mixed formulation

Let us now consider the mixed variational formulation of (5.1a)-(5.1c): Find $(p,\mathbf{q}) \in L^2_{\alpha-1}(\Omega) \times V_{\alpha+1}(\mathrm{div};\Omega)$ such that

$$(\kappa^{-1}\mathbf{q}, \mathbf{v}) - (p, \nabla\cdot\mathbf{v}) = 0 \qquad \forall\, \mathbf{v} \in V_{-\alpha+1}(\mathrm{div};\Omega), \tag{5.23a}$$

$$(\nabla\cdot\mathbf{q}, \theta) = (f\delta_\Lambda, \theta)_\Omega \qquad \forall\, \theta \in L^2_{-\alpha-1}(\Omega), \tag{5.23b}$$

where δ_Λ is defined as the limit of the series of nascent Dirac delta functions (3.14). The main result of this section is the following existence theorem:

Theorem 5.2.5. *Let $f \in C^0(\bar{\Omega})$ and $\kappa \in L^\infty(\mathbb{R})$. For $\alpha > 0$, there then exists $(p,\mathbf{q}) \in L^2_{\alpha-1}(\Omega) \times V_{\alpha+1}(\mathrm{div};\Omega)$ solving (5.23a)-(5.23b).*

A proof of Theorem 5.2.5 is given in Paper B. The proof itself relies on two lemmas, the first of which guarantees a solution to (5.23a)-(5.23b) for a source term $g \in L^2_{\alpha+1}(\Omega)$ with $\alpha \in \mathbb{R}$:

Lemma 5.2.6. *Let $g \in L^2_{\alpha+1}(\Omega)$. Under the assumptions of Theorem 5.2.5, there then exists $(p,\mathbf{q}) \in L^2_{\alpha-1}(\Omega) \times V_{\alpha+1}(\mathrm{div};\Omega)$ solving*

$$(\kappa^{-1}\mathbf{q}, \mathbf{v}) - (\nabla\cdot\mathbf{v}, p) = 0 \qquad \forall\, \mathbf{v} \in V_{-\alpha+1}(\mathrm{div};\Omega), \tag{5.24a}$$

$$(\nabla\cdot\mathbf{q}, \theta) = (g, \theta) \qquad \forall\, \theta \in L^2_{-\alpha-1}(\Omega). \tag{5.24b}$$

The proof is by verification of the assumptions of Theorem 5.2.3. The second lemma addresses the line source:

Lemma 5.2.7. *For $\alpha > 0$ and δ_Λ defined in the limit sense (3.14), one has $\delta_\Lambda \in L^2_{\alpha+1}(\Omega)$.*

The proof of this lemma is by showing that the sequence δ^ϵ_Λ is Cauchy in $L^2_{\alpha+1}(\Omega)$ (which is complete) and thus converges in $L^2_{\alpha+1}(\Omega)$. It follows that the line source δ_Λ belongs to $L^2_{\alpha+1}(\Omega)$.

5.3 Finite Element Methods

In the previous section, we gave existence theorems for the solution to the primal and mixed variational formulations of the line source problem (5.1a)-(5.1c). With these in hand, we are now ready to introduce discretization methods with which the solution can be approximated. As in Section 4.3, we restrict our attention to the standard and mixed finite element method.

5.3.1 The primal finite element method

Let Ω, $\mathcal{T}_h$ and $\mathbb{CG}_h^k$ be as in Section 4.3.1. The discrete weak formulation of (5.12) reads: Find $p_h \in \mathbb{CG}_h^k$ such that

$$a(p_h, v_h) = L(v_h) \text{ for all } v_h \in \mathbb{CG}_h^k, \tag{5.25}$$

where $a(p_h, v_h) = (\nabla p_h, \nabla v_h)_\Omega$ and $L(v_h) = (f, v_h)_\Lambda$. The stability and well-posedness of this formulation was proved in [22]. Therein, D'Angelo also proved the following convergence theorem:

Theorem 5.3.1. *Let $0 < \alpha < 1$, $p \in V_{k+\epsilon}^{k+1}(\Omega)$ solve (4.15a)-(4.15c) for some $\epsilon \in (0, \alpha)$ and $p_h \in \mathbb{CG}_h^k$ solve (5.25). The approximation error can then be bounded by*

$$\|p - p_h\|_{V_\alpha^1(\Omega)} \leq Ch^{\alpha-\epsilon}\|p\|_{V_{k+\epsilon}^{k+1}(\Omega)}. \tag{5.26}$$

As $\epsilon > 0$ is allowed arbitrarily small, it is not noticeable in numerical experiments. Thus, one formally observes $\mathcal{O}(h^\alpha)$ convergence in the V_α^1-norm. In the same work, D'Angelo provided numerical evidence for the following convergence rates:

$$\|p - p_h\|_{L_\alpha^2(\Omega)} = \mathcal{O}(h^{1+\alpha}) \text{ for } 0 \leq \alpha < 1, \tag{5.27}$$

In particular, let us note that this yields convergence of order $\mathcal{O}(h^1)$ in the standard L^2-norm. This is in agreement with the results found in [74] for the 2D point source problem.

Remark 5.3.2. As is evident from these error rates, the singular behaviour of the solution degrades the numerical convergence order. An increase in the polynomial degree k is not seen to improve the convergence rate as the solution is not regular enough to benefit from this. An increase of the weight α is seen to improve the convergence rate, with the convergence rate becoming semi-optimal as $\alpha \to 1$. This can be interpreted as giving up an increasing amount of control of the solution around the line. As $\alpha \to 0$, the convergence rate decreases; in the standard L^2-norm, one observes a rate of only $\mathcal{O}(h^1)$. This is one order lower than the $\mathcal{O}(h^2)$ convergence rate expected for solutions belonging to $H^2(\Omega)$.

Köppl et al. proved that the convergence issues are local to the singularity around the line source [46; 47]. To be more precise, the convergence rates are quasi-optimal (i.e. optimal up to a log factor) with respect to the $\|\cdot\|_{L^2(\Omega\setminus\Sigma_\epsilon)}$-norm for $\epsilon > 0$, where Σ_ϵ is the cylinder of radius ϵ with centreline Λ. This can be interpreted as saying that the line source does not pollute the approximation away from Λ.

In [22], it was shown that quasi-optimal convergence can be retrieved in the entire domain Ω by a suitable grading (i.e. refinement) of the mesh around the line. Again, this was

in agreement with results known for the 2D point source problem [24; 35; 7] and for corner-point problems [6]. Considering, however, the complex structure of a vascular network (as illustrated in Figure 1.2), it is clear that this approach of mesh grading would be computationally intractable for simulations of flow through vascularized tissue.

5.3.2 The mixed finite element

Let Ω, $\mathcal{T}_h$, $\mathbb{DG}_h^k$ and $\mathbb{RT}_h^k$ be as in Section 4.3.2. The discrete weak formulation of (5.23a)-(5.23b) then reads: Find $(p_h, \mathbf{q}_h) \in \mathbb{DG}_h^k \times \mathbb{RT}_h^k$ such that

$$a(\mathbf{q}_h, \mathbf{v}_h) - b(p_h, \mathbf{v}_h) = 0 \qquad \forall\, \mathbf{v}_h \in \mathbb{RT}_h^k, \tag{5.28a}$$

$$b(\theta_h, \mathbf{q}_h) = L(f) \qquad \forall\, \theta_h \in \mathbb{DG}_h^k. \tag{5.28b}$$

where $a(\mathbf{q}_h, \mathbf{v}_h) = (\mathbf{q}_h, \mathbf{v}_h)_\Omega$, $b(p_h, \mathbf{v}_h) = -(p_h, \nabla \cdot \mathbf{v}_h)_\Omega$ and $L(\theta_h) = (f, \theta_h)_\Lambda$. The convergence rates of the line source problem were tested numerically in Paper B. The following convergence rates were observed using $0 < \alpha < 1$:

$$\|p - p_h\|_{L^2_\alpha(\Omega)} = \mathcal{O}(h^1) \qquad \text{for } k = 1, \tag{5.29a}$$

$$\|p - p_h\|_{L^2_\alpha(\Omega)} = \mathcal{O}(h^{1+\alpha}) \qquad \text{for } k = \{2, 3\}, \tag{5.29b}$$

$$\|\mathbf{q} - \mathbf{q}_h\|_{L^2_\alpha(\Omega)} = \mathcal{O}(h^\alpha) \qquad \text{for } k = \{1, 2, 3\}. \tag{5.29c}$$

From Theorem 4.3.2, we know that the $\|p - p_h\|_{L^2_\alpha(\Omega)}$ will converge with optimal order k provided that $p \in H^k(\Omega)$. As p falls just shy of belonging to $H^1(\Omega)$, we therefore observe optimal convergence for $k = 1$. By the same theorem, the flux $\mathbf{q}$ will converge optimally provided it belongs to $(H^2(\Omega))^3$. Note, however, that $\mathbf{q}$ does not even belong to $(L^2(\Omega))^3$. For this reason, the flux cannot converge in the standard L^2-sense.

5.4 Solution Splitting Methods

In the previous sections, we found that the finite element approximation of the line source problem (5.1a)-(5.1c) will converge sub-optimally due to the low regularity of the solution. This was particularly evident for the mixed finite element approximation of the problem, for which the flux fails to converge in the standard L^2-sense.

Given some restrictions on the problem parameters, it was shown in Papers A and B that this issue can be resolved by the formulation of a *singularity removal method*. This method is commonly known for point sources [29, p. 14], where it has been applied in the context of e.g. electromagnetic problems [25; 88] and 2D reservoir models [35].

Assume $\kappa \in W^{2,\infty}(\Omega)$, $f \in H^2(\Lambda) \cap C(\Omega)$ and $\Lambda = \cup_{i=1}^n \Lambda_i$ consists of a collection of (straight) line segments. The singularity removal is based on a splitting of the solution into higher and lower regularity terms. Let us now sketch the main steps involved in formulating such a splitting. Consider the strong formulation of the line source problem with $\kappa = 1$:

$$\mathbf{q} + \nabla p = 0 \qquad \text{in } \Omega, \tag{5.30a}$$

$$\nabla \cdot \mathbf{q} = f\delta_\Lambda \qquad \text{in } \Omega, \tag{5.30b}$$

$$p = 0 \qquad \text{on } \partial\Omega. \tag{5.30c}$$

Take $0 < \alpha < 1$. A solution splitting can then be constructed as

$$(p, \mathbf{q}) = (p_r, \mathbf{q}_r) + (p_r, \mathbf{q}_r) \quad \text{where} \begin{cases} (p_s, \mathbf{q}_s) \in L^2_{\alpha-1}(\Omega) \times V_{\alpha+1}(\text{div}; \Omega), \\ (p_r, \mathbf{q}_r) \in L^2(\Omega) \times H(\text{div}; \Omega). \end{cases} \tag{5.31}$$

The terms p_s and $\mathbf{q}_s$ are here given explicitly as

$$p_s = E(f)\Psi G, \quad \mathbf{q}_s = -\nabla p_s, \tag{5.32}$$

with $E : H^1(\Lambda) \to H^2(\Omega) \cap C^0(\Omega)$ denoting a linear extension operator satisfying $E(f)|_\Lambda = f$ and $\Psi \in C_0^\infty(\Omega)$ some smooth cut-off function satisfying $0 < \Psi < 1$ in Ω, $\Psi = 1$ on Λ and $\Psi = 0$ on $\partial\Omega$. Finally, G denotes a logarithmic term that satisfies $-\Delta G = \delta_\Lambda$ with the line source interpreted in the sense of (3.15):

$$\int_\Omega -\Delta G\, v \, \mathrm{d}\Omega = \int_\Lambda v \, \mathrm{d}\Lambda \quad \forall v \in C^0(\Omega). \tag{5.33}$$

By Green's function theory, such a function G can be constructed by integrating the 3D Green's function for the Laplacian over Λ. The result is a logarithmic function similar to the ones derived in [78; 12]. To construct G, consider first a single line segment Λ_i with endpoints $\mathbf{a}_i$ and $\mathbf{b}_i$. The line Λ_i is described by the parametrization $\mathbf{y}_i = \mathbf{a}_i + \mathbf{T}_i s_i \quad \text{for } s_i \in (0, L_i)$, where $L_i = \|\mathbf{b}_i - \mathbf{a}_i\|$ and $\mathbf{T}_i = (\mathbf{b}_i - \mathbf{a}_i)/L_i$ is the normalized tangent vector of Λ_i. For the domain $\mathbb{R}^3$, the Green's function for the Laplacian is given by

$$G_{3D}(\mathbf{x}, \mathbf{y}) = \frac{1}{4\pi} \frac{1}{\|\mathbf{x} - \mathbf{y}\|}. \tag{5.34}$$

By the theory of Green's functions, a function G_i solving (5.33) can now be constructed by a convolution of δ_{Λ_i} and $G_{3D}(\mathbf{x}, \mathbf{y})$:

$$\begin{aligned} G_i(\mathbf{x}) &= \frac{1}{4\pi} \int_\Omega \frac{\delta_\Lambda}{\|\mathbf{x} - \mathbf{y}\|} \, \mathrm{d}\mathbf{y} \\ &= \frac{1}{4\pi} \ln\left(\frac{r_{b_i} + L_i + \mathbf{T}_i \cdot (\mathbf{a}_i - \mathbf{x})}{r_{a_i} + \mathbf{T}_i \cdot (\mathbf{a}_i - \mathbf{x})} \right), \end{aligned} \tag{5.35}$$

where $r_{b_i}(\mathbf{x}) = \|\mathbf{x} - \mathbf{b}_i\|$ and $r_{a_i}(\mathbf{x}) = \|\mathbf{x} - \mathbf{a}_i\|$. Returning then to the general case $\Lambda = \cup_{i=1}^n \Lambda_i$, the function G satisfying (5.33) can now be found by an application of the superposition principle:

$$G(\mathbf{x}) = \frac{1}{4\pi} \sum_{i=1}^n \ln\left(\frac{r_{b_i} + L_i + \mathbf{T}_i \cdot (\mathbf{a}_i - \mathbf{x})}{r_{a_i} + \mathbf{T}_i \cdot (\mathbf{a}_i - \mathbf{x})} \right). \tag{5.36}$$

The remainder term in (5.31) can now be defined as the solution of

$$\mathbf{q}_r + \nabla p_r = 0 \qquad \text{in } \Omega \tag{5.37a}$$

$$\nabla \cdot \mathbf{q}_r = F \qquad \text{in } \Omega \tag{5.37b}$$

$$p_r = 0 \qquad \text{on } \partial\Omega \tag{5.37c}$$

with right-hand side F given by

$$F(f) = \Delta(\Psi E(f))G + 2\nabla(\Psi E(f)) \cdot \nabla G. \tag{5.38}$$

By construction, the solution splitting $(p, \mathbf{q}) = (p_s, \mathbf{q}_s) + (p_r, \mathbf{q}_r)$ satisfies (5.30a) and (5.30c). To verify that it satisfies (5.30b), note that

$$\nabla \cdot \mathbf{q} = -\Delta p = -(\Delta G)\Psi E(f) \underbrace{-2\nabla G \cdot \nabla(\Psi E(f)) - G\Delta(\Psi E(f)) - \Delta p_r}_{=0}. \tag{5.39}$$

Moreover, by (5.33), $\Delta G = \delta_\Lambda$ weakly. As $E(f) = f$ and $\Psi = 1$ on Λ, it follows that

$$\nabla \cdot \mathbf{q} = f\delta_\Lambda. \tag{5.40}$$

The practical value of the solution splitting lies in the fact that it forms a splitting into higher and lower regularity terms. In Papers A and B, it was found that

$$p_s \in L^2_{\alpha-1} \quad \text{and } \mathbf{q}_s = V_{\alpha+1}(\text{div}; \Omega). \tag{5.41}$$

To understand the regularity of the remainder pair $(p_r, \mathbf{q}_r)$, note that $F \in L^2(\Omega)$. To see this, note that

$$\begin{aligned} \|F\|_{L^2(\Omega)} &\leq \|\Delta(\Psi E(f))G\|_{L^2(\Omega)} + 2\|\nabla(\Psi E(f)) \cdot \nabla G\|_{L^2(\Omega)} \\ &\leq C\left(\|\Delta E(f)G\|_{L^2(\Omega)} + 2\|\nabla E(f) \cdot \nabla G\|_{L^2(\Omega)}\right) \\ &\leq C\left(\|\Delta E(f)\|_{L^2(\Omega)}\|G\|_{L^2(\Omega)} + 2\|\nabla E(f)\|_{L^2_{-\alpha}(\Omega)}\|\nabla G\|_{L^2_\alpha(\Omega)}\right), \end{aligned} \tag{5.42}$$

where the constant $C > 0$ will depend on the smoothness of Ψ. It was shown in Paper A that $G \in L^2(\Omega)$ and $\nabla G \in L^2_\alpha(\Omega)$ for all $\alpha > 0$. By definition, $\Delta E(f) \in L^2(\Omega)$. Recall now that $E(f) \in H^2(\Omega) \cap C^0(\bar{\Omega})$. By the embedding $H^2(\Omega) \subset H^2_\epsilon(\Omega) \subset H^1_{\epsilon-1}(\Omega)$ for $0 < \epsilon < 1$ one has $\nabla E(f) \in L^2_{-\epsilon}(\Omega)$. It follows that $F \in L^2(\Omega)$.

As $F \in L^2(\Omega)$, the analysis and approximation of p_r follow from the standard theory introduced in Chapter 4. By Theorem 4.2.3, there exists $p_r \in H^2(\Omega)$ solving the primal variational formulation of (5.37a)-(5.37b). By Theorem 4.2.5, there exists $(p_r, \mathbf{q}_r) \in L^2(\Omega) \times H(\text{div}; \Omega)$ solving the mixed variational formulation of (5.37a)-(5.37b).

Clearly, the remainder pair $(p_r, \mathbf{q}_r)$ enjoys higher regularity than the full solution $(p, \mathbf{q})$. Based on this observation, an alternative numerical method can be formulated, in which only $(p_r, \mathbf{q}_r)$ is approximated and the full solution $(p, \mathbf{q})$ reconstructed via (5.31). We shall refer to this as the *singularity removal method*. This approach was tested numerically for the standard finite element method in Paper A and the mixed finite element method in Paper B. In both papers, this approach was found to yield optimal convergence rates for lowest-order elements.

Remark 5.4.1. To conclude, let us comment on the limitations of the solution splitting method. Firstly, the method requires the 1D domain to consist of straight line segments. This is in our opinion reasonable; in applications, the curve Λ is usually discretized so that it is given in terms of line segments.

Secondly, the method handles only linear problems. Moreover, the solution splitting and singularity removal has to be reformulated if the underlying model is changed. Depending on the model, this could be cumbersome in practice. For this reason, the singularity removal method is best suited for problems that are linearized and decoupled. As an example, we have successfully applied this method to the quasi-static, linear Biot model with line sources

[76]. Here the model was decoupled using a fixed stress splitting scheme to decouple the equations describing flow and mechanics, ultimately reducing the flow equations to be on the form (5.1a)-(5.1c). Thus, the singularity removal could be readily applied.

Finally, the method requires a scalar-valued permeability $\kappa \in W^{2,\infty}(\Omega)$. In this case, a solution splitting can be constructed setting $p_s = E(f)\Psi G/\kappa$. Letting $\Omega_\Psi = \text{supp}(\Psi)$, this can be relaxed to having a locally smooth $\kappa \in L^\infty(\Omega) \cap W^{2,\infty}(\Omega_\Psi)$. We have not yet succeeded in formulating a solution splitting when κ is tensor-valued.

Chapter 6

Coupled 1D-3D Flow Models

In this section, we will consider the numerical approximation of the coupled 1D-3D flow model introduced in Chapter 3.4. Recall first the geometrical setting of the problem: Let $\Omega \subset \mathbb{R}^3$ denote a bounded, convex 3D domain with smooth boundary $\partial\Omega$. Let $\Sigma \subset \mathbb{R}$ denote a generalized cylinder embedded in this domain with radius $R(s)$ and a C^2 centreline denoted $\Lambda \subset \Omega$. The boundary of this cylinder is denoted Γ. The coupled 1D-3D flow problem then reads the following:

$$\mathbf{q} + \kappa \nabla p = 0 \qquad \text{in } \Omega, \tag{6.1a}$$

$$\nabla \cdot \mathbf{q} = \beta(\hat{p} - \bar{p})\delta_\Lambda \qquad \text{in } \Omega, \tag{6.1b}$$

$$\hat{q} + \hat{\kappa}\frac{\mathrm{d}}{\mathrm{d}s}\hat{p} = 0 \qquad \text{in } \Lambda, \tag{6.1c}$$

$$\frac{\mathrm{d}}{\mathrm{d}s}\hat{q} = \beta(\hat{p} - \bar{p}) \qquad \text{in } \Lambda, \tag{6.1d}$$

where $\kappa \in L^\infty(\Omega)$ and $\hat{\kappa} \in L^\infty(\Lambda)$ are strictly positive scalars, δ_Λ a Dirac line source concentrated on Λ and $\bar{p} = \Pi p$ with Π denoting the averaging operator defined in (3.13):

$$\Pi p = \frac{1}{2\pi}\int_0^{2\pi} p(s, R, \theta)\,\mathrm{d}\theta. \tag{6.2}$$

For the sake of notational simplicity, the boundary conditions are taken homogeneous and Dirichlet, i.e., $p = 0$ on $\partial\Omega$ and $\hat{p} = 0$ on $\partial\Lambda$.

The chapter will proceed as follows. In Section 6.1, we give the primal variational formulation of (6.1a)-(6.1b) and the corresponding finite element discretization. We then discuss the convergence issues the approximation might suffer due to the singular nature of the solution. Next, we formulate in Section 6.2.1 a solution splitting of p into higher and lower-regularity terms, and show how it can be used to formulate a singularity removal method. As we will see, this leads to a reformulated coupled 1D-3D flow model posed in terms of the variables $\hat{p}$ and p_r, where the latter denotes a 3D remainder pressure. In Section 6.2.2, we show that there exists a solution $(p_r, \hat{p}) \in H^2(\Omega) \times H^2(\Lambda)$ to the primal variational formulation of this model.

Remark 6.0.1. The mixed variational formulation of the coupled 1D-3D flow problem has, to the best of our knowledge, not yet been shown to be well-posed. Moreover, the analysis requires some consideration as the resulting problem does not fit the saddle point framework of Theorem 4.2.4. With this in mind, we leave this as future work and restrict our attention to the primal variational formulation of the problem.

6.1 Variational Formulation and Discretization

Let P and V denote the pairs $P := (p, \hat{p})$ and $V := (v, \hat{v})$. Recall that $W^1_\alpha(\Omega) = \{p \in H^1_\alpha(\Omega) : Tu = 0 \text{ on } \partial\Omega\}$. We take $\mathbf{V}^1_\alpha$ to denote the function space

$$\mathbf{V}^1_\alpha = \{(p, \hat{p}) \text{ such that } \ p \in W^1_\alpha(\Omega),\, \hat{p} \in H^1_0(\Lambda)\},$$

with norm $\|P\|_{\mathbf{V}^1_\alpha} = \|p\|_{H^1_\alpha(\Omega)} + \|\hat{p}\|_{H^1(\Lambda)}$. Eliminating the fluxes $\mathbf{q}$ and $\hat{q}$ from (6.1a)-(6.1d), multiplying (6.1a) and (6.1c) with test functions $v \in W^1_{-\alpha}(\Omega)$ and $\hat{v} \in H^1_0(\Lambda)$, respectively, and integrating over their domains then yields the following variational formulation:

Find $P \in \mathbf{V}^1_\alpha$ such that

$$a\,(P, V) = 0 \quad \text{for all } V \in \mathbf{V}^1_{-\alpha}, \tag{6.3}$$

where

$$a(P, V) = (\nabla p, \nabla v)_\Omega + \left(\frac{\mathrm{d}\hat{p}}{\mathrm{d}s}, \frac{\mathrm{d}\hat{v}}{\mathrm{d}s}\right)_\Lambda - (\beta(\hat{p} - \bar{p}), v)_\Lambda + (\beta(\hat{p} - \bar{p}), \hat{v})_\Lambda. \tag{6.4}$$

The existence of $P \in \mathbf{V}^1_\alpha$ solving this problem was proven by D'Angelo in [23]. The proof itself follows in a straightforward manner from the proof of Theorem 5.2.4.

Let $\mathbb{CG}^k_h$ and $\hat{\mathbb{CG}}^k_{\hat{h}}$ denote the continuous Lagrange finite element spaces on Ω and Λ, respectively. The primal discretization of (6.3) then reads:

Find $P_{h,\hat{h}} \in \mathbb{CG}^k_h \times \hat{\mathbb{CG}}^k_{\hat{h}}$ such that

$$a(P_{h,\hat{h}}, V_{h,\hat{h}}) = 0 \quad \text{for all } V_{h,\hat{h}} \in \mathbb{CG}^k_h \times \hat{\mathbb{CG}}^k_{\hat{h}}. \tag{6.5}$$

where $P_{h,\hat{h}} = (p_h, \hat{p}_{\hat{h}})$ and $V_{h,\hat{h}} = (v_h, \hat{v}_{\hat{h}})$. The stability and well-posedness of this formulation was proven in [22]. Convergence rates have been observed numerically in [21; 49]. In Paper D, the convergence properties of this method where tested with R varying over several orders of magnitude. It was found that the solution *failed* to converge in cases where $R \ll h$. This is a troublesome observation considering that the coupled 1D-3D flow problem was formulated precisely to handle applications with R negligible.

Remark 6.1.1. Why does the approximation of the coupled 1D-3D flow model fail to converge when $R \ll h$? The answer has to do with the logarithmic nature of p as well as the averaging operator Π. Firstly, the logarithmic nature of p is difficult to resolve numerically in the near vicinity of Λ. For $R \ll h$, this leads to a large discrepancy between $\bar{p}$ and the numerically computed value $\bar{p}_h$. As an example of this, Figure 6.1 shows the function $p = \ln(r)$ on the unit interval, along with the value $\bar{p}$ for different radii R. Next, the figure shows interpolations $p_h = \mathcal{I}_h(p)$ of p using $\mathbb{CG}^1_h$ elements with different mesh sizes h. From the figure, one sees that for $R < h/2$ the value of $\bar{p}_h$ does not depend on the averaging radius R. Moreover, it is clear that when $R \ll h$, the values of $\bar{p}$ and $\bar{p}_h$ differ significantly. This has serious implications for the approximation of the coupling conditions.

This issue is well known in the context of well modelling, where it is typically resolved by means of a Peaceman well correction [69; 68; 55]. By analytic arguments, the parameter β is altered so that the approximation of $\beta(\hat{p} - \bar{p})$ better approximates the true value. The precise correction depends on the flow equations, the discretization method, the mesh for

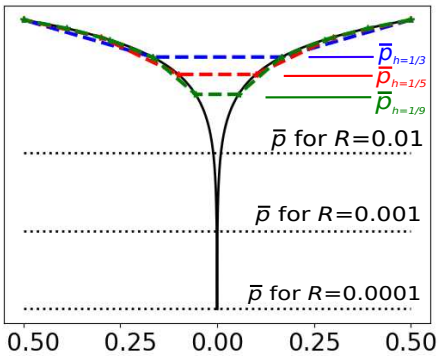

Figure 6.1: The function $p = \ln(r)$ along with its average value $\bar{p}$ for different values of R. Interpolations $p_h = \mathcal{I}_h(p)$ are also shown using $\mathbb{CG}$ elements on the unit interval mesh with different mesh sizes h. As is evident from the plot, the interpolation does not resolve the singularity in p. For $R \ll h$, this leads to a large discpreancy between $\bar{p}$ and $\bar{p}_h$.

Ω and the spatial configuration of Λ. Peaceman's original formulation was formulated for the two-point flux approximation method on square grids with the well aligned with one of its axes. Considerable research effort has been put into generalizing the Peaceman correction to different discretization methods [20], more generalized grids [69; 2; 1; 3], and more generalized well placements [42; 4; 86; 8].

In [44], the line source δ_Λ is replaced by a distributed source using a smooth kernel function Φ of radius ρ. The parameter β is then multiplied by a scaling factor to ensure the model agrees with the coupled 1D-3D flow problem as $\rho \to 0$. In contrast to the Peaceman well correction, this approach has the advantage of being independent of the discretization method. The scaling factor depends on the choice of Φ and ρ and can be analytically derived under certain assumptions of the geometry of Λ.

6.2 Singularity Removal Method

In the previous section, we discussed how the coupled 1D-3D flow model suffers approximation problems due to the singular nature of the solution. We further discussed how this problem could be alleviated by the use of a Peaceman well correction. Considering now e.g. the vascular network illustrated in Figure 1.2, the 1D domain Λ here has a highly complicated structure with a large number of branches. For this reason, it is, in our opinion, not viable to use the Peaceman well correction for simulations of flow through vascularized tissue.

With this in mind, we will now extend the singularity removal method defined in Section 5.4 to the coupled 1D-3D flow model. This will be done in two parts. In Section 6.2.1, we formulate a solution splitting for the pressure p into higher and lower regularity terms. By algebraic manipulation of the coupling condition, the model is then reformulated, so that is given only with respect to the higher regularity remainder pressure p_r. In Section 6.2.2, we give the primal variational formulation of the reformulated coupled 1D-3D flow model, and prove the existence of a solution $(p_r, \hat{p}) \in H^2(\Omega) \times H^2(\Lambda)$.

6.2.1 Solution splitting and model reformulation

As in Section 5.4, we assume $\kappa = 1$ for the sake of simplicity. To begin, let us assume the solution to (6.1a)-(6.1d) admits a splitting

$$p = p_s + p_r, \text{ where } \begin{cases} p_s \in W^1_\alpha(\Omega), \\ p_r \in H^2_0(\Omega). \end{cases} \tag{6.6}$$

The singular part of the solution splitting is given as

$$p_s = E(f)\Psi G, \tag{6.7}$$

with G being as in (5.36), Ψ denoting some smooth cut-off function, assumed to satisfy $0 \leq \Psi \leq 1$ in Ω, $\Psi = 1$ in Σ and $\Psi = 0$ on $\partial\Omega$, and $E : H^1(\Lambda) \to H^2(\Omega) \cap C(\Omega)$ denoting a linear extension operator. Recalling the parametrization of Σ as introduced in Section 3.1, the extension is assumed to satisfy $E(f)(s, r, \theta) = f(s)$ for each point $(s, r, \theta) \in \Sigma$. Finally, f denotes the previously introduced pressure difference $f = \beta(\hat{p} - \bar{p})$.

The remainder pressure p_r can then defined as the solution of the elliptic problem

$$-\Delta p_r = F(f) \qquad \text{in } \Omega, \tag{6.8a}$$

$$p_r = 0 \qquad \text{on } \partial\Omega, \tag{6.8b}$$

with

$$F(f) = G\Delta(\Psi E(f)) + 2\nabla G \cdot \nabla(\Psi E(f)). \tag{6.9}$$

Note that unlike in Section 5.4, one here has $f = f(p, \hat{p})$. I.e., one now has f implicitly given from the solutions $\hat{p}$ and p of the coupled 1D-3D flow problem. The next step is therefore to reformulate f so that $f = f(p_r, \hat{p})$, p_r being the solution of (6.8b). To do so, let us first average (6.7) using the averaging operator defined by (6.2):

$$\begin{aligned} \bar{p} = \Pi p &= \Pi(\Psi E(f)G + p_r) \\ &= \Pi(\Psi E(f)G) + \Pi p_r, \end{aligned} \tag{6.10}$$

where we used the linearity of Π. Note now that $G = G(s, r)$, i.e. G is invariant with respect to θ. Next, $\Psi = 1$ in Σ. Moreover, the extension operator is assumed to satisfy $E(f) = f(s)$ in Σ. Thus,

$$\begin{aligned} \Pi(\Psi E(f)G) &= \int_0^{2\pi} f(s)\, G(s, R)\, \mathrm{d}\theta \\ &= f(s)G(s, R) = f(s)\overline{G}(s). \end{aligned} \tag{6.11}$$

It follows that

$$\bar{p} = f\bar{G} + \bar{p}_r = \beta\,(\hat{p} - \bar{p})\,\bar{G} + \bar{p}_r, \tag{6.12}$$

where $\bar{G}(s) = G(s, R)$. Manipulating this result algebraically yields

$$\begin{aligned} &\bar{p} = \frac{\beta\overline{G}\hat{p} + \bar{p}_r}{1 + \beta\overline{G}}, \\ \Rightarrow\ &f = \beta(\hat{p} - \bar{p}) = \frac{\beta}{1 + \beta\overline{G}}(\hat{p} - \bar{p}_r) = \beta^*(\hat{p} - \bar{p}_r) \quad \text{with } \beta^* = \frac{\beta}{1 + \beta\overline{G}}. \end{aligned} \tag{6.13}$$

From this, we can state the reformulated coupled 1D-3D flow model:

$$
\begin{aligned}
-\Delta p_r &= F(\beta^*(\hat{p} - \bar{p}_r)) && \text{in } \Omega, && (6.14a)\\
p_r &= 0 && \text{on } \partial\Omega, && (6.14b)\\
-\frac{\mathrm{d}^2\hat{p}}{\mathrm{d}s^2} &= -\beta^*(\hat{p} - \bar{p}_r) && \text{in } \Lambda, && (6.14c)\\
\hat{p} &= 0 && \text{on } \partial\Lambda. && (6.14d)
\end{aligned}
$$

6.2.2 Weak solution of the reformulated model

Next, we state a weak formulation of the reformulated coupled 1D-3D flow problem (6.14a)-(6.14d). As the solution singularity has here been removed from the governing equations, this can be done using standard Sobolev spaces.

Multiplying (6.14a) and (6.14c) with test functions $v \in H_0^2(\Omega)$ and $\hat{v} \in H_0^2(\Lambda)$, respectively, and integrating over their respective domains yields the following:

$$
\begin{aligned}
(\nabla p_r, \nabla v)_\Omega &= (F(\beta^*(\hat{p} - \bar{p}_r)), v)_\Omega, && (6.15a)\\
\left(\frac{\mathrm{d}\hat{p}}{\mathrm{d}s}, \frac{\mathrm{d}\hat{v}}{\mathrm{d}s}\right)_\Lambda &= -(\beta^*(\hat{p} - \bar{p}_r), \hat{v})_\Lambda, && (6.15b)
\end{aligned}
$$

with the right-hand side in (6.15a) given by

$$
(F(f), v)_\Omega = (G\Delta(\Psi E(f)), v)_\Omega + (2\nabla(\Psi E(f)) \cdot \nabla G, v)_\Omega.
$$

Next, let $\mathbf{V}^2$ denote the function space

$$
\mathbf{V}^2 = \{(p, \hat{p}) : p \in H_0^2(\Omega),\ \hat{p} \in H_0^2(\Lambda)\}
$$

with norm $\|P\|_{\mathbf{V}^2} = \|p\|_{H_0^2(\Omega)} + \|\hat{p}\|_{H_0^2(\Lambda)}$. Finally, let P and V denote the pairs $P := (p_r, \hat{p})$ and $V := (v, \hat{v})$, and $a(P, V)$ the bilinear form given by

$$
a(P, V) = (\nabla p_r, \nabla v)_\Omega + \left(\frac{\mathrm{d}\hat{p}}{\mathrm{d}s}, \frac{\mathrm{d}\hat{v}}{\mathrm{d}s}\right)_\Lambda - (F(\beta^*(\hat{p} - \bar{p}_r)), v)_\Omega + (\beta^*(\hat{p} - \bar{p}_r), \hat{v})_\Lambda. \tag{6.16}
$$

The variational formulation of (6.14a)-(6.14d) then reads the following: Find $P \in \mathbf{V}^2$ such that

$$
a(P, V) = 0 \quad \text{for all } V \in \mathbf{V}^2. \tag{6.17}
$$

The following theorem guarantees, for small enough β^*, the existence of $P = (p_r, \hat{p}) \in \mathbf{V}^2$ solving (6.17):

Theorem 6.2.1. *Let* $\|\beta^*\|_{W^{1,\infty}(\Lambda)} < 1/C$ *with* $C = \max(1, C_\Pi)(2\sqrt{2}MC_\Psi C_E C_L + \hat{C}_L)$, $E : H^1(\Lambda) \to H^2(\Omega) \cap C(\Omega)$ *be a continuous linear extension operator and* $\Psi \in C^\infty(\bar{\Omega})$ *a cut-off function satisfying* $0 \le \Psi \le 1$ *in* Ω, $\Psi = 1$ *in* Σ *and* $\Psi = 0$ *on* $\partial\Omega$. *Then there exists* $(p_r, \hat{p}) \in \mathbf{V}^2$ *solving* (6.17).

We here take $p \in H^2(\Omega)$ so that $\Pi p_r = \bar{p}_r \in H^1(\Lambda)$ (for a verification of this, see Lemma 6.2.2 given at the end of the section). This ensures $f = \beta^*(\hat{p} - \bar{p}_r) \in H^1(\Omega)$. The extension operator can then be defined in a manner consistent with what was required for the solution

splitting in Section 6.2.1, i.e., as a linear mapping $E : H^1(\Lambda) \to H^2(\Omega) \cap C(\Omega)$ satisfying $E(f)(s,r,\theta) = f(s)$ for all $(s,r,\theta) \in \Sigma$.

The result $p_r \in H^2(\Omega)$ is further consistent with the numerical results presented in Paper D. We there considered the primal finite element discretization of (6.17), which reads: Find $P_{h,\hat{h}} \in \mathbb{C}\mathbb{G}^k_h \times \hat{\mathbb{C}\mathbb{G}}^k_{\hat{h}}$ such that

$$a(P_{h,\hat{h}}, V_{h,\hat{h}}) = 0 \quad \text{for all } V_{h,\hat{h}} \in \mathbb{C}\mathbb{G}^k_h \times \hat{\mathbb{C}\mathbb{G}}^k_{\hat{h}}. \tag{6.18}$$

where $P_{h,\hat{h}} = (p_{r,h}, \hat{p}_{\hat{h}})$ and $V_{h,\hat{h}} = (v_h, \hat{v}_{\hat{h}})$. A numerical test case with $k = 1$ then showed $\mathcal{O}(h^2)$ convergence in the $L^2(\Omega)$-norm and $\mathcal{O}(\hat{h}^2)$ convergence in the $L^2(\Lambda)$-norm. Given that $(p_r, \hat{p}) \in H^2(\Omega) \times H^2(\Lambda)$, this is formally consistent with the convergence rates given by Theorem 4.3.1

Finally, let us conclude by giving a proof of Theorem 6.2.2. The proof is by the Banach fixed point theorem applied to an iteration procedure similar to the one proposed in Paper C. A bound is necessary on $\|\beta^*\|_{W^{1,\infty}(\Lambda)}$ for the iterations to contract. Recalling from (3.11) that $\beta = 2\pi R L_p$, this will further set a restriction on the radius R relative to L_p. Let us note that the bound most likely could be improved. In the future, however, we plan to look at a different formulation of the coupled 1D-3D flow model. This will be further discussed in Section 7.2. With this in mind, we leave the proof as is.

Proof. Given $(p_r^k, \hat{p}^k) \in H^2_0(\Omega) \times H^2_0(\Lambda)$, we define the following iteration procedure:

Step 1: Let $f^k = \beta^*(\hat{p}^k - \bar{p}_r^k)$. Find $p_r^{k+1} \in H^2_0(\Omega)$ solving

$$(\nabla p_r^{k+1}, \nabla v)_\Omega = (F(f^k), v)_\Omega \quad \text{for all } v \in H^2_0(\Omega). \tag{6.19}$$

Step 2: Find $\hat{p}_{k+1} \in H^2_0(\Lambda)$ solving

$$(\nabla \hat{p}_{k+1}, \nabla \hat{v})_\Lambda = -(\beta^*(\hat{p}^k - \bar{p}_r^k), \hat{v})_\Lambda \quad \text{for all } \hat{v} \in H^2_0(\Lambda) \tag{6.20}$$

The proof is by showing that this iteration procedure is a contraction.

Firstly, let us verify that there exists $p_r^{k+1} \in H^2_0(\Omega)$ solving (6.19). This readily follows from Theorem 4.2.3 given that $F(f^k) \in L^2(\Omega)$. From Lemma 6.2.2, $\bar{p}_r^k = \Pi p_r^k \in H^1(\Lambda)$, meaning that $f^k = \hat{p}^k - \bar{p}_r^k \in H^1(\Lambda)$. The extension $E(f^k)$ is thus well defined. Let $\Omega_\Psi = \text{supp}(\Psi)$. A calculation shows

$$\begin{aligned}\|F(f^k)\|_{L^2(\Omega)} &\leq \|\Delta\left(\Psi E\left(f^k\right)\right) G\|_{L^2(\Omega_\Psi)} + \|\nabla\left(\Psi E\left(f^k\right)\right) \cdot \nabla G\|_{L^2(\Omega_\Psi)} \\ &\leq \|G\|_{L^2(\Omega_\Psi)} \|\Delta(\Psi E\left(f^k\right))\|_{L^2(\Omega_\Psi)} + \|\nabla G\|_{L^2_\alpha(\Omega_\Psi)} \|\nabla(\Psi E\left(f^k\right))\|_{L^2_{-\alpha}(\Omega_\Psi)}\end{aligned}$$

where $0 < \alpha < 1$. Let

$$C_\Psi = \max(1, \|\nabla\Psi\|_{L^\infty(\Omega)}, \|\Delta\Psi\|_{L^\infty(\Omega)}). \tag{6.21}$$

Applying the product rule to the terms $\Delta(\Psi E(f^k))$ and $\nabla(\Psi E(f^k))$ then yields

$$\|F(f^k)\|_{L^2(\Omega)} \leq C_\Psi \left(2\|G\|_{L^2(\Omega_\Psi)} \|E\left(f^k\right)\|_{H^2(\Omega_\Psi)} + \|\nabla G\|_{L^2_\alpha(\Omega_\Psi)} \|E\left(f^k\right)\|_{H^1_{-\alpha}(\Omega_\Psi)}\right).$$

By the embedding (5.10), we further have

$$\|E\left(f^k\right)\|_{H^1_{-\alpha}(\Omega_\Psi)} \leq C_\alpha \|E\left(f^k\right)\|_{H^2_{-\alpha+1}(\Omega_\Psi)} \leq C_\alpha \|E\left(f^k\right)\|_{H^2(\Omega_\Psi)}$$

where we used that $-\alpha+1>0$ meaning that $\|\cdot\|_{H^2_{-\alpha+1}(\Omega)} \leq \|\cdot\|_{H^2(\Omega)}$. Letting

$$M = \max(2\|G\|_{L^2(\Omega_\Psi)}, C_\alpha \|\nabla G\|_{L^2_\alpha(\Omega_\Psi)}), \tag{6.22}$$

one then has

$$\begin{aligned}\|F(f^k)\|_{L^2(\Omega)} &\leq 2C_\Psi M \|E\left(f^k\right)\|_{H^2(\Omega_\Psi)} \\ &\leq 2C_\Psi M \|E\left(f^k\right)\|_{H^2(\Omega)}\end{aligned}$$

Finally, using that $E: H^1(\Lambda) \to H^2(\Omega) \cap C(\Omega)$ is a bounded operator, one then has

$$\begin{aligned}\|F(f^k)\|_{L^2(\Omega)} &\leq 2MC_\Psi \|E(f^k)\|_{H^2(\Omega)} \\ &\leq 2MC_\Psi C_E \|f^k\|_{H^1(\Lambda)}.\end{aligned} \tag{6.23}$$

It follows that $F(f^k) \in L^2(\Omega)$.

Next, let us bound the iteration errors in Step 1, i.e. (6.19). Clearly, $p_r^{k+1}-p_r^k$ should satisfy the following problem: Find $p_r^{k+1}-p_r^k \in H_0^2(\Omega)$

$$(\nabla(p_r^{k+1}-p_r^k), \nabla v)_\Omega = (F(f^k-f^{k-1}), v)_\Omega \quad \text{for all } v \in H_0^2(\Omega) \tag{6.24}$$

where we used the linearity of F. By (6.23), $F(f^k-f^{k-1}) \in L^2(\Omega)$. Applying Theorem 4.2.3 with the constant C_L then yields

$$\begin{aligned}\|p_r^{k+1}-p_r^k\|_{H^2(\Omega)} &\leq C_L \|F(f^k-f^{k-1})\|_{L^2(\Omega)} \\ &\leq 2MC_\Psi C_E C_L \|f^k-f^{k-1}\|_{H^1(\Lambda)} \\ &\leq 2MC_\Psi C_E C_L \left(\|\beta^*\left(\hat{p}^k-\hat{p}^{k-1}\right)\|_{H^1(\Lambda)} + \|\beta^*\left(\bar{p}_r^k-\bar{p}_r^{k-1}\right)\|_{H^1(\Lambda)}\right) \\ &\leq 2\sqrt{2}MC_\Psi C_E C_L \|\beta^*\|_{W^{1,\infty}(\Lambda)} \left(\|\hat{p}^k-\hat{p}^{k-1}\|_{H^1(\Lambda)} + \|\bar{p}_r^k-\bar{p}_r^{k-1}\|_{H^1(\Lambda)}\right) \\ &\leq 2\sqrt{2}MC_\Psi C_E C_L \|\beta^*\|_{W^{1,\infty}(\Lambda)} \left(\|\hat{p}^k-\hat{p}^{k-1}\|_{H^1(\Lambda)} + C_\Pi \|p_r^k-p_r^{k-1}\|_{H^2(\Omega)}\right),\end{aligned}$$

where the last line used Lemma 6.2.2 with the constant C_Π. Thus, one has

$$\|p_r^{k+1}-p_r^k\|_{H^2(\Omega)} \quad \leq C_1 \|\beta^*\|_{W^{1,\infty}(\Lambda)} \left(\|\hat{p}^k-\hat{p}^{k-1}\|_{H^2(\Lambda)} + \|p_r^k-p_r^{k-1}\|_{H^2(\Omega)}\right), \tag{6.25}$$

with $C_1 = 2\sqrt{2}MC_\Psi C_E C_L \max(1, C_\Pi)$.

Next, let us bound the iteration error from Step 2, i.e. (6.20). Firstly, $\hat{p}^k - \bar{p}_r^k \in L^2(\Lambda)$. Applying Theorem 4.2.3 with the constant $\hat{C}_L$ then yields

$$\begin{aligned}\|\hat{p}^{k+1}-\hat{p}^k\|_{H_0^2(\Lambda)} &\leq \hat{C}_L \|\beta^*\left(\hat{p}^k-\hat{p}^{k-1}\right)\|_{L^2(\Lambda)} + \|\beta^*\left(\bar{p}_r^k-\bar{p}_r^{k-1}\right)\|_{L^2(\Lambda)} \\ &\leq \hat{C}_L \|\beta^*\|_{L^\infty(\Omega)} \left(\|\hat{p}^k-\hat{p}^{k-1}\|_{L^2(\Lambda)} + \|\bar{p}_r^k-\bar{p}^{k-1}\|_{L^2(\Lambda)}\right) \\ &\leq \hat{C}_L \|\beta^*\|_{W^{1,\infty}(\Lambda)} \left(\|\hat{p}^k-\hat{p}^{k-1}\|_{H^1(\Lambda)} + \|\bar{p}_r^k-\bar{p}^{k-1}\|_{H^1(\Lambda)}\right) \\ &\leq \hat{C}_L \|\beta^*\|_{W^{1,\infty}(\Lambda)} \left(\|\hat{p}^k-\hat{p}^{k-1}\|_{H^1(\Lambda)} + C_\Pi \|p_r^k-p_r^{k-1}\|_{H^2(\Omega)}\right)\end{aligned}$$

where the last line used Lemma 6.2.2. Thus,

$$\|\hat{p}^{k+1}-\hat{p}^k\|_{H_0^2(\Lambda)} \leq C_2 \|\beta^*\|_{W^{1,\infty}(\Lambda)} \left(\|\hat{p}^k-\hat{p}^{k-1}\|_{H^2(\Lambda)} + \|p_r^k-p_r^{k-1}\|_{H^2(\Omega)}\right), \tag{6.26}$$

with $C_2 = \hat{C}_L \max(1, C_\Pi)$.

Combining (6.25) and (6.26), one then has

$$\begin{aligned}\|P^{k+1} - P^k\|_{\mathbf{v}} &= \|p_r^{k+1} - p_r^k\|_{H_0^2(\Omega)} + \|\hat{p}^{k+1} - \hat{p}^k\|_{H^2(\Omega)} \\ &\leq (C_1 + C_2)\|\beta^*\|_{W^{1,\infty}(\Lambda)} \left(\|p_r^k - p_r^{k-1}\|_{H^2(\Omega)} + \|\hat{p}^k - \hat{p}^{k-1}\|_{H_0^2(\Lambda)}\right) \\ &= C\|\beta^*\|_{W^{1,\infty}(\Lambda)}\|P^k - P^{k-1}\|_{\mathbf{v}}.\end{aligned}$$

where $C = C_1 + C_2$ is given by

$$C = \max(1, C_\Pi)(2\sqrt{2}MC_\Psi C_E C_L + \hat{C}_L). \tag{6.27}$$

By assumption, one then has $C\|\beta^*\|_{W^{1,\infty}(\Lambda)} < 1$ and the iteration procedure defined by (6.19)-(6.20) thus has a fixed point solving (6.17). □

Lemma 6.2.2. *The averaging operator $\Pi : H^2(\Omega) \to H^1(\Lambda)$ is a bounded linear operator satisfying*

$$\|\Pi p\|_{H^1(\Lambda)} \leq C_\Pi \|p\|_{H^2(\Omega)} \tag{6.28}$$

with the constant $C_\Pi = 1/2\pi$.

Proof. Firstly, it is well known that for $p \in H^2(\Omega)$ one has $T_\Gamma p \in H^1(\Gamma)$ satisfying the trace inequality

$$\|T_\Gamma p\|_{H^1(\Gamma)} \leq C_\Gamma \|p\|_{H^2(\Omega)}. \tag{6.29}$$

Using the polar coordinate system with respect to the Frenet-Serret frame of Σ, $T_\Gamma p$ then has a weak derivative satisfying

$$\int_\Lambda \int_0^{2\pi} \frac{\partial}{\partial s} T_\Gamma p \, \phi \, \mathrm{d}\theta \mathrm{d}s = -\int_\Lambda \int_0^{2\pi} T_\Gamma p \frac{\partial}{\partial s}\phi \, \mathrm{d}\theta \mathrm{d}s$$

for all $\phi \in L^1_{\mathrm{loc}}(\Gamma)$.

Let us now show that the function Πp has a weak derivative $\frac{\mathrm{d}}{\mathrm{d}s}\Pi p$. By Theorem 4.1.1, there exists a sequence $p_k \in C_0^\infty(\Omega)$ such that $\lim_{k\to\infty} p_k = p$ in $H^2(\Omega)$. From this, let us define the weak derivative of Πp by $\frac{\mathrm{d}}{\mathrm{d}s}\Pi p = \lim_{k\to\infty}(\frac{\mathrm{d}}{\mathrm{d}s}\Pi p_k)$. For each element $p_k \in C_0^\infty(\Omega)$, one has

$$\begin{aligned}\int_\Lambda \frac{\mathrm{d}}{\mathrm{d}s}\Pi p_k \, \phi \, \mathrm{d}s &= \frac{1}{2\pi}\int_\Lambda \frac{\mathrm{d}}{\mathrm{d}s}\left(\int_0^{2\pi} p_k(s, R, \theta)\, \mathrm{d}\theta\right) \phi(s)\, \mathrm{d}s \\ &= \frac{1}{2\pi}\int_\Lambda \int_0^{2\pi} \frac{\partial}{\partial s} p_k(s, R, \theta)\, \phi(s)\, \mathrm{d}\theta \; \mathrm{d}s \\ &= -\frac{1}{2\pi}\int_\Lambda \int_0^{2\pi} p_k(s, R, \theta) \frac{\mathrm{d}}{\mathrm{d}s}\phi(s)\, \mathrm{d}\theta \; \mathrm{d}s \\ &= -\int_\Lambda \Pi p_k \frac{\mathrm{d}}{\mathrm{d}s}\phi \, \mathrm{d}s\end{aligned}$$

for all $\phi \in L^1_{\mathrm{loc}}(\Lambda)$, where we used Leibniz integral rule and integration by parts. By a limit argument one then has

$$\int_\Lambda \frac{\mathrm{d}}{\mathrm{d}s}\Pi p \, \phi \, \mathrm{d}s = -\int_\Lambda \Pi p \frac{\mathrm{d}}{\mathrm{d}s}\phi \, \mathrm{d}s \quad \text{for all } \phi \in L^1_{\mathrm{loc}}(\Lambda).$$

Next, $\Pi p \in L^2(\Gamma)$:

$$\begin{aligned}\|\Pi p\|^2_{L^2(\Lambda)} &= \int_\Lambda (\Pi p)^2 \mathrm{d}s = \left(\frac{1}{2\pi}\right)^2 \int_\Lambda \left(\int_0^{2\pi} T_\Gamma p \,\mathrm{d}\theta\right)^2 \mathrm{d}s \\ &\le \left(\frac{1}{2\pi}\right)^2 \int_\Lambda \int_0^{2\pi} (T_\Gamma p)^2 \mathrm{d}\theta \,\mathrm{d}s = \left(\frac{1}{2\pi}\right)^2 \|T_\Gamma p\|^2_{L^2(\Gamma)}.\end{aligned}$$

Similarly one finds $\frac{\mathrm{d}}{\mathrm{d}s}\Pi p \in L^2(\Gamma)$:

$$\begin{aligned}\|\frac{\mathrm{d}}{\mathrm{d}s}\Pi p\|^2_{L^2(\Lambda)} &= \int_\Lambda (\frac{\mathrm{d}}{\mathrm{d}s}\Pi p)^2 \mathrm{d}s = \left(\frac{1}{2\pi}\right)^2 \int_\Lambda \left(\frac{\mathrm{d}}{\mathrm{d}s}\int_0^{2\pi} T_\Gamma p \,\mathrm{d}\theta\right)^2 \mathrm{d}s \\ &\le \left(\frac{1}{2\pi}\right)^2 \int_\Lambda \int_0^{2\pi} \frac{\mathrm{d}}{\mathrm{d}s} T_\Gamma p(s,\theta)^2 \mathrm{d}\theta \,\mathrm{d}s = \left(\frac{1}{2\pi}\right)^2 \|\frac{\mathrm{d}}{\mathrm{d}s} T_\Gamma p\|^2_{L^2(\Gamma)}.\end{aligned}$$

It follows that $\Pi p \in H^1(\Lambda)$. Combining this with (6.29), one has

$$\|\Pi p\|_{H^1(\Lambda)} \le \left(\frac{1}{2\pi}\right) \|T_\Gamma p\|_{H^1(\Gamma)} \le \left(\frac{1}{2\pi}\right) C_\Gamma \|p\|_{H^2(\Omega)}. \tag{6.30}$$

Thus, (6.28) holds with a constant $C_\Pi = {}^1\!/_{2\pi} C_\Gamma$.

□

Chapter 7

Summary and Outlook

In this chapter we summarize the scientific results presented in the form of three scientific articles and one conference proceeding.

7.1 Summary of the Papers

Paper A: Splitting method for elliptic equations with line sources

In the first paper, we focus on the strong formulation of an elliptic equation with a line source in the right-hand side. Given some assumptions on the problem parameters, we show that the solution admits a splitting into higher and lower regularity terms. The lower regularity terms are given as explicitly known functions. The higher regularity term, denoted as the remainder function, is defined as the solution of its own elliptic equation. Centrally, the right-hand side of this equation is found to belong to $L^2(\Omega)$. The existence and approximation properties of the remainder term then follow from standard elliptic theory.

The contributions of this paper are both analytical and numerical in nature. Firstly, the solution splitting makes clear the mathematical structure of the solution. In particular, it gives an explicit representation of the logarithmic behaviour of the pressure around the line source. As the properties of the remainder term follow from standard elliptic theory, a regularity analysis of the full solution now reduces to straightforward computation of the regularity properties of the (explicitly known) logarithmic term. Such an analysis is performed and the results found to agree with previous results regarding the regularity of the solution, considering both weighted Sobolev spaces as in [23; 22] and fractional Sobolev spaces as in [51]. Moreover, the results are in full agreement with the pollution issue addressed in [46; 47].

Secondly, we formulate in this paper a new numerical method with which to approximate the solution. The idea of the method is to approximate the remainder term and then use the solution splitting to reconstruct the full solution. We refer to this method as the *singularity removal method*. The method itself has several advantages compared to the standard discretization method considered in [22]. Recall that remainder term is defined as the solution of a (standard) elliptic equation with a right-hand side belong to $L^2(\Omega)$. Discretization methods and solvers are therefore readily available from standard theory. Moreover, this method significantly increases the approximation properties of the solution. Lastly, it makes the discretization independent of the discretization of Λ. To conclude the article, we illustrate these advantages by performing simulations where the line sources are concentrated on lines rep-

resenting the vascular network found from the MRI of a human brain [81].

Paper B: A Mixed Approach to the Poisson Problem with Line Sources

In the second paper, we consider the mixed formulation of the same problem considered in Paper A. The main contribution of the article is the proof of the existence of a solution and a discussion regarding its regularity and approximation properties. We start by identifying the appropriate weighted Sobolev spaces for the solution and prove its existence by the use of a generalized Lax-Milgram lemma. Here, we find that the flux requires the use of a non-standard Sobolev space, in the sense that the weighing required for the divergence of the flux is non-Muckenhoupt. This raises concerns about the approximation properties of the flux as the analysis cannot guarantee that the flux is integrable in the sense of $L^1(\Omega)$. Next, we test numerically the approximation properties of the mixed finite element method when applied to this problem. The tests utilize both standard and weighted norms. We identify a relationship between the weighing of the norm, the order of the discretization space, and the convergence rate similar to the one proved in [22].

Centrally, the numerical tests find that the flux does not converge in the standard sense. I.e., the flux requires a weighing of the L^2-norm in order to converge; this can be interpreted as giving up control of the solution around the line. With this in mind, we extend the singularity removal method proposed in Paper A to the case of mixed elliptic problems. In this approach, both the pressure and flux are split into higher and lower regularity terms. The lower regularity terms are again given explicitly, while the higher-regularity term is defined as the solution of its own mixed elliptic problem. As the source term in this problem belongs to $L^2(\Omega)$, the remainder flux is found to belong to the standard $H(\mathrm{div};\Omega)$ space. Finally, we use the solution splitting to formulate a singularity removal based finite element method in which only the higher-regularity remainder terms are approximated numerically. We provide numerical evidence that this method converges optimally for lowest-order mixed finite elements. This is shown to hold also when the line sources are concentrated on a complex geometry taken from the vascular network taken of a rat carcinoma [75].

Paper C: Well Modelling By Means Of Coupled 1D-3D Flow Models

In the third paper, we consider how the singularity removal method from Papers A and B can be extended to approximate the coupled 1D-3D flow problem. The paper is focused on a fixed-point iteration scheme with its fixed point solving the coupled 1D-3D model. The scheme decouples the interaction between well and reservoir so that each problem can be approximated separately. To be more precise, the scheme takes as an initial guess f^0 for the pressure difference between the (1D) well and (3D) reservoir pressure. The iteration process involves three steps: (i) computation of the reservoir pressure field given a line source of intensity f^0, (ii) an update of the averaged 3D pressure and resulting pressure difference f^1, (iii) a computation of the well pressure given the right-hand side f^1.

The main contribution of the paper is this division of the coupled 1D-3D flow problem into subproblems, each of which can be approximated using standard numerical methods. The reservoir pressure is now defined as the solution of an elliptic problem with a line source of given intensity f^0. Thus, the singularity removal method from paper A and B can now be used to approximate the solution.

Paper D: A Singularity Removal Method for Coupled 1D-3D Flow Models

In the final paper, we extend the singularity removal method from Papers A and B so that it holds for the (fully) coupled 1D-3D flow problem. To do so, we first formulate a solution splitting of the 3D pressure into higher and lower regularity terms. Via algebraic manipulations, the pressure difference between domains is reformulated so that it is given with respect to the 3D remainder pressure. A reformulated coupled 1D-3D flow model is then given depending only on the 1D pressure and the 3D remainder pressure. As in Papers A and B, the remainder pressure is defined as the solution of its own elliptic equation.

Centrally, the 1D pressure and 3D remainder pressure are both expected to enjoy full H^2-regularity. For this reason, the approximation of the reformulated coupled 1D-3D flow model can now be carried out using any standard numerical method. We refer to this as the singularity removal based approach. Next, we show results obtained using the Galerkin finite element method with and without singularity removal. Numerical evidence is provided showing that a straightforward approximation can fail to converge for $R \ll h$. The singularity removal based method is found to resolve this problem. For this reason, it is found to be suitable for problems containing a large number of inclusions, as it would in this case not be computationally feasible to refine around each line segment.

7.2 Outlook

The overarching goal of this thesis has been to develop robust and accurate approximation methods for the coupled 1D-3D flow problem. This model is well known to be difficult to approximate due to the influence of the line source.

Following the same methodology as previous research on this problem, we began by considering the Poisson equation with line sources. It is our opinion that this particular problem is now well understood. In particular, one knows

- The existence and regularity of the solution, both for the primal [23] and mixed formulation (Paper B) of the problem.
- the approximation properties of the primal [22] and mixed finite element method (Paper B) when applied to this problem.
- the local pollution effect of the Dirac line source [46; 47].
- an alternative numerical method which restores optimal convergence for lowest order conformal (Paper A) and mixed finite element method (Paper B).

Next, it is our opinion that the coupled 1D-3D flow model is in need of more research. In particular, let us note that

- The existence and regularity of the solution are known for the primal formulation of the problem [23]. Similar results are not known for the mixed formulation.
- The primal and mixed finite element methods for this problem have both been shown to be stable [22; 64]. However, the numerical experiments in Paper D showed that the primal finite element method failed to converge for $R \ll h$. This result agrees with earlier results regarding approximation issues encountered in well-modelling [68; 69; 20; 87; 55].

The last point is especially pressing as this defeats the purpose of the coupled 1D-3D flow model (which was introduced precisely to handle cases where $R \ll h$). Thus, there is a pressing need to develop efficient and robust approximation methods for this model.

The singularity removal method proposed in Paper D may be one alternative. In particular, it was found that this method is robust with respect to having $R \ll h$. Let us note, however, that there are a number of improvements one could make to this approach. In particular,

- the solution splitting could be extended to handle tensor valued permeability. This would be an important contribution to well modelling, as the currently used Peaceman well correction is difficult to extend to cases involving anisotropic permeability.
- the method could be made more efficient by introducing cut-off functions that localize the effect of the logarithmic term capturing the solution singularity, such as in [65; 27]. This would be an important contribution to simulations of flow in vascularized tissue. Here, the number of line sources can only be expected to increase as MRI image resolution increases, meaning one can capture smaller and smaller blood vessels. Thus, it is important to formulate numerical methods that are scalable with respect to the number of line segments in the 1D domain.

One possible way of handling anisotropy would be to use the solution splitting to formulate a Generalized Finite Element Method [79] for the problem. The Generalized Finite Element Method works by enriching the basis functions at locations where the analytical solution corresponding to the singularity is known. In the case of the coupled 1D-3D flow problem, this would mean enriching the space with the logarithmic term G.

Finally, let us note a recent improvement in the formulation of the coupled 1D-3D flow model. Recalling the geometrical setting of presented in Section 3.1, $\Omega \subset \mathbb{R}^3$ denotes a domain embedded with generalized cylinders $\Sigma \subset \Omega$, the cylinders having centreline $\Lambda \subset \mathbb{R}^1$ and boundary $\Gamma \subset \mathbb{R}^2$. In [48; 53; 18], the coupled 1D-3D flow model has been reformulated so that the source term is concentrated on the 2D cylinder boundary Γ [53; 18]. As Ω and Γ have codimension one, this improves the regularity of the solution. In particular, the pressure p is no longer singular, and one has $p \in H^{\frac{3}{2}}(\Omega)$.

While the regularity of the solution is improved, the pressure still admits a logarithmic pressure profile around the 1D domain Λ. Thus, while the solution is no longer singular, it is still multiscale in nature. I.e., the majority of the spatial pressure variation still occurs in the near vicinity of Λ, leading to the same approximation issue as was discussed in Remark 6.1.1.

With this in mind, we are currently investigating the approximation properties of this model as $R \ll h$. To resolve the multiscale nature of the problem, we are further formulating a logarithm removal method for the 3D pressure. The method itself bears many similarities with the singularity removal method presented in this work, with the function G now describing the pressure profile expected around a cylinder source. This will be communicated in future work.

Bibliography

[1] I. Aavatsmark. Interpretation of well-cell pressures on hexagonal grids in numerical reservoir simulation. *Computational Geosciences*, 20(5):1029–1042, 2016. doi: 10.1007/s10596-016-9575-2.

[2] I. Aavatsmark. Equivalent well-cell radius for hexagonal k-orthogonal grids in numerical reservoir simulation. *Applied Mathematics Letters*, 61:122 – 128, 2016. doi: 10.1016/j.aml.2016.05.013.

[3] I. Aavatsmark. Interpretation of well-cell pressures on stretched hexagonal grids in numerical reservoir simulation. *Computational Geosciences*, 20(5):1043–1060, 2016. doi: 10.1007/s10596-016-9575-2.

[4] I. Aavatsmark and R. A. Klausen. Well index in reservoir simulation for slanted and slightly curved wells in 3d grids. *SPE Journal*, 8:41–48, 2003. doi: 10.2118/75275-PA.

[5] R. Al−Khoury, P. G. Bonnier, and R. B. J. Brinkgreve. Efficient finite element formulation for geothermal heating systems. part i: steady state. *International Journal for Numerical Methods in Engineering*, 63(7):988–1013, 2005. doi: 10.1002/nme.1313.

[6] T. Apel, A.-M. Sändig, and J. R. Whiteman. Graded mesh refinement and error estimates for finite element solutions of elliptic boundary value problems in non-smooth domains. *Mathematical Methods in the Applied Sciences*, 19(1):63–85, 1996. doi: 10.1002/(SICI)1099-1476(19960110)19:1<63::AID-MMA764>3.0.CO;2-S.

[7] T. Apel, O. Benedix, D. Sirch, and B. Vexler. A priori mesh grading for an elliptic problem with dirac right-hand side. *SIAM Journal on Numerical Analysis*, 49(3): 992–1005, 2011. doi: 10.1137/090778018.

[8] D. K. Babu, A. S. Odeh, A. J. Al-Khalifa, and R. C. McCann. The relation between wellblock and wellbore pressures in numerical simulation of horizontal wells. *SPE Journal*, 6, 1991. doi: 10.2118/20161-PA.

[9] I. Babuška. Error-bounds for finite element method. *Numerische Mathematik*, 16(4): 322–333, 1971. doi: 10.1007/bf02165003.

[10] I. Babuška and M. B. Rosenzweig. A finite element scheme for domains with corners. *Numerische Mathematik*, 20(1):1–21, 1972. doi: 10.1007/BF01436639.

[11] C. Bernardi, C. Canuto, and Y. Maday. Generalized inf-sup conditions for chebyshev spectral approximation of the stokes problem. *SIAM Journal on Numerical Analysis*, 25(6):1237–1271, 1988. doi: 10.1137/0725070.

[12] S. Bertoluzza, A. Decoene, L. Lacouture, and S. Martin. Local error estimates of the finite element method for an elliptic problem with a dirac source term. *Numerical Methods for Partial Differential Equations*, 34(1):97–120, 2018. doi: 10.1002/num.22186.

[13] D. Boffi, F. Brezzi, and M. Fortin. *Mixed Finite Element Methods and Applications*. Springer-Verlag Berlin Heidelberg, 2013. ISBN 978-3-642-36519-5.

[14] D. Braess. *Finite Elements: Theory, Fast Solvers, and Applications in Solid Mechanics*. Cambridge University Press, 2001. ISBN 0521011957.

[15] S. Brenner and L. Scott. *The Mathematical Theory of Finite Element Methods*. Texts in Applied Mathematics. Springer New York, 2002. ISBN 9780387954516.

[16] C. Bromley, M. Mongillo, G. Hiriart, B. Goldstein, R. Bertani, E. Huenges, Á. Ragnarsson, J. Tester, H. Muraoka, and V. Zui. Contribution of geothermal energy to climate change mitigation: the ipcc renewable energy report. *Proceedings World Geothermal Congress*, pages 25–29, 2010.

[17] L. Cattaneo and P. Zunino. A computational model of drug delivery through microcirculation to compare different tumor treatments. *International Journal for Numerical Methods in Biomedical Engineering*, 30(11):1347–1371, 2014. doi: 10.1002/cnm.2661.

[18] D. Cerroni, F. Laurino, and P. Zunino. Mathematical analysis, finite element approximation and numerical solvers for the interaction of 3d reservoirs with 1d wells. *GEM - International Journal on Geomathematics*, 10(1):4, 2019. doi: 10.1007/s13137-019-0115-9.

[19] Y. Chen, D. Wolk, J. Reddin, M. Korczykowski, P. Martinez, E. Musiek, A. Newberg, P. Julin, S. Arnold, J. Greenberg, and J. Detre. Voxel-level comparison of arterial spin-labeled perfusion mri and fdg-pet in alzheimer disease. *Neurology*, 77(22): 1977–1985, 2011. doi: 10.1212/WNL.0b013e31823a0ef7.

[20] Z. Chen and Y. Zhang. Well flow models for various numerical methods. *International Journal of Numerical Analysis and Modeling*, 3:375–388, 2009.

[21] C. D'Angelo. *Multiscale modelling of metabolism and transport phenomena in living tissues*. PhD thesis, Politecnico di Milano, 2007. URL https://infoscience.epfl.ch/record/103742?ln=en.

[22] C. D'Angelo. Finite element approximation of elliptic problems with dirac measure terms in weighted spaces: Applications to one- and three-dimensional coupled problems. *SIAM Journal on Numerical Analysis*, 0(1):194–215, 2012. doi: 10.1137/100813853.

[23] C. D'Angelo and A. Quarteroni. On the coupling of 1d and 3d diffusion-reaction equations: Application to tissue perfusion problems. *Mathematical Models and Methods in Applied Sciences*, 18(08):1481–1504, 2008. doi: 10.1142/S0218202508003108.

[24] Y. Ding and L. Jeannin. A new methodology for singularity modelling in flow simulations in reservoir engineering. *Computational Geosciences*, 5(2):93–119, 2001. doi: 10.1023/A:1013123029671.

[25] F. Drechsler, C. Wolters, T. Dierkes, H. Si, and L. Grasedyck. A full subtraction approach for finite element method based source analysis using constrained delaunay tetrahedralisation. *NeuroImage*, 46(4):1055 – 1065, 2009. doi: 10.1016/j.neuroimage.2009.02.024.

[26] O. Edenhofer, R. Madruga, Y. Sokona, K. Seyboth, P. Matschoss, S. Kadner, T. Zwickel, P. Eickemeier, G. Hansen, S. Schlömer, and C. Stechow. Renewable energy sources and climate change mitigation: Special report of the intergovernmental panel on climate change. *Renewable Energy Sources and Climate Change Mitigation: Special Report of the Intergovernmental Panel on Climate Change*, pages 1–1075, 2011. doi: 10.1017/CBO9781139151153.

[27] C. Engwer, J. Vorwerk, J. Ludewig, and C. H. Wolters. A discontinuous galerkin method to solve the EEG forward problem using the subtraction approach. *SIAM Journal on Scientific Computing*, 39(1):B138–B164, 2017. doi: 10.1137/15m1048392.

[28] L. C. Evans. *Partial differential equations*. American Mathematical Society, Providence, R.I., 2010. ISBN 9780821849743 0821849743.

[29] R. E. Ewing, editor. *The mathematics of reservoir simulation*, volume 1 of *Frontiers in Applied Mathematics*. Society for Industrial and Applied Mathematics (SIAM), Philadelphia, PA, 1983. ISBN 0-89871-192-4.

[30] Q. Fang, S. Sakadzić, L. Ruvinskaya, A. Devor, A. D. D.A., and Boas. Oxygen advection and diffusion in a three- dimensional vascular anatomical network. *Opt Express*, 16(22), 2008. doi: 10.1364/oe.16.17530.

[31] L. Formaggia, A. Quarteroni, and A. Veneziani. Multiscale models of the vascular system. In L. Formaggia, A. Quarteroni, and A. Veneziani, editors, *Cardiovascular Mathematics: Modeling and simulation of the circulatory system*, pages 395–446, Milano, 2009. Springer Milan. ISBN 978-88-470-1152-6. doi: 10.1007/978-88-470-1152-6_11.

[32] I. Gansca, W. Bronsvoort, G. Coman, and L. Tambulea. Self-intersection avoidance and integral properties of generalized cylinders. *Computer Aided Geometric Design*, 19(9):695 – 707, 2002. doi: 10.1016/S0167-8396(02)00163-2.

[33] R. J. Gillies, P. A. Schomack, T. W. Secomb, and N. Raghunand. Causes and effects of heterogeneous perfusion in tumors. *Neoplasia*, 1(3):197–207, 1999. doi: 10.1038/sj.neo.7900037.

[34] L. Grinberg, E. Cheever, T. Anor, J. R. Madsen, and G. E. Karniadakis. Modeling blood flow circulation in intracranial arterial networks: A comparative 3d/1d simulation study. *Annals of Biomedical Engineering*, 39(1):297–309, 2011. doi: 10.1007/s10439-010-0132-1.

[35] H. B. Hales. An improved method for simulating reservoir pressures through the incorporation of analytical well functions. *SPE Journal*, 1977. doi: 10.2118/39065-MS.

[36] E. Hodneland, E. Hanson, O. Sævareid, G. Nævdal, A. Lundervold, V. Šoltészová, A. Z. Munthe-Kaas, A. Deistung, J. R. Reichenbach, and J. M. Nordbotten. A new framework for assessing subject-specific whole brain circulation and perfusion using mri-based measurements and a multi-scale continuous flow model. *PLOS Computational Biology*, 15(6):1–31, 2019. doi: 10.1371/journal.pcbi.1007073.

[37] International Energy Agency. World Energy Balances Overview. ISBN: 9789264318922, https://www.iea.org/statistics/balances/, 2019.

[38] Y. Iturria-Medina, , R. C. Sotero, P. J. Toussaint, J. M. Mateos-Pérez, and A. C. Evans. Early role of vascular dysregulation on late-onset alzheimer's disease based on multifactorial data-driven analysis. *Nature Communications*, 7(1), 2016. doi: 10.1038/ncomms11934.

[39] M. Javaux, T. Schröder, J. Vanderborght, and H. Vereecken. Use of a Three-Dimensional Detailed Modeling Approach for Predicting Root Water Uptake. *Vadose Zone J.*, 7, 2008. doi: 10.2136/vzj2007.0115.

[40] A.-R. Khaled and K. Vafai. The role of porous media in modeling flow and heat transfer in biological tissues. *International Journal of Heat and Mass Transfer*, 46 (26):4989 – 5003, 2003. doi: 10.1016/S0017-9310(03)00301-6.

[41] T. Kilpelainen, J. Heinonen, and O. Martio. *Nonlinear Potential Theory of Degenerate Elliptic Equations*. Courier Corporation, 2012, 2006. ISBN 0486450503.

[42] M. J. King and M. Mansfield. Flow simulation of geologic models. *Society of Petroleum Engineers*, 1997. doi: doi:10.2118/39065-MS.

[43] T. Koch, K. Heck, N. Schröder, H. Class, and R. Helmig. A new simulation framework for soil–root interaction, evaporation, root growth, and solute transport. *Vadose Zone J.*, 17, 2018. doi: 10.2136/vzj2017.12.0210.

[44] T. Koch, M. Schneider, R. Helmig, and P. Jenny. Modeling tissue perfusion in terms of 1d-3d embedded mixed-dimension coupled problems with distributed sources, 2019.

[45] V. A. Kondratiev and O. A. Oleinik. Boundary-value problems for partial differential equations in non-smooth domains. *Russian Mathematical Surveys*, 38(2):1–86, 1983. doi: 10.1070/RM1983v038n02ABEH003470.

[46] T. Köppl and B. Wohlmuth. Optimal a priori error estimates for an elliptic problem with dirac right-hand side. *SIAM Journal on Numerical Analysis*, 52(4):1753–1769, 2014. doi: 10.1137/130927619.

[47] T. Köppl, E. Vidotto, and B. Wohlmuth. A local error estimate for the poisson equation with a line source term. In B. Karasözen, M. Manguoğlu, M. Tezer-Sezgin, S. Göktepe, and Ö. Uğur, editors, *Numerical Mathematics and Advanced Applications ENUMATH 2015*, pages 421–429, Cham, 2016. Springer International Publishing. ISBN 978-3-319-39929-4.

[48] T. Köppl, E. Vidotto, B. Wohlmuth, and P. Zunino. Mathematical modeling, analysis and numerical approximation of second-order elliptic problems with inclusions. *Mathematical Models and Methods in Applied Sciences*, 28(05):953–978, 2018. doi: 10.1142/S0218202518500252.

[49] T. T. Köppl. *Multi-scale modeling of flow and transport processes in arterial networks and tissue*. PhD thesis, Universität München, 2015. URL https://mediatum.ub.tum.de/1237433.

[50] V. A. Koslov, V. G. Mazya, and J. Rossman. Elliptic boundary value problems in domains with point singularities. *Mathematical Surveys and Monographs*, 52, 1997.

[51] M. Kuchta, K.-A. Mardal, and M. Mortensen. Preconditioning trace coupled 3d-1d systems using fractional laplacian. *Numerical Methods for Partial Differential Equations*, 35(1):375–393, 2019. doi: 10.1002/num.22304.

[52] A. Kufner. *Weighted Sobolev Spaces*. John Wiley and Sons, 1993.

[53] F. Laurino and P. Zunino. Derivation and analysis of coupled pdes on manifolds with high dimensionality gap arising from topological model reduction. *ESAIM: M2AN*, 2019. doi: 10.1051/m2an/2019042. in press.

[54] K. S. Lee. A review on concepts, applications, and models of aquifer thermal energy storage systems. *Energies*, 3(6):1320–1334, 2010. doi: 10.3390/en3061320.

[55] K.-A. Lie. *An Introduction to Reservoir Simulation Using MATLAB/GNU Octave: User Guide for the MATLAB Reservoir Simulation Toolbox (MRST)*. Cambridge University Press, 2019. doi: 10.1017/9781108591416.

[56] A. A. Linninger, I. G. Gould, T. Marinnan, C.-Y. Hsu, M. Chojecki, and A. Alaraj. Cerebral microcirculation and oxygen tension in the human secondary cortex. *Annals of Biomedical Engineering*, 41(11):2264–2284, 2013. doi: 10.1007/s10439-013-0828-0.

[57] A. Llau, L. Jason, F. Dufour, and J. Baroth. Finite element modelling of 1d steel components in reinforced and prestressed concrete structures. *Engineering Structures*, 127:769–783, 2016. doi: 10.1016/j.engstruct.2016.09.023.

[58] H. S. Markus. Cerebral perfusion and stroke. *Journal of Neurology, Neurosurgery & Psychiatry*, 75(3):353–361, 2004. doi: 10.1136/jnnp.2003.025825.

[59] J. N. McDonald and N. A. Weiss. *International Edition A Course in Real Analysis*, volume 2. Elsevier, 1999. ISBN 0123877741.

[60] A. Mullard. Anti-amyloid failures stack up as alzheimer antibody flops. *Nature Reviews Drug Discovery*, 2019. doi: 10.1038/d41573-019-00064-1.

[61] M. Nabil and P. Zunino. A computational study of cancer hyperthermia based on vascular magnetic nanoconstructs. *Royal Society Open Science*, 3(9), 2016. doi: 10.1098/rsos.160287.

[62] R. A. Nicolaides. Existence, uniqueness and approximation for generalized saddle point problems. *SIAM Journal on Numerical Analysis*, 19(2):349–357, 1982. doi: 10.1137/0719021.

[63] J. M. Nordbotten and M. Celia. *Geological Storage of CO2: Modeling Approaches for Large-Scale Simulation*. Wiley, 2011. ISBN 9781118137079.

[64] D. Notaro, L. Cattaneo, L. Formaggia, A. Scotti, and P. Zunino. A mixed finite element method for modeling the fluid exchange between microcirculation and tissue interstitium. In G. Ventura and E. Benvenuti, editors, *Advances in Discretization Methods: Discontinuities, Virtual Elements, Fictitious Domain Methods*, pages 3–25, Cham, 2016. Springer International Publishing. ISBN 978-3-319-41246-7. doi: 10.1007/978-3-319-41246-7_1.

[65] A. Nüßing. *Fitted and unfitted finite element methods for solving the EEG forward problem*. PhD thesis, University of Münster, 2018. URL https://miami.uni-muenster.de/Record/a0133fee-1ead-4ee8-9cd8-62cfefff775b.

[66] M. Olufsen and A. Nadim. On deriving lumped models for blood flow and pressure in the systemic arteries. *Mathematical biosciences and engineering : MBE*, 1:61–80, 2004. doi: 10.3934/mbe.2004.1.61.

[67] W. H. Organization. The top 10 causes of death worldwide. https://www.who.int/news-room/fact-sheets/detail/the-top-10-causes-of-death, 2019. Accessed: 08-08-2019.

[68] D. W. Peaceman. Interpretation of well-block pressures in numerical reservoir simulation. *Society of Petroleum Engineers Journal*, 18(03):183–194, 1978. doi: 10.2118/10528-PA.

[69] D. W. Peaceman. Interpretation of well-block pressures in numerical reservoir simulation with nonsquare grid blocks and anisotropic permeability. *Society of Petroleum Engineers Journal*, 23(3), 1983. doi: 10.2118/10528-PA.

[70] J. Peiró and A. Veneziani. Reduced models of the cardiovascular system. In L. Formaggia, A. Quarteroni, and A. Veneziani, editors, *Cardiovascular Mathematics: Modeling and simulation of the circulatory system*, pages 347–394, Milano, 2009. Springer Milan. ISBN 978-88-470-1152-6. doi: 10.1007/978-88-470-1152-6_10.

[71] L. Possenti, G. Casagrande, S. D. Gregorio, P. Zunino, and M. L. Costantino. Numerical simulations of the microvascular fluid balance with a non-linear model of the lymphatic system. *Microvascular Research*, 122:101 – 110, 2019. doi: 10.1016/j.mvr.2018.11.003.

[72] A. R. Pries, T. W. Secomb, and P. A. L. Gaehtgens. Biophysical aspects of blood flow in the microvasculature. *Cardiovascular research*, 32 4:654–67, 1996. doi: 10.1016/s0008-6363(96)00065-x.

[73] J. Reichold, M. Stampanoni, A. L. Keller, A. Buck, P. Jenny, and B. Weber. Vascular graph model to simulate the cerebral blood flow in realistic vascular networks. *Journal of Cerebral Blood Flow & Metabolism*, 29(8):1429–1443, 2009. doi: 10.1038/jcbfm.2009.58.

[74] R. Scott. Finite element convergence for singular data. *Numerische Mathematik*, 21 (4):317–327, 1973. doi: 10.1007/BF01436386.

[75] T. Secomb, R. Hsu, M. Dewhirst, B. Klitzman, and J. Gross. Analysis of oxygen transport to tumor tissue by microvascular networks. *International Journal of Radiation Oncology Biology Physics*, 25(3):481 – 489, 1993.

[76] N. E. Skoglund. Simulation of flow and mechanics in the brain. Master's thesis, University of Bergen, 2019. URL http://bora.uib.no/handle/1956/20035.

[77] E. H. Starling. On the absorption of fluids from the connective tissue spaces. *The Journal of Physiology*, 19(4):312–326, 1896. doi: 10.1113/jphysiol.1896.sp000596.

[78] O. Strack. *Analytical Groundwater Mechanics*. Cambridge University Press, 2017. doi: 10.1017/9781316563144.

[79] T. Strouboulis, I. Babuška, and K. Copps. The design and analysis of the generalized finite element method. *Computer Methods in Applied Mechanics and Engineering*, 181(1):43 – 69, 2000. doi: 10.1016/S0045-7825(99)00072-9.

[80] Y. Tang and Y. He. Numerical modeling of fluid and oxygen exchanges through microcirculation for the assessment of microcirculation alterations caused by type 2 diabetes. *Microvascular Research*, 117:61 – 73, 2018. doi: 10.1016/j.mvr.2018.01.006.

[81] C. L. Tardif, A. Schäfer, R. Trampel, A. Villringer, R. Turner, and P.-L. Bazin. Open science cbs neuroimaging repository: Sharing ultra-high-field mr images of the brain. *NeuroImage*, 124:1143 – 1148, 2016. doi: 10.1016/j.neuroimage.2015.08.042. Sharing the wealth: Brain Imaging Repositories in 2015.

[82] B. O. Turesson. *Nonlinear Potential Theory and Weighted Sobolev Spaces*. Springer Berlin Heidelberg, 2000. doi: 10.1007/bfb0103908.

[83] E. Vidotto, T. Koch, T. Köppl, R. Helmig, and B. Wohlmuth. Hybrid models for simulating blood flow in microvascular networks. *Multiscale Modeling & Simulation*, 17(3):1076–1102, 2019. doi: 10.1137/18m1228712.

[84] C. J. Weiss. Finite-element analysis for model parameters distributed on a hierarchy of geometric simplices. *GEOPHYSICS*, 82(4):E155–E167, 2017. doi: 10.1190/geo2017-0058.1.

[85] S. Whitaker. Flow in porous media i: A theoretical derivation of darcy's law. *Transport in Porous Media*, 1:3–25, 1986. doi: 10.1007/BF01036523.

[86] C. Wolfsteiner, L. J. Durlofsky, and K. Aziz. Calculation of well index for nonconventional wells on arbitrary grids. *Computational Geosciences*, 7(1):61–82, 2003. doi: 10.1023/A:1022431729275.

[87] C. Wolfsteiner, S. Lee, and H. Tchelepi. Well modeling in the multiscale finite volume method for subsurface flow simulation. *Multiscale Modeling & Simulation*, 5(3): 900–917, 2006. doi: 10.1137/050640771.

[88] C. H. Wolters, H. Köstler, C. Möller, J. Härdtlein, L. Grasedyck, and W. Hackbusch. Numerical mathematics of the subtraction method for the modeling of a current dipole in eeg source reconstruction using finite element head models. *SIAM J. Scientific Computing*, 30:24–45, 2007. doi: 10.1137/060659053.

Part II:

Scientific Results

Paper A

Splitting method for elliptic equations with line sources

Ingeborg G. Gjerde, Kundan Kumar, Jan M. Nordbotten, Barbara Wohlmuth

ESAIM: M2AN **53(5)** (2019), p. 1715–1739

doi: 10.1051/m2an/2019027

ESAIM: M2AN 53 (2019) 1715–1739
https://doi.org/10.1051/m2an/2019027

ESAIM: Mathematical Modelling and Numerical Analysis
www.esaim-m2an.org

SPLITTING METHOD FOR ELLIPTIC EQUATIONS WITH LINE SOURCES

Ingeborg G. Gjerde[1,*], Kundan Kumar[1,2], Jan M. Nordbotten[1] and Barbara Wohlmuth[3]

Abstract. In this paper, we study the mathematical structure and numerical approximation of elliptic problems posed in a (3D) domain Ω when the right-hand side is a (1D) line source Λ. The analysis and approximation of such problems is known to be non-standard as the line source causes the solution to be singular. Our main result is a splitting theorem for the solution; we show that the solution admits a split into an explicit, low regularity term capturing the singularity, and a high-regularity correction term w being the solution of a suitable elliptic equation. The splitting theorem states the mathematical structure of the solution; in particular, we find that the solution has anisotropic regularity. More precisely, the solution fails to belong to H^1 in the neighbourhood of Λ, but exhibits piecewise H^2-regularity parallel to Λ. The splitting theorem can further be used to formulate a numerical method in which the solution is approximated *via* its correction function w. This recasts the problem as a 3D elliptic problem with a 3D right-hand side belonging to L^2, a problem for which the discretizations and solvers are readily available. Moreover, as w enjoys higher regularity than the full solution, this improves the approximation properties of the numerical method. We consider here the Galerkin finite element method, and show that the singularity subtraction then recovers optimal convergence rates on uniform meshes, *i.e.*, without needing to refine the mesh around each line segment. The numerical method presented in this paper is therefore well-suited for applications involving a large number of line segments. We illustrate this by treating a dataset (consisting of ∼3000 line segments) describing the vascular system of the brain.

Mathematics Subject Classification. 35J75, 65M60, 65N80.

Received October 25, 2018. Accepted April 18, 2019.

1. Introduction

Let $\Omega \subset \mathbb{R}^3$ be an open domain with the smooth boundary $\partial\Omega$, $\Lambda = \cup_{i=1}^n \Lambda_i$ be a collection of line segments Λ_i, and $\kappa \in W^{2,\infty}(\Omega)$ be a uniformly positive, scalar-valued coefficient. We consider elliptic problems with line sources of the type

$$-\nabla \cdot (\kappa \nabla u) = f\delta_\Lambda \quad \text{in } \Omega, \tag{1.1a}$$

$$\int_\Omega f\delta_\Lambda \, v \, \mathrm{d}\Omega = \sum_{i=1}^n \int_{\Lambda_i} f(s_i) v(s_i) \mathrm{d}s \quad \forall v \in C^0(\Omega), \tag{1.1b}$$

Keywords and phrases. Singular elliptic equations, finite-elements, Green's functions methods.

[1] Department of Mathematics, University of Bergen, Bergen, Norway.
[2] Department of Mathematics, Karlstad University, Karlstad, Sweden.
[3] Department of Mathematics, Technical University of Munich, Garching, Germany.
*Corresponding author: ingeborg.gjerde@uib.no

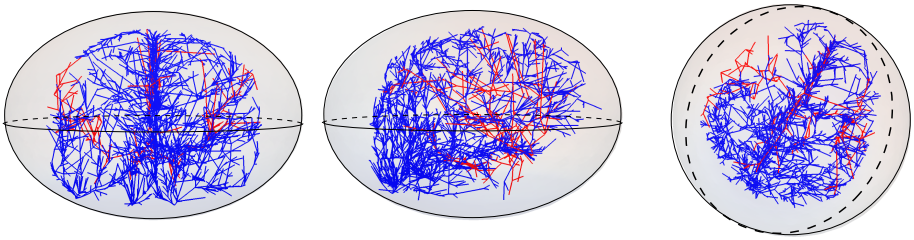

FIGURE 1. Front, side and perspective view of the arteries (red) and veins (blue) in a human brain. The arterial system is responsible for providing oxygenated blood to the brain tissue; its counterpart, the venous system, then carries deoxygenated blood back to the heart. Both systems are composed of a collection of blood vessels that individually resemble line segments Λ_i. It is therefore natural to model the arterial and venous systems as graphs $\Lambda_a = \cup_{i=1}^{n} \Lambda_{a,i}$ and $\Lambda_v = \cup_{i=1}^{n} \Lambda_{v,i}$ respectively. The dataset consists of ∼3000 line segments and was constructed from an MRI scan [42].

s_i being the arc-length of line segment i. The right-hand side f is supported on Λ and models a collection of 1D sources and sinks. The line source can be interpreted as a 1D fracture in the domain, with the variable $f : \Lambda \to \mathbb{R}$ denoting the linear mass flux from Λ into the domain. This fracture is modelled mathematically by means of a Dirac distribution on the line, understood in the sense of (1.1b).

Models of this type arise in a variety of applications, *e.g.*, in the modelling of 1D steel components in concrete structures [29] or the interference of metallic pipelines and bore-casings in electromagnetic modelling of reservoirs [43]. Of special interest are coupled 1D–3D models, where (1.1a) is coupled with a 1D flow equation defined on Λ [12]. The coupled 1D–3D model is more commonly used for biological applications, *e.g.*, in the study of blood flow in the vascularized tissue of the brain [20,37], the efficiency of cancer treatment by hyperthermia [33] and by drug delivery through microcirculation [9,35]. The use of a 1D source term is motivated by the observation that roots, blood vessels, steel components and pipelines all have negligible radii compared to the size of the simulation domain. It would therefore be quite expensive to resolve these structures as 3D objects in a mesh, and we model them instead as 1D structures embedded in Ω.

The coupled 1D–3D problem is a particular instance of mixed-dimensional PDEs, where an d-dimensional PDE is coupled to some $d-k, k < d$-dimensional PDE. A typical example can be found in fracture modelling, where a fracture is considered as a $d-1$ dimensional manifold embedded in a d-dimensional domain. We refer to [16,17,31] and references therein for dealing with some examples, Kuchta *et al.* [26] for suitable preconditioners, and Boon *et al.* [8] for a general mathematical framework to handle the d to $d-1$-dimensional coupling. The results in these works are, however, not easily transferred to the coupled 1D–3D problem, as the dimensional gap impacts the mathematical structure of the solution. In particular, an increase in the dimensional gap negatively affects the solution regularity. In fact, the line source in the right-hand side of (1.1a) induces a logarithmic type singularity in the solution, ultimately causing the solution not to be in $H^1(\Omega)$. The approximation and analysis of the line source problem therefore requires special consideration.

The existence of a solution to (1.1a) was proven in [12] by means of weighted Sobolev spaces. Convergence rates for the Galerkin finite element (FE) method were proven in [11] in terms of weighted Sobolev spaces, with results similar to those found in [3] for the 2D problem with a point source. In both of these works, the high dimensional gap was found to cause sub-optimal convergence rates on uniform meshes, with the L^2-error converging with order less than one, and no convergence in the H^1 norm. These sub-optimal convergence rates for the 2D–0D problem were found to be local to the point source in [23, 24], in the sense that linear finite elements converge optimal up to a log-factor in the L^2-norm if a small neighbourhood is removed around the

point. A similar result was proved for the 3D problem with a line source in [7, 24]. Optimal convergence rates can be retrieved in the entire domain by use of a graded mesh, *i.e.*, by a particular refinement of the mesh around each point [3] or line segment [11].

The numerical approximation of coupled 1D–3D models is similarly known to be difficult due to the presence of a line source in the 3D flow equation. We refer to [26] for preconditioners developed to treat the ill-conditioning this coupling introduces in the discretization matrix A. In this work, negative fractional Sobolev norms were found suitable to precondition the Schur complement of the system, with an extension to the positive fractional Sobolev norms considered in [4]. In [24], an alternative coupling scheme was introduced, where the source term was taken to live on the boundary of the inclusions. The result is a 1D–(2D)–3D method where the dimensional gap has been reduced to 1. This improves the regularity and thus the approximation properties of the problem, at the expense of having to resolve the 2D boundary of the inclusions.

Our approach is based on exploiting certain splitting properties of the solution, where the solution u is split into a collection of low-regularity logarithmic terms G_i, each corresponding to a line segment Λ_i, and a high-regularity correction term $w \in H^2(\Omega)$:

$$u = \sum_{i=1}^{n} E_i(f) G_i + w. \tag{1.2}$$

The term $E_i(f)$ here denotes an extension of f from the line segment Λ_i to the entire domain, the precise definition of which will be given at a later point. The logarithmic term was found by an integration of the 3D Green's function for the Laplacian over each line segment, resulting in an analytic function for the line source similar to the ones derived in [7, 40]. The correction term w solves its own elliptic equation on Ω with a given right-hand side $F \in L^{2-\epsilon}(\Omega)$ for some arbitrarily small $\epsilon > 0$. F depends on the line source intensities f_i, the endpoints of each line segment, and the coefficient κ; its regularity can be improved to $F \in L^2(\Omega)$ given some assumptions on the structure of κ.

The G_i terms completely capture the singular parts of the solution, and the sum $\sum_{i=1}^{n} f_i G_i$ therefore constitutes the low-regularity part of the split. The mathematical structure and regularity properties of u can thus be found by inspection of this term. In particular, this will reveal to us that the solution u exhibits anisotropic regularity, with the low regularity of u occurring in the plane perpendicular to the line. Formally, the line singularity acts at each surface normal to a line segment as a Dirac source term in a 2D plane, whereas along the line it inherits the regularity of f.

Besides informing us about the mathematical structure of the solution, the splitting in (1.2) suggests an alternative numerical method in which u is solved for indirectly by a correction term w. A similar approach is known for the point source problem, where it is often referred to as a singularity subtraction technique [13, 44]. With this in mind, we will refer to our method as the *singularity subtraction technique for the line source problem*. The singularity subtraction recasts (1.1a) and (1.1b) as a (3D) elliptic problem with a (3D) right-hand side belonging to $L^2(\Omega)$, a standard problem for which suitable approximation methods are well known. As the splitting works at the continuous level, this method is readily adapted to different discretization schemes; for example, we provide in [19] a mixed method adaptation of the ideas developed here. The technique can also be extended to the handle the coupled 1D–3D flow model. We show in [18] that this results in a reformulated coupled 1D–3D flow model in which all variables are smooth.

The singularity subtraction is associated with a number of advantages, the main ones being that it results in numerical methods that are (i) easy to implement, (ii) can be adapted to a variety of discretization methods, and (iii) have significantly improved convergence properties. We consider here the use of a Galerkin FE method, in which case the singularity subtraction technique can be considered as a special case of the Generalized Finite Element Method [41]. The Generalized Finite Element Method works by enriching the basis functions at locations where the analytical solution corresponding to the singularity is known (*e.g.*, displacement in a corner in an elasticity equation). This improves the convergence properties of the method; we show in this work that the singularity subtraction recovers optimal convergence rates on uniform meshes.

The singularity subtraction based methods presented in this paper are particularly well suited for problems involving a large number of line sources. This type of problem arises for example when considering flow through the vascularized tissue of the brain; the dataset describing the arterial and venous systems of the brain (shown in Fig. 1) consists of ∼3000 line segments. Moreover, this dataset is incomplete in the sense that the imaging captures only blood vessels of a certain radii. The size of this type of dataset can therefore be expected to increase as image quality is increased with improved technology. The main limitation of our approach is that it handles only a certain collection of problems. The study presented here requires the problem to be linear, moreover, the permeability coefficients has to be scalar-valued and smooth. This can be relaxed to have locally smooth coefficients, however, when the number of line segments is large, ensuring a smooth permeability even locally is restrictive.

Our approach is similar to the seminal work of Peaceman [34] in that way it uses the properties of the analytical solution to inform and improve the approximation of more general problems. The Peaceman well correction is used to account for the fact that bottom-hole pressure in a well differs greatly from the cell pressure of the cell in which it is located [15]. The correction factor itself is strongly dependent on the spatial relationsship between well and discretization, thus requiring various adaptations in order to handle different types of grids and discretizations [1,28]. The singularity subtraction, conversely, works on the continuous level, thus making it independent of the specific discretization method.

The article is structured as follows. In Section 2, we introduce the notation that will be used to state the regularity properties of the solution. We introduce here both weighted and fractional Sobolev spaces, as these are the spaces we have seen used for the coupled 1D–3D problem in the aforementioned references. In Section 3, we show that the solution admits a splitting into high and low-regularity terms, and discuss how this informs us of the mathematical structure of the solution. We start in Section 3.1 with the special case of f smooth and Λ consisting of a single line segment. With these assumptions the splitting is quite trivial, making it easier to illustrate the splitting technique itself and discuss the regularity properties of the solution. We then proceed to generalize the splitting technique, showing in Section 3.2 how to treat an arbitrary line segment Λ_i, and then in Section 3.3 how to treat the case of κ varying spatially. The decomposition section is then concluded in Section 3.4 with a splitting theorem valid for any graph Λ.

The next two sections are dedicated to the numerical approximation of (1.1a); from this point on, we treat only the case of $\kappa = 1$. In Section 4, we present two different FE methods, the first being the straight-forward discretization of (1.1a) and (1.1b). In this method, the line source is assembled explicitly into the right-hand side as a line integral; this is the same discretization as was presented in [11]. The second method is a singularity subtraction approach based on the splitting theorem in Section 3.4, where the correction function w is approximated using FE. We denote this method as the singularity subtraction based finite element (SSB-FE) method. In Section 4, we then show how the singularity subtraction leads to an improvement in the convergence rates of the method. We also discuss the modelling error introduced by neglecting some of the line segments in Λ. The article is then concluded with three numerical experiments. The first two of these serve to verify the mathematical properties and error estimates found in Sections 3 and 4, respectively. The last example uses the graph shown in Figure 1 to demonstrate the capabilities of the SSB-FE method in handling datasets with a large number of line segments.

2. Background and notation

In this section we will introduce the function spaces used in this work. Let $W^{k,p}(\Omega)$ be the standard Sobolev space,

$$W^{k,p}(\Omega) = \{u \in L^p(\Omega) : D^\beta u \in L^p(\Omega) \text{ for } |\beta| \leq k\},$$

with β denoting a multi-index and D^β the corresponding weak distributional derivative of u. This is a Banach space endowed with the norm

$$\|u\|^p_{W^{k,p}(\Omega)} = \sum_{|\beta|\le k} \|D^\beta u\|^p_{L^p(\Omega)}.$$

For $p = 2$ it is also a Hilbert space, customarily denoted $H^k(\Omega) = W^{k,2}(\Omega)$, with inner product

$$(u, v)_{H^k(\Omega)} = \sum_{|\beta|\le k} \int_\Omega D^\beta u \, D^\beta v \, \mathrm{d}\Omega.$$

As we will see, solutions to (1.1a) and (1.1b) fail to belong to $H^1(\Omega)$; for this reason, we consider also weighted and fractional Sobolev spaces. To define the weighted Sobolev space, let $-1 < \alpha < 1$, and take L^2_α to denote the weighted Hilbert space

$$L^2_\alpha(\Omega) := \left\{ u : \int_\Omega u^2 r^{2\alpha} \mathrm{d}\Omega < \infty \right\},$$

equipped with the inner product

$$(u, v)_{L^2_\alpha} = \int_\Omega r^{2\alpha} uv \, \mathrm{d}\Omega.$$

For $\alpha > 0$, the weight r^α has the power to dampen out singular behaviour in the function being normed, and we have the relation $L^2_{-\alpha}(\Omega) \subset L^2(\Omega) \subset L^2_\alpha(\Omega)$. A weighted Sobolev space $V^k_\alpha(\Omega)$ can now be constructed as [21, 25]

$$V^k_\alpha(\Omega) = \{D^\beta u \in L^2_{\alpha+|\beta|-k}(\Omega), |\beta| \le m\},$$

equipped with the norm

$$\|u\|^2_{V^k_\alpha(\Omega)} = \sum_{|\beta|\le k} \|D^\beta u\|^2_{L^2_{\alpha+|\beta|-k}}.$$

This weighted space takes the order of the derivative into consideration when computing the weight function, increasing the weighting-factor to compensate for the regularity loss due to an extra derivative. We shall use mainly $V^1_\alpha(\Omega)$, in which the norm can be stated more simply as $\|u\|^2_{V^1_\alpha(\Omega)} = \|u\|^2_{L^2_{\alpha-1}(\Omega)} + \|\nabla u\|^2_{L^2_\alpha(\Omega)}$. The space $V^k_\alpha(\Omega)$ admits weighted properties analogously to those of the regular Sobolev space, *e.g.*, a weighted version of the Poincar inequality [27]:

$$\|u\|_{L^2_{\alpha-1}(\Omega)} \le C_\alpha \|\nabla u\|_{L^2_\alpha(\Omega)} \quad \forall\, u \in V^1_\alpha(\Omega) : u_{|\partial\Omega} = 0.$$

Finally, let us also define the fractional Sobolev space. For $\Omega \subset \mathbb{R}^d$, we define fractional Sobolev space $H^s(\Omega), s \in (0, 1)$ using the norm,

$$\|u\|_{H^s(\Omega)} = \|u\|_{L^2(\Omega)} + \int_\Omega \int_\Omega \frac{|u(x) - u(y)|^2}{|x - y|^{d+2s}} \mathrm{d}x\mathrm{d}y.$$

We also recall the embedding result of $W^{1,p}(\Omega)$, $\dfrac{2d}{d+2} < p < 2$ in $H^s(\Omega)$ for $s = 1 - d(\frac{1}{p} - \frac{1}{2})$ (see *e.g.*, [2], Thm 7.58).

3. Decomposition and regularity properties

We consider the model in (1.1a) and (1.1b), posed in a bounded, open domain Ω with smooth boundary $\partial\Omega$, and Dirichlet boundary conditions;

$$-\nabla\cdot(\kappa\nabla u) = f\delta_\Lambda \qquad \text{in } \Omega, \tag{3.1a}$$

$$u = u_D \qquad \text{on } \partial\Omega, \tag{3.1b}$$

where $\Lambda = \cup_{i=1}^n \Lambda_i$ denotes a collection of line segments $\Lambda_i \subset \Omega$, $u_D \in C^2(\bar{\Omega})$ some given boundary data, and $\kappa \in W^{2,\infty}(\Omega)$ a uniformly positive, scalar-valued permeability coefficient. In this section we will show that solutions to (3.1a) and (3.1b) admit a split into singular and high-regularity parts. We start in Section 3.1 by illustrating the splitting technique itself and discussing the information it reveals concerning the structure and regularity of the solution. We do this by treating the simple case of $\kappa = 1$ and Λ consisting of a single line with its endpoints contained in the boundary of Ω. In Section 3.2, we then extend the splitting technique to handle arbitrary line sources in the domain, and show that this yields similar results for the regularity. We then proceed to treat the case of κ varying in Section 3.3, before concluding in Section 3.4 with a general proof of the splitting properties of solutions to (1.1a). The proof relies on the discussions in the preceding parts and a simple application of the superposition principle.

3.1. The splitting technique

Let us assume $f \in H^2(\Lambda)$, $\kappa = 1$ and Λ consists of a single line segment passing through the domain Ω, meaning Λ has its endpoints contained in $\partial\Omega$. For simplicity, we assume $f = 0$ on $\partial\Omega$, meaning that the line source is in-active on the boundary. Next, we orient the coordinate system s.t. Λ lies along the z-axis, $\Lambda = (0,0,z) \in \Omega$, and employ a cylindrical coordinate system with $r = \sqrt{x^2+y^2}$. The solution to (3.1a) now admits a splitting into an explicit, low-regularity term $f(z)G(r)$ and a high-regularity correction term w:

$$u(r,z) = -\frac{1}{2\pi}\left(\underbrace{f(z)G(r)}_{\text{line singularity}} + \underbrace{w(r,z)}_{\text{correction}}\right), \tag{3.2}$$

where $G = \ln(r)$ and the correction term w is defined as the solution of

$$-\Delta w = f''(z)G(r) \qquad \text{in } \Omega, \tag{3.3a}$$

$$w = -2\pi u_D - f(z)G(r) \qquad \text{on } \partial\Omega, \tag{3.3b}$$

The choice of $G = \ln(r)$ is motivated by the observation that $-\ln(r)/2\pi$ is the fundamental solution for $d = 2$. Letting S_{z_0} be the intersection of Ω with the plane perpendicular to Λ at a given height z_0, *i.e.*, $S_{z_0} = \{(r, z_0) \in \Omega\}$, it is well known that the Laplacian of $\ln(r)$ in the domain S_{z_0} returns a Dirac point source located in $(0,0,z_0)$, *i.e.*,

$$-\frac{1}{2\pi}\int_{S_{z_0}} \Delta\ln(r) v \,\mathrm{d}S = v(0,z_0) \quad \forall\, v \in C^0(\bar{\Omega}). \tag{3.4}$$

It follows then that the Laplacian of G returns the line source on Λ, *i.e.*:

$$-\frac{1}{2\pi}\int_\Omega \Delta G\, v \,\mathrm{d}\Omega = -\frac{1}{2\pi}\int_z\int_{S_z} \Delta\ln(r)\, v \,\mathrm{d}S\,\mathrm{d}x \tag{3.5}$$

$$= \int_\Lambda v \,\mathrm{d}\Lambda \quad \forall v \in C^0(\bar{\Omega}). \tag{3.6}$$

The $f(z)G(r)$ term in the decomposition thus acts by prescribing in u a line source of the correct intensity f, with the correction function w acting to ensure that u satisfies the given boundary conditions.

The existence of the correction function w follows from standard elliptic theory. By assumption, $f''(z) \in L^2(\Lambda)$, and $G(r) \in L^2(\Omega)$ can be shown by calculation. It follows that the right-hand side in (3.3a) belongs to $L^2(\Omega)$, and that a $w \in H^2(\Omega)$ exists solving (3.3a) and (3.3b) in a weak sense. For an example of what each term in the split might look like, the reader is invited to examine Figure 4.

To see that u in (3.2) indeed solves (1.1a), let us calculate its Laplacian:

$$-\Delta u = \frac{1}{2\pi}\left(\underbrace{f(z)\Delta_\perp G(r)}_{f(z)\delta_\Lambda} + \underbrace{2\nabla_\perp G(r)\cdot\nabla_\parallel f}_{=0 \text{ as } \nabla f \perp \nabla G} + G(r)\Delta_\parallel f(z) + \Delta w(r,z) \right), \tag{3.7}$$

where $\nabla_\parallel$ and $\nabla_\perp$ denote the gradient taken in the line parallel to the line and in the plane perpendicular to the line, respectively; the gradient can then be written as $\nabla = \nabla_\perp + \nabla_\parallel$. By construction, the two last terms in (3.7) cancel, and we are left with

$$\frac{1}{2\pi}\int_\Omega f(z)\Delta_\perp G(r)\, v \,\mathrm{d}\Omega = \int_\Lambda f v \,\mathrm{d}\Lambda \quad \forall v \in C^0(\bar{\Omega}). \tag{3.8}$$

It follows that the u given by (3.2) solves (1.1a) in a weak sense.

From the decomposition, we can now investigate the regularity of the solution. Provided that the only source of regularity loss stems from the right-hand side, the correction term w was found to belong to $H^2(\Omega)$; for this reason, we refer to it as being the high-regularity term in the split (3.2). To see that $f\ln(r)$ is the low regularity term in u, let us consider the gradient of $\ln(r)$. A straightforward calculation shows us that $\ln(r) \in L^p(S_{z_0})$ for any $p < \infty$. Similarly, we have $\ln(r) \in L^2_{\alpha-1}$ for any $\alpha > 0$. As for the gradient, another calculation shows

$$\nabla_\perp \ln(r) = \frac{(x,y)}{r^2} \in \begin{cases} L^p(S) & \text{for } p < 2, \\ L^2_\alpha(\Omega) & \text{for } \alpha > 0. \end{cases} \tag{3.9}$$

In terms of fractional Sobolev space we have $W^{1,p}(S), 1 < p < 2$ embedded in $H^s(\Omega)$ for $s = 1 - 2(\frac{1}{p} - \frac{1}{2})$. Thus, the solution u belonging to $\{u \in W^{1,p}(\Omega), u_{zz} \in L^2(\Omega)\}$ implies $\{u \in H^s(\Omega), u_{zz} \in L^2(\Omega)\}$, $s \in (0,1)$.

To summarize, we have the following results for the regularity of u:

$$u \in \begin{cases} W^{1,p}(\Omega) \cap \{u : u_{zz} \in L^2(\Omega)\} & \text{for } p < 2, \\ V^1_\alpha(\Omega) & \text{for } \alpha > 0 \\ H^s(\Omega) \cap \{u : u_{zz} \in L^2(\Omega)\} & \text{for } s \in (0,1). \end{cases} \tag{3.10}$$

We see that the solution u evades $H^1(\Omega)$, with the regularity loss due to the singular behaviour in the plane normal to Λ. Moreover, the regularity loss is local to the region surrounding Λ, meaning that u retrieves full H^2 regularity if a small region is removed around Λ. To be more precise, let U_ϵ denote a tubular radius surrounding Λ,

$$U_\epsilon = \{(x,y,z) : \sqrt{x^2+y^2} < \epsilon\}, \tag{3.11}$$

and Ω_ϵ what remains when this region is removed, *i.e.*, $\Omega_\epsilon = \Omega \setminus U_\epsilon$. We then have $u \in H^2(\Omega_\epsilon)$ for any $\epsilon > 0$. Lastly, we see that parallel with Λ the solution inherits the regularity of f, and therefore exhibits high regularity in the z-direction.

3.2. Decomposition and regularity for arbitrary line sources

The decomposition presented in the previous section is valid for the case $f \in H^2(\Lambda)$ with the line Λ passing through the domain and $f = 0$ on $\Lambda \cap \partial\Omega$. This excludes, however, a number of interesting scenarios, *e.g.*, when Λ is allowed to branch. For this reason, let us now extend the decomposition technique to handle Λ being some arbitrary line segment between the points $\mathbf{a}, \mathbf{b} \in \Omega$, keeping the assumptions of $\kappa = 1$ and $f \in H^2(\Lambda)$.

The line Λ can be described by the parametrization $\mathbf{y} = \mathbf{a} + \boldsymbol{\tau} t \quad \text{for } t \in (0, L)$, where $L = \|\mathbf{b} - \mathbf{a}\|$ denotes the Euclidean norm and $\boldsymbol{\tau} = (\mathbf{b} - \mathbf{a})/L$ is the normalized tangent vector of Λ. As in Section 3.1, we want to construct a function G so that its Laplacian satisfies

$$\int_\Omega -\Delta G\, v \,\mathrm{d}\Omega = \int_\Lambda v \,\mathrm{d}\Lambda \quad \forall v \in C^0(\bar{\Omega}). \tag{3.12}$$

Considering for the moment $\Omega = \mathbb{R}^3$, the Green's function for the Laplacian is given by

$$G_{3D}(\mathbf{x}, \mathbf{y}) = \frac{1}{4\pi} \frac{1}{\|\mathbf{x} - \mathbf{y}\|}, \tag{3.13}$$

and a candidate G can now be found by the convolution of δ_Λ and $G_{3D}(\mathbf{x}, \mathbf{y})$:

$$G(\mathbf{x}) = \int_\Omega \frac{\delta_\Lambda}{\|\mathbf{x} - \mathbf{y}\|} \,\mathrm{d}\mathbf{y} \tag{3.14}$$

$$= \int_0^L \frac{1}{\|\mathbf{x} - (\mathbf{a} + \boldsymbol{\tau} t)\|} \,\mathrm{d}t \tag{3.15}$$

$$= \ln\left(\frac{r_b + L + \boldsymbol{\tau} \cdot (\mathbf{a} - \mathbf{x})}{r_a + \boldsymbol{\tau} \cdot (\mathbf{a} - \mathbf{x})} \right), \tag{3.16}$$

where $r_b(\mathbf{x}) = \|\mathbf{x} - \mathbf{b}\|$ and $r_a(\mathbf{x}) = \|\mathbf{x} - \mathbf{a}\|$.

Solving now the line source problem with f as the line source intensity, the solution admits the decomposition

$$u = \frac{1}{4\pi} \left(\underbrace{E(f)G}_{\text{line singularity}} + \underbrace{w}_{\text{correction}} \right), \tag{3.17}$$

where $E : H^2(\Lambda) \to H^2(\Omega) \cap C^2(\bar{\Omega})$ denotes a suitable extension of the line source intensity f into the domain Ω. Depending on the choice of extension, the correction term w must solve

$$-\Delta w = F \qquad \text{in } \Omega, \tag{3.18a}$$

$$w = 4\pi u_D - fG \qquad \text{on } \partial\Omega., \tag{3.18b}$$

with right-hand side F given by

$$F = \Delta E(f) G + 2 \nabla E(f) \cdot \nabla G. \tag{3.19}$$

The $1/4\pi$-scaling of G in (3.17) differs from the $-1/2\pi$-scaling in Section 3.1 as we now used the fundamental solution for $d = 3$. To be more precise, the scalings $1/2\pi$ and $1/4\pi$ enter in the fundamental solution as the volume of a unit ball in $\mathbb{R}^d$ for dimensions $d = 2$ and $d = 3$, respectively (see *e.g.*, [14], p. 22). The relation

$$\lim_{L \to \infty} \frac{1}{4\pi} \ln\left(\frac{r_b + L + \boldsymbol{\tau} \cdot (\mathbf{a} - \mathbf{x})}{r_a + \boldsymbol{\tau} \cdot (\mathbf{a} - \mathbf{x})} \right) \approx -\frac{1}{2\pi} \ln(r);$$

is used in electromagnetism to approximate the potential of an infinite length line charge. The splitting with $-\ln(r)/2\pi$ introduced in Section 3.1 can thus be thought of to hold for any infinite length line segment. It is

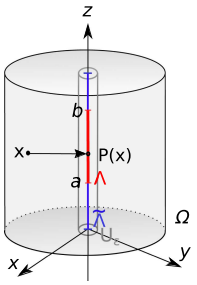

FIGURE 2. A cylindrical domain Ω and the line segment $\Lambda = \{(0,0,z) : z \in [a,b]\}$, its elongation $\tilde{\Lambda} = \{(0,0,z) \in \Omega\}$, and a projection operator $P : \Omega \to \tilde{\Lambda}$ taking a point in the domain to the closest point on $\tilde{\Lambda}$.

further valid for a smooth line source intensity f as f is then H^2-extendible to the infinite extension of the line segment. The same does not hold if f is discontinuous along Λ; for this case, it is necessary to use G as it is given in (3.16).

The regularity of the correction function w thus depends now on the choice of extension E; for $w \in H^2(\Omega)$, it is necessary to require $F \in L^2(\Omega)$. By a calculation, one finds that $\nabla G_\perp$ fails to be L^2-integrable in the neighbourhood of Λ. The result $w \in H^2(\Omega)$ thus requires choosing E so that the term involving $\nabla G_\perp$ is cancelled; this can be achieved, for example, by choosing $E(f)$ s.t. $\nabla_\perp E(f) = (0,0)$ in U_ϵ. Assuming $f = f(s)$ is a given, analytic function with respect to the arc length parameter s, the extension operator can be chosen as

$$E(f)(\mathbf{x}) = f(P(\mathbf{x})) \text{ for } \mathbf{x} \in \Omega \tag{3.20}$$

where $P : \Omega \to \tilde{\Lambda}$, $\mathbf{x} \to (\mathbf{x} - \mathbf{a}) \cdot \boldsymbol{\tau}$ denotes the orthogonal projection of a point $\mathbf{x}$ onto the elongation of Λ, as is illustrated in Figure 2. For an example of what the splitting might look like with this choice of extension, the reader is invited to examine Figure 5.

Given the extension (3.20), the right-hand side F can be stated more explicitly. To see this, let us first note that

$$\nabla G = \frac{\frac{\mathbf{x}-\mathbf{b}}{r_b} - \boldsymbol{\tau}}{L + r_b + \boldsymbol{\tau} \cdot (\mathbf{a} - \mathbf{x})} - \frac{\frac{\mathbf{x}-\mathbf{a}}{r_a} - \boldsymbol{\tau}}{r_a + \boldsymbol{\tau} \cdot (\mathbf{a} - \mathbf{x})}, \tag{3.21}$$

and that the gradient and Laplacian of $E(f)$ are given by $\nabla E(f) = f'(P(\mathbf{x}))\boldsymbol{\tau}$ and $\Delta E(f) = f''(P(\mathbf{x}))\|\boldsymbol{\tau}\| = f''(P(\mathbf{x}))$. It follows that F, for this particular choice of extension operator, is given by

$$F = f''(p(\mathbf{x}))G + f'(p(\mathbf{x}))\left(\frac{1}{r_a} - \frac{1}{r_b}\right). \tag{3.22}$$

To see that $F \in L^2(\Omega)$, let us for simplicity assume the domain to be cylindrical around Λ, and shift the coordinate system so that Λ lies along the z-axis, $\Lambda = \{(0,0,z) : \ z \in [a,b]\}$. The extension $E(f)$ can then be expressed more simply as $E(f) = f(z)$ and the function G as

$$G(r,z)\frac{1}{4\pi}\ln\left(\frac{r_b - (z-b)}{r_a - (z-a)}\right) \quad \text{where } r_a = \sqrt{r^2 + (z-a)^2} \quad \text{and } r_b = \sqrt{r^2 + (z-b)^2}. \tag{3.23}$$

Without loss of generality, let us shift the coordinate system so that the endpoint $(0,0,b)$ is the origin: a calculation then shows us that $f'(z)/r_b \in L^2(\Omega)$:

$$\|f'(z)/r_b\|^2_{L^2(\Omega)} = \int_0^{2\pi}\int_0^Z f'(z)^2 \int_0^R \frac{1}{r^2+z^2} r \,\mathrm{d}r\mathrm{d}z\,\mathrm{d}\theta \tag{3.24}$$

$$= 2\pi \int_0^Z f'(z)^2 \ln\left(\frac{R^2}{z^2}+1\right)\mathrm{d}z < \infty, \tag{3.25}$$

and that $f(z)\ln(r_b-(z-b)) \in L^2(\Omega)$:

$$\|\ln(r_b-z)\|^2_{L^2(\Omega)} = \int_0^{2\pi}\int_0^Z f(z)^2 \int_0^R \ln(\sqrt{r^2+z^2}-z)^2 r\,\mathrm{d}r\mathrm{d}z\mathrm{d}\theta < \infty. \tag{3.26}$$

The terms depending on r_a can be similarly treated by shifting the origin to $(0,0,a)$.

It only remains to understand the regularity properties of the solution. As before, the correction term w and extension $E(f)$ both belong to $H^2(\Omega)$, and the low regularity terms in u are now $\ln(r_b-(z-b))$ and $\ln(r_a-(z-a))$. Both of these logarithmic terms belong to $L^2_{\alpha-1}(\Omega)$. To understand the regularity of their gradients, considering the domain Ω/Λ, in which case the gradient of $\ln(r_b-(z-b))$ is given by

$$\nabla \ln(r_b-z) = \left(\frac{x}{r^2+z^2-z\sqrt{r^z+z^2}}, \frac{y}{r^2+z^2-z\sqrt{r^z+z^2}}, -\frac{1}{r_b}\right). \tag{3.27}$$

Shifting again the coordinate system so that $(0,0,b)$ is the origin, we can examine the norm of this gradient in a weighted $L^2_\alpha(\Omega)$. A straightforward calculation reveals

$$\|\nabla_\parallel \ln(r_b-z)\|^2_{L^2_\alpha(\Omega)} = \int_\Omega \frac{r^{2+\alpha}}{(r^2+z^2-z\sqrt{r^z+z^2})^2}\,\mathrm{d}\Omega \tag{3.28}$$

$$= \int_0^{2\pi}\int_0^R\int_a^b \frac{r^{3+\alpha}}{(r^2+z^2-z\sqrt{r^z+z^2})^2}\,\mathrm{d}z\,\mathrm{d}r\,\mathrm{d}\theta \tag{3.29}$$

$$= 2\pi\int_0^R \left[2r^{\alpha-1}\left(\sqrt{z^2+r^2}+z\right) - r^\alpha \arctan\left(\frac{z}{r}\right)\right]_a^0 \mathrm{d}r \tag{3.30}$$

$$= 2\pi\int_0^R 2r^{\alpha-1}\left(r-\sqrt{a^2+r^2}-a\right) + r^\alpha \arctan\left(\frac{a}{r}\right)\mathrm{d}r \tag{3.31}$$

$$< \infty \quad \text{if } \alpha > 0. \tag{3.32}$$

A similar argument holds for $\nabla\ln(r_a-(z-a))$, and for the L^p-norm with $p<2$. For the z-component of these gradients, recall $1/r_b, 1/r_a \in L^2(\Omega)$. Notice however, that u_{zz} falls just short of belonging to $L^2(\Omega)$. The regularity properties are therefore as follows:

$$u \in \begin{cases} W^{1,p}(\Omega)\cap\{u_{zz}\in L^p(\Omega)\} & \text{for } p<2, \\ V^1_\alpha(\Omega) & \text{for } \alpha>0, \\ H^s(\Omega)\cap\{u_{zz}\in L^p(\Omega)\} & \text{for } s<1, p<2. \end{cases} \tag{3.33}$$

As in the previous section, the solution u thus barely eludes $H^1(\Omega)$. The regularity loss is again local to the region surrounding Λ, meaning $u \in H^2(\Omega_\epsilon)$ for any $\epsilon > 0$. Moreover, the solution exhibits anisotropic regularity properties, with improved regularity parallel to the line.

3.3. Spatially varying permeability

Let us now extend the splitting technique to handle spatially varying κ. Assuming $\kappa \in W^{2,\infty}(\Omega)$ and $\kappa > 0$, the solution u to (1.1a) admits the splitting

$$u = \frac{1}{4\pi}\left(\underbrace{\frac{E(f)G}{\kappa}}_{\text{line singularity}} + \underbrace{w}_{\text{correction}} \right), \tag{3.34}$$

with the correction term w solving

$$-\nabla \cdot (\kappa \nabla w) = F \qquad \text{in } \Omega, \tag{3.35a}$$

$$w = 4\pi u_D - fG \qquad \text{on } \partial\Omega \tag{3.35b}$$

with right-hand side

$$F = \left(\Delta E(f) - \frac{E(f)\,\Delta\kappa + \nabla E(f) \nabla \kappa}{\kappa} + \frac{E(f)|\nabla \kappa|^2}{\kappa^2} \right) G + \left(2\nabla E(f) - \frac{E(f)\nabla\kappa}{\kappa^2} \right) \cdot \nabla G \tag{3.36}$$

To see that (3.34) solves (1.1a), we calculate $-\nabla \cdot (\kappa \nabla u)$. By construction, this yields the single term

$$-\nabla \cdot (\kappa \nabla u) = -\frac{1}{4\pi} f \Delta G. \tag{3.37}$$

Furthermore, we know from Section 3.2 that this term returns the line source with required intensity f.

The regularity of w depends now on the behaviour of κ. Recall that $\nabla_\perp G$ falls just short of belonging to $L^2(\Omega)$, and consequently

$$F \in \begin{cases} L^p(\Omega) & \text{for } p < 2, \\ L^2_\alpha(\Omega) & \text{for } \alpha > 0, \end{cases} \qquad \Rightarrow \qquad w \in \begin{cases} W^{2,p}(\Omega) & \text{for } p < 2, \\ V^1_\alpha(\Omega) & \text{for } \alpha > 0, \\ H^k(\Omega) & \text{for } k < 2. \end{cases} \tag{3.38}$$

We see that for general $\kappa \in W^{2,p}(\Omega)$ the correction function w falls just short of belonging to $H^2(\Omega)$. Notice, however, that it still constitutes a higher regularity term compared to the full solution $u \not\in H^1(\Omega)$. Moreover, given the existence of some $\epsilon > 0$ such that $\nabla_\perp \kappa = 0$ in the small tubular neighbourhood U_ϵ, R will indeed belong to $L^2(\Omega)$ and we recover $w \in H^2(\Omega)$.

3.4. Splitting theorem

We are now ready to summarize the results of Sections 3.1-3.3 with a splitting theorem. The results hold for any collection of line sources δ_Λ when Λ is a collection of line segments and f is piecewise H^2 on each line segment. The line source intensity f is thus allowed to contain jumps. The jump can be handled by splitting the line segment containing it into two pieces. By superposition, these two line segments can be handled separately using the splitting technique shown in Section 3.2.

Theorem 3.1 (Singularity splitting theorem for elliptic equations with line sources)**.** *Let $\Lambda = \cup_{i=1}^n \Lambda_i$ be a collection of line segments Λ_i, f be a piecewise H^2 function on each line segment Λ_i, and $\kappa \in W^{2,p}(\Omega)$ be a positive, scalar-valued permeability. The solution $u \in W^{1,p}(\Omega)$ for $p < 2$ solving (1.1a) then admits the split*

$$u(\mathbf{x}) = \frac{1}{4\pi}\left(\sum_{i=1}^n \frac{E_i(f)G_i}{\kappa} + w \right), \tag{3.39}$$

where G_i is the logarithmic term

$$G_i(\mathbf{x}) = \ln\left(\frac{r_{b,i} + L_i + \boldsymbol{\tau}_i \cdot (\mathbf{a}_i - \mathbf{x})}{r_{a,i} + \boldsymbol{\tau}_i \cdot (\mathbf{a}_i - \mathbf{x})}\right), \tag{3.40}$$

$E_i(f)$ is an extension operator $E_i(f) : H^2(\Lambda) \to H^2(\Omega)$ that extends f from line segment Λ_i into the domain, assumed to satisfy

$$\begin{aligned} &\text{(i)} \quad E_i(f)(\mathbf{x}) = f(\mathbf{x}) \text{ for } \mathbf{x} \in \Lambda_i, \\ &\text{(ii)} \quad E_i(f) \in H^2(\Omega), \\ &\text{(iii)} \quad \nabla G_i \cdot \nabla E_i(f) \in L^2(\Omega), \end{aligned}$$

and w solves

$$-\nabla \cdot (\kappa \nabla w) = F \qquad \text{in } \Omega, \tag{3.41}$$

$$w = w_D \qquad \text{on } \partial\Omega, \tag{3.42}$$

with right-hand side F given by

$$F = \sum_{i=1}^{n} \left(\Delta E_i(f) - \frac{E_i(f)\Delta\kappa + \nabla E_i(f) \cdot \nabla\kappa}{\kappa} + \frac{E_i(f)|\nabla\kappa|^2}{\kappa^2}\right) G_i + \left(2\nabla E_i(f) - \frac{E_i(f)\nabla\kappa}{\kappa}\right) \cdot \nabla G_i, \tag{3.43}$$

and boundary data w_D given by

$$w_D = 4\pi u_D - \sum_{i=1}^{n} E_i(f) G_i. \tag{3.44}$$

Proof. A direct calculation shows that, for u being the solution given in (3.39),

$$-\nabla \cdot (\kappa \nabla u) = \frac{1}{4\pi}\left(\sum_{i=1}^{n} E_i(f)\Delta G_i + \Delta E_i(f) G_i + 2\nabla E_i(f) \cdot \nabla G_i - \nabla \cdot \left(\frac{\nabla\kappa}{\kappa} E_i(f) G_i\right) - \nabla \cdot (\kappa \nabla w)\right) \tag{3.45}$$

By construction, all these terms cancel except the first, and we have

$$-\nabla \cdot (\kappa \nabla u) = \frac{1}{4\pi}\left(\sum_{i=1}^{n} E_i(f)\Delta G_i)\right). \tag{3.46}$$

Recalling now from Section 3.2 that

$$\int_\Omega -(\Delta G_i) v \, \mathrm{d}\Omega = \int_{\Lambda_i} v \, \mathrm{d}\Lambda_i \quad \forall v \in C^0(\bar{\Omega}), \tag{3.47}$$

we see that

$$-\nabla \cdot (\kappa \nabla u) = f \delta_\Lambda, \tag{3.48}$$

where the Dirac distribution on the line is understood in the sense of (1.1b). Moreover, by construction, u matches the prescribed boundary conditions. It follows that the u constructed in (3.39) solves (3.1a) and (3.1b) in a weak sense. □

4. Numerical methods

Let us now consider the numerical approximation of (3.1a) and (3.1b) by finite element methods. From this point on, we consider only $\kappa = 1$. For the numerical discretization we will make use of both simplicial and prismatic Lagrange elements, the latter as it lets us study the anisotropic properties of the solution. We consider two different numerical methods, where the first is the standard lowest-order Galerkin FE method (3.1a) introduced in [11]. The second method is based on the splitting properties of the solution: Using Theorem 3.1, we can formulate a numerical method in which u is approximated *via* its correction function w. We shall refer to this method as the Singularity Subtraction Based Finite Element (SSB-FE) method for the line source problem.

4.1. Discretization

Let us assume the domain Ω is a polyhedron that readily admits a partitioning $\mathcal{T}_{K,h}$ into simplicials K,

$$\bar{\Omega} = \bigcup_{K \in \mathcal{T}_{K,h}} K,$$

as well as a partitioning $\mathcal{T}_{P,h}$ into prisms P,

$$\bar{\Omega} = \bigcup_{P \in \mathcal{T}_{P,h}} P.$$

The prismatic elements $P \in \mathcal{T}_{P,h}$ consist of the product $T \times I$ between a triangle T in the x, y-plane and an interval I in the z-axis. The simplicial mesh is characterized by the mesh discretization parameter h, taken as maximum element size $h = \max_{K \in \mathcal{T}_{K,h}} h_K$. The prismatic element is characterized by the two mesh discretization parameters $h_\perp$ and $h_\parallel$, where $h_\perp = \max_{T \times I \in \mathcal{T}_{P,h}} h_T$ measures the size of the triangles in the x, y-plane, and $h_\parallel = \max_{T \times I \in \mathcal{T}_{P,h}} h_I$ measures the discretization of the interval along the z-axis. Both meshes $\mathcal{T}_{K,h}$ and $\mathcal{T}_{P,h}$ are assumed to satisfy all the requirements of a conforming mesh.

The partitionings can now be associated with discrete spaces. For the simplicial partitioning $\mathcal{T}_{K,h}$ we pick the standard conforming space

$$V_{u_D}^{K,h} = \{v_h \in C_{u_D}^0(\Omega),\ v_h|_K \in \mathbb{P}_1 \text{ where } K \in \mathcal{T}_{K,h}\},$$

where $\mathbb{P}^1$ denotes the space of polynomials of degree 1 and $C_{u_D}^0(\Omega)$ the space of continuous elements that equal the interpolation of u_D on the boundary, *i.e.*,

$$C_{u_D}^0(\Omega) = \{u \in C^0(\Omega) : u|_{\partial\Omega} = \mathcal{I}_h u_D\}.$$

Similarly, for the prismatic partitioning $\mathcal{T}_{P,h}$ we pick the conforming space

$$V_{u_D}^{P,h} = \Big\{v_h \in C_{u_D}^0(\Omega),\ v_h(x,y,z)|_P = \sum_{i=1}^{3}\sum_{j=2}^{3} \sigma_{ij}\lambda_i(x,y)l_j(z), \\ \text{where } P \in \mathcal{T}_{P,h}, P = T \times I, \sigma_{ij} \in \mathbb{R}, \lambda_i \in \mathbb{P}^1(T), l_j \in \mathbb{P}^1(I)\Big\}, \quad (4.1)$$

defined on each prism $P = T \times I$ as the Cartesian product between linear elements defined on the triangle T and linear elements defined on each interval I. Similar to the simplicial elements, the degree of freedoms for the prismatic element are defined on its vertices, as is illustrated in Figure 3.

The first order Galerkin approximation of (1.1a), which we shall denote as the standard FE method, can now be introduced: Find $u_h \in V_{u_D}^h$ s.t.

$$(\nabla u_h, \nabla v_h)_\Omega = (f, v_h)_\Lambda \qquad \text{for all } v_h \in V_0^h, \quad (4.2)$$

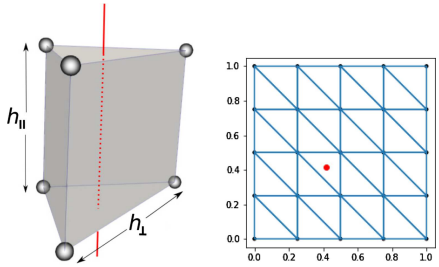

FIGURE 3. *Right panel*: prismatic element used in the finite element methods, with its degrees of freedom indicated by grey spheres, and line placement in red. *Left panel*: line placement in a horizontal cross-section of the coarsest mesh.

where V^h can be either $V^{K,h}$ or $V^{P,h}$. The stability of this approximation was shown in [11] for the simplicial type space $V^{K,h}$, and we choose here to assume this can be extended to hold also for the prismatic type space $V^{P,h}$.

The line source in the right-hand side of (4.2) is well known to cause sub-optimal convergence rates for the approximation. For this reason, we define the SSB-FE method, in which u is solved for *via* its correction function w: Find $w_h \in V^h_{w_D}$ such that

$$(\nabla w_h, \nabla v_h)_\Omega = (F, v_h)_\Omega \qquad \text{for all } v_h \in V^h_0, \tag{4.3}$$

where the right-hand side F and boundary data w_D are given by (3.43) and (3.44), respectively.

4.2. Error estimates

The logarithmic term in the analytic solution of u is well known to cause sub-optimal convergence rates when solving u_h directly *via* (4.2). In [38], it was found that approximating $\ln(r)$ near the origin with piecewise linears yields errors in the $L^2(\Omega)$ norm of order $\mathcal{O}(h^{1-\epsilon})$, $\epsilon > 0$ being some arbitrarily small parameter. In [11], the following error estimate was found for the approximation (4.2) with simplicial elements:

$$\|u - u_h\|_{V^1_\alpha(\Omega)} \leq C_\alpha h^{\alpha-\epsilon} \|u\|_{V^2_{\alpha+1}(\Omega)},$$

where α is assumed to satisfy $0 < \alpha < 1$ and $\epsilon \in (0, \alpha)$. Note that convergence is not possible in the standard H^1-norm as u fails to belong to $H^1(\Omega)$. The Aubin-Nitsche theorem in weighted norms then predicts convergence of order $1 + \alpha - \epsilon$ in the $L^2_\alpha(\Omega)$ norm; in particular, we expect the sub-optimal error estimate

$$\|u - u_h\|_{L^2(\Omega)} \lesssim h^{1-\epsilon} \|u\|_{H^1_\alpha(\Omega)}.$$

in the standard L^2-norm, where $X \lesssim Y$ is taken to denote $X \leq CY$ for some constant $C > 0$.

As w belongs to $H^2(\Omega)$, the approximation of w by (4.3) will yield optimal convergence rates. For simplicial elements with mesh size h, we expect the following error estimates:

$$\|w - w_h\|_{L^2(\Omega)} \lesssim h^2 \|w\|_{H^2(\Omega)}, \tag{4.4}$$
$$\|w - w_h\|_{H^1(\Omega)} \lesssim h^1 \|w\|_{H^2(\Omega)}. \tag{4.5}$$

For prismatic elements with mesh size $h_\perp$ and $h_\parallel$, we expect the following error estimates:

$$\|w - w_h\|_{L^2(\Omega)} \lesssim h_\perp^2 \|w\|_{H^2(\Omega)}, \tag{4.6}$$
$$\|w - w_h\|_{H^1(\Omega)} \lesssim h_\perp^1 \|w\|_{H^2(\Omega)}, \tag{4.7}$$

provided that $h_\parallel$ is sufficiently small.

4.3. Modelling error

Let us now consider the effect of removing a collection of line segments from Λ. The motivation for such a removal may be to improve simulation runtime by removing line segments that offer a negligible contribution to the total solution. Another motivation might be to assess the effect of imperfect data acquisition, or to investigate the effect a disease such as stroke has in altering the blood flow to the surrounding tissue.

We start by defining u_0 to be the solution of the boundary-value problem

$$-\Delta u_0 = 0 \qquad \text{in } \Omega, \tag{4.8}$$
$$u_0 = u_D \qquad \text{on } \partial\Omega, \tag{4.9}$$

and u_i, $i = 1, 2, \ldots, n$, to be the solution found when considering line source i, *i.e.*,

$$-\Delta u_i = f\delta_{\Lambda_i} \qquad \text{in } \Omega, \tag{4.10}$$
$$u_i = 0 \qquad \text{on } \partial\Omega. \tag{4.11}$$

The total solution u, solving the full system (1.1a) and (1.1b), can then be found by summation:

$$u_n = u_0 + \sum_{i=1}^{n} E_i(f)G_i + w_i,$$

where w_0 solves the boundary value problem

$$-\Delta w_0 = 0 \qquad \text{in } \Omega, \tag{4.12}$$
$$w_0 = w_D \qquad \text{on } \partial\Omega, \tag{4.13}$$

with $w_D = -4\pi u_D$. The remaining terms w_i, $i = 1, ..., n$, each constitute the correction term associated with line source i, and are defined as the solution to

$$-\Delta w_i = F_i \qquad \text{in } \Omega, \tag{4.14}$$
$$w_i = -E_i(f)G_i \qquad \text{on } \partial\Omega, \tag{4.15}$$

with

$$F_i = \Delta E_i(f)G_i + 2\nabla E_i(f) \cdot \nabla G_i. \tag{4.16}$$

Next, we define u_{n_0} to be the solution found when considering only $n_0 - 1 < n = n_a + n_v$ of the line sources:

$$u_{n_0} = \frac{1}{4\pi}\left(\sum_{i=0}^{n_0-1} E_i(f)G_i + w_i\right).$$

The error $\|u - u_h\|_{L^2(\Omega)}$ will then consist of two terms,

$$\|u - u_h\|_{L^2(\Omega)} \leq \|u_{n_0} - u_h\|_{L^2(\Omega)} + \|u - u_{n_0}\|_{L^2(\Omega)},$$

where the first term is the usual numerical error, with u_h being the FE approximation of u_{n_0}, and the second term is the modelling error. From the splitting properties of the solution, we find that this modelling error

satisfies

$$\|u - u_{n_0}\|_{L^2(\Omega)} \lesssim \sum_{i=n_0}^{n} \|E_i(f)G_i + w_i\|_{L^2(\Omega)} \tag{4.17}$$

$$\lesssim \sum_{i=n_0}^{n} \|E_i(f)G_i\|_{L^2(\Omega)} + \|F_i\|_{L^2(\Omega)} + \|w_i\|_{H^{\frac{1}{2}}(\partial\Omega)} \tag{4.18}$$

$$\lesssim \sum_{i=n_0}^{n} \|E_i(f)G_i\|_{L^2(\Omega)} + \|E_i(f)G_i\|_{H^{\frac{1}{2}}(\partial\Omega)} + \|\Delta E_i(f)G_i\|_{L^2(\Omega)} + 2\|\nabla E_i(f)\cdot\nabla G_i\|_{L^2(\Omega)} \tag{4.19}$$

While this estimate is not sharp, it suggests that the modelling error introduced when neglecting line segment i depends on two factors: the line source intensity f_i, as well as the logarithmic term G_i associated with it. The exact interplay between the two is hard to quantify; care must therefore be taken when considering the impact of removing a line segment. We will return to this thought in Section 5.3.

5. Numerical results

The purpose of this section is twofold. Firstly, we want to verify numerically the regularity properties and error estimates found in Sections 3 and 4, respectively. To this end, we have performed numerical experiments on the simple unit cube domain $\Omega = (0,1)^3$, with Λ taken as a single, vertical line. Physically, these experiments can be interpreted as modelling a single well injecting fluid into a box-shaped reservoir. We test the two different numerical approaches presented in Section 4, the first one being the straightforward FE method described by equations (4.2), and the second being the SSB-FE method given by (4.3). Furthermore, we utilize here a prismatic mesh; this allows us to refine independently in the directions parallel with and perpendicular to the line. Prismatic meshes are more commonly used in reservoir engineering as it allows for a finer discretization in the horizontal plane; in particular, it allows for easy grading of the mesh around a well [32]. Here, we will use it to probe the anisotropic properties of the solutions. The computations for this first part were performed using the finite element framework Firedrake [10,36], which relies on PetSc [5,6].

The second purpose of this section is to demonstrate the capabilities of the SSB-FE method in handling problems with a large number of line segments. To this end, we test it on a dataset describing the vascular system in a human brain. As this dataset contains nearly 3000 line segments, it would be computationally challenging to resolve using the standard FE method. We show that our numerical approach for this test case is advantageous, in that it allows for a fine resolution of the pressure profile around each line segment and facilitates model reduction techniques. Here, the computations were performed using the finite element framework FEniCS [30].

5.1. Convergence test for smooth f

Let

$$\Lambda = \{(x_0, y_0, z) : z \in (0,1)\}$$

be a line cutting vertically through the unit cube domain Ω, with x_0, y_0 chosen as is illustrated in Figure 3. We solve (3.1a) and (3.1b) with line intensity $f(z) = z^3$ and Dirichlet boundary conditions

$$u_D = -\frac{1}{2\pi}\left(z^3\ln(r) - 1.5z\,r^2\left(\ln(r) - 1\right)\right) \text{ on } \partial\Omega, \tag{5.1}$$

for which we have the analytic solution

$$u_a = -\frac{1}{2\pi}\left(z^3 G + w\right), \quad G = \ln(r), \quad w = -1.5z\,r^2\left(\ln(r) - 1\right). \tag{5.2}$$

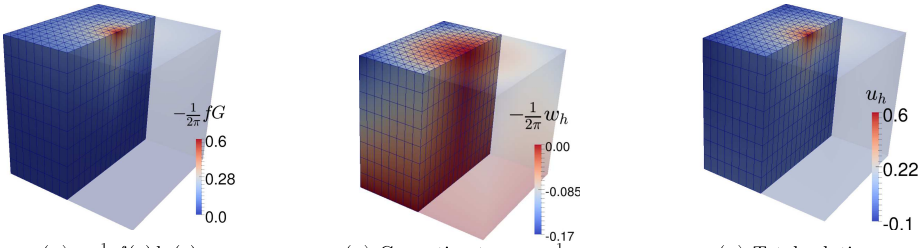

(A) $-\frac{1}{2\pi}f(z)\ln(r)$ (B) Correction term: $-\frac{1}{2\pi}w_h$ (C) Total solution u_h

FIGURE 4. The splitting terms and solution itself found when solving (3.1a) and (3.1b) on the unit domain with line source intensity $f(z) = z^3$ and the Dirichlet boundary data given in (5.1).

The solution and its splitting terms are shown in Figure 4.

Table 1A shows the numerical results obtained when solving for u_h directly by (4.2). Examining the $L^2(\Omega)$-error of the solution, we see that the solution converges in this norm sub-optimally, *i.e.*, with only order $h^{1-\epsilon}$ for some small $\epsilon > 0$. The convergence order improves to order h^2, *i.e.*, optimal, when a small region is removed around the line. This agrees with the results in [22], where quasi-optimal convergence was proven for the point source in a 2D domain as long as a small area was removed around the point source. The H^1-error for the entire domain is not given as the error does not converge in this norm.

The results in Table 1A are also consistent with our observation that u exhibits anisotropic regularity. Comparing the errors for $h_\parallel = 1/16$ and $h_\parallel = 1/64$, one can conclude that a refinement along with the line makes close to no difference in the L^2-error taken on the full domain. It follows that the perpendicular error dominates the parallel error; this is consistent with our observation in Section 3 that the solution exhibits a regularity loss in the plane perpendicular to the line. In contrast, both L^2 and H^1-errors are affected by the vertical refinement when the cylinder $U_{R=0.2}$ is removed from the domain. This is to be expected as we know from Section 3 that the solution exhibits high and isotropic regularity as long as a small volume is removed around the line.

Table 1B shows the numerical results obtained when solving for w_h by (4.3) and comparing with the analytical expression for w. As the correction term here solves the Poisson equation with right-hand side $f''(z)\ln(r) = z\ln(r) \in L^2(\Omega)$, we see here optimal convergence rates. The error is not affected by removing a small region around the line; this makes sense as w is H^2 regular in the entire domain. We also here see evidence of solution anisotropy, as the error is comparable for $h_\parallel = 1/16$ and $h_\parallel = 1/64$. This is natural as w adopts the regularity of f in the vertical direction, meaning that the correction function w for this test case is smooth with respect to z. The table also lists the convergence properties of the error in the H^1-norm, which was similarly found to be of optimal order.

5.2. Convergence test for arbitrary line source

We again solve (3.1a) and (3.1b) on the unit cube, with Λ as in Section 5.1, with the exception that it now has two endpoints contained in the interior of Ω:

$$\Lambda = \{(x, y, z) \in \Omega : x = x_0, y = y_0, z \in (0.2, 0.8)\}. \tag{5.3}$$

TABLE 1. Convergence rates p of the error in different norms, found when applying either the standard FE or SSB-FE method.

(A) Convergence rates p of the error $\|u - u_h\|$ obtained when applying the standard FEM.							
$h_\parallel$	$h_\perp$	$L^2(\Omega)$	p	$L^2(\Omega_R)$	p	$H^1(\Omega_R)$	p
1/16	1/4	1.4e-2		5.0e-3		8.3e-2	
	1/8	6.0e-3	1.2	1.4e-3	1.9	4.4e-2	0.9
	1/16	2.9e-3	1.1	3.6e-4	1.9	2.3e-2	1.0
	1/32	1.5e-3	1.0	1.5e-4	1.3	1.4e-2	0.7
	1/64	7.8e-4	0.9	1.3e-4	0.2	1.1e-2	0.3
1/64	1/4	1.4e-2		5.0e-3		8.3e-2	
	1/8	6.0e-3	1.2	1.4e-3	1.9	4.3e-2	0.9
	1/16	2.8e-3	1.1	3.6e-4	1.9	2.1e-2	1.0
	1/32	1.4e-3	1.0	1.0e-4	1.8	1.0e-2	1.0
	1/64	7.0e-4	1.0	4.4e-5	1.2	5.7e-3	0.9

(B) Convergence rates p of the error $\|w - w_h\|$ obtained when applying the SSB-FEM.									
$h_\parallel$	$h_\perp$	$L^2(\Omega)$	p	$H^1(\Omega)$	p	$L^2(\Omega_R)$	p	$H^1(\Omega_R)$	p
1/16	1/4	2.4e-2		2.4e-1		1.9e-2		2.2e-1	
	1/8	6.0e-3	2.0	1.2e-1	1.0	4.5e-3	2.1	1.0e-1	1.1
	1/16	1.5e-3	2.0	5.9e-2	1.0	1.1e-3	2.0	4.9e-2	1.1
	1/32	3.8e-4	2.0	2.9e-2	1.0	2.8e-4	2.0	2.4e-2	1.0
	1/64	9.5e-5	2.0	1.5e-2	1.0	7.1e-5	2.0	1.2e-2	1.0
1/64	1/4	2.4e-2		2.4e-1		1.9e-2		2.2e-1	
	1/8	6.0e-3	2.0	1.2e-1	1.0	4.5e-3	2.1	1.0e-1	1.1
	1/16	1.5e-3	2.0	5.9e-2	1.0	1.1e-3	2.0	4.9e-2	1.1
	1/32	3.8e-4	2.0	2.9e-2	1.0	2.8e-4	2.0	2.4e-2	1.0
	1/64	9.4e-5	2.0	1.5e-2	1.0	7.1e-5	2.0	1.2e-2	1.0

Notes. The error is computed for the full domain Ω as well as for the domain with the singularity removed, *i.e.*, Ω_R ($R = 0.2$).

The line source is prescribed an intensity $f(z) = z$ and Dirichlet boundary conditions are assigned on the boundary,

$$u_D = \frac{1}{4\pi}\left(z\ln\left(\frac{\sqrt{r^2+(z-b)^2}-(z-b)}{\sqrt{r^2+(z-a)^2}-(z-a)}\right)\right. \tag{5.4}$$

$$\left. -\left(\sqrt{(z-a)^2+r^2}-\sqrt{(z-b)^2+r^2}\right)\right) \text{ on } \partial\Omega. \tag{5.5}$$

The solution to (3.1a) and (3.1b) then admits an analytic solution, namely

$$u = \frac{1}{4\pi}\left(E(f)G + w\right), \quad E(f) = z, \quad w = -\sqrt{(z-a)^2+r^2}+\sqrt{(z-b)^2+r^2}, \tag{5.6}$$

where G is given by (3.16). The solution, along with its splitting terms, is shown in Figure 5.

Table 2A shows the numerical results obtained when solving for u_h by the standard FE method. Examining again the $L^2(\Omega)$-error of the solution, we see that the solution converges in this norm sub-optimally, *i.e.*, with only order $h^{1-\epsilon}$ for some small $\epsilon > 0$. The convergence order becomes optimal, *i.e.*, of order h^2, when a small region is removed around the line.

As in the previous example, the L^2-error shows the anisotropic nature of the solution, with an increase in the vertical refinement from $h_\parallel = 1/16$ to $h_\parallel = 1/128$ leading only to a small reduction in the error. It is thus clear that the error for this test case is also dominated by the horizontal error. Removing a small region around the

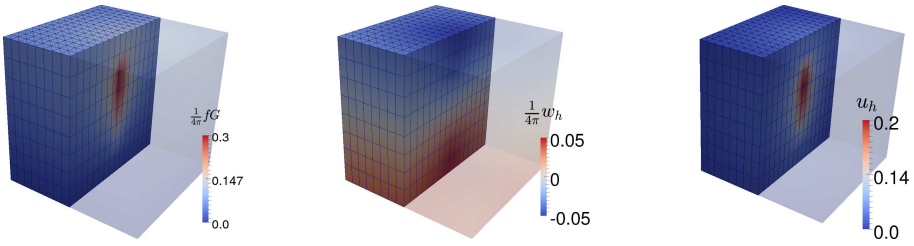

(A) $\frac{1}{4\pi}f(z)G$ (B) Correction $\frac{1}{4\pi}w_h$ (C) Total solution u_h

FIGURE 5. The splitting terms and solution itself found when solving (3.1a) and (3.1b) on the unit cube domain with line source intensity $f(z) = z$ and the Dirichlet boundary data in (5.1).

TABLE 2. Convergence rates p of the error in different norms found when applying either the standard FE method or the SSB-FE method.

(A) Convergence rates p of the error $\|u - u_h\|$ obtained when applying the standard FEM.

$h_\parallel$	$h_\perp$	$L^2(\Omega)$	p	$L^2(\Omega_R)$	p	$H^1(\Omega_R)$	p
1/16	1/4	1.0e-2		6.5e-3		1.4e-1	
	1/8	5.8e-3	0.8	2.2e-3	1.6	6.3e-2	1.2
	1/16	3.2e-3	0.9	6.4e-4	1.7	3.3e-2	0.9
	1/32	1.8e-3	0.9	4.5e-4	0.5	1.6e-2	1.0
	1/64	1.1e-3	0.7	4.6e-4		9.8e-3	0.7
1/128	1/4	1.0e-2		6.5e-3		1.4e-1	
	1/8	5.6e-3	0.9	2.2e-3	1.6	6.4e-2	1.1
	1/16	3.0e-3	0.9	5.5e-4	2.0	3.3e-2	1.0
	1/32	1.6e-3	0.9	1.8e-4	1.6	1.5e-2	1.1
	1/64	8.3e-4	0.9	1.3e-4	0.4	8.0e-3	0.9

(B) Convergence rates p of the error $\|w - w_h\|$ obtained when applying the SSB-FEM.

$h_\parallel$	$h_\perp$	$L^2(\Omega)$	p	$H^1(\Omega)$	p	$L^2(\Omega_R)$	p	$H^1(\Omega_R)$	p
1/16	1/4	9.7e-4		1.4e-2		7.5e-4		1.2e-2	
	1/8	2.9e-4	1.7	7.8e-3	0.8	2.0e-4	1.9	6.2e-3	1.0
	1/16	1.1e-4	1.4	4.9e-3	0.7	7.9e-5	1.4	4.0e-3	0.6
	1/32	7.4e-5	0.6	3.8e-3	0.4	6.0e-5	0.4	3.2e-3	0.3
	1/64	6.7e-5	0.1	3.4e-3	0.2	5.7e-5	0.1	3.0e-3	0.0
1/128	1/4	9.5e-4		1.3e-2		7.4e-4		1.2e-2	
	1/8	2.7e-4	1.8	7.1e-3	0.9	1.8e-4	2.0	5.5e-3	1.1
	1/16	7.3e-5	1.9	3.7e-3	0.9	4.3e-5	2.1	2.8e-3	1.0
	1/32	1.9e-5	1.9	1.9e-3	0.9	1.1e-5	2.0	1.4e-3	1.0
	1/64	5.1e-6	1.9	1.0e-3	0.9	3.0e-6	1.9	7.9e-4	0.9

Notes. The error is computed for the full domain Ω as well as for the domain with the singularity removed, *i.e.*, Ω_R ($R = 0.2$).

line again removes the anisotropic nature of the error; this is evident from the fact that the convergence rates of the error in $L^2(\Omega_R)$ and $H^1(\Omega_R)$-norms quickly deteriorate when the vertical refinement becomes coarser than the horizontal refinement.

Table 2B shows the numerical results obtained when solving for w_h with the SSB-FE method and comparing the solution with the analytical expression for w. The results are again better when compared to solving for

u_h directly, with optimal order convergence observed in both L^2 and H^1-norms. The convergence rates remain nearly unaltered when a small volume is removed around, confirming our observation that w exhibits high-regularity on the entire domain Ω.

5.3. Vascular network of the brain

Finally, let us demonstrate the capability of the SSB-FE method in handling problems with a large number of line segments. To this end, we solve the line source problem with both Dirichlet and Neumann type boundary conditions,

$$-\Delta u = f\delta_\Lambda \quad \text{in } \Omega, \tag{5.7a}$$

$$u = u_D \quad \text{on } \partial\Omega_D, \tag{5.7b}$$

$$\nabla u \cdot \mathbf{n} = 0 \quad \text{on } \partial\Omega_N, \tag{5.7c}$$

where $\mathbf{n}$ denotes the outward directed boundary normal of the domain, u_D some given boundary data, and $\partial\Omega_D$ and $\partial\Omega_N$ the Dirichlet and Neumann boundaries respectively, assumed to satisfy $\partial\Omega_D \cap \partial\Omega_N = \emptyset$ and $\partial\Omega_D \cup \partial\Omega_N = \partial\Omega$. The line sources are taken from a graph describing the vascular network in a human brain [42], the same dataset as was illustrated in Figure 1. This dataset consists of $n_a = 264$ and $n_v = 2606$ line segments describing the arterial and venous systems of the brain, respectively. The arterial system is responsible for providing the brain with oxygenated blood; its counterpart is the venous system, which is tasked with returning de-oxygenated blood back to the heart.

The process of oxygen delivery to biological tissue by micro-circulation is commonly modelled by means of coupled 1D–3D flow models, where the graph is seen as a 1D network and endowed with its own flow equation. The 1D flow equation can then be coupled to the 3D flow equation for the tissue by Starling's law of filtration. In this work, however, we consider only the 3D flow equation with a collection of line sources. For this reason, it is necessary to prescribe a certain mass flux to each line segment. For the test case presented here, the linear mass flux from each vessel i was taken proportional to its (given) vessel radius R_i:

$$f_i(t) = \gamma_i R_i \quad \text{for } t \in (0, L_i), \tag{5.8}$$

where the proportionality constant is taken as $\gamma_i = 1.0$ for arterial blood vessels and $\gamma_i = -0.1$ for venous blood vessels. The graph was then embedded in a spherical domain loosely representing the skull. A Dirichlet pressure was assigned to the bottom portion of the domain,

$$u_D = 1 \text{ for } \mathbf{x} \in \partial\Omega_D, \quad \partial\Omega_D = \{(x, y, z) \in \partial\Omega : x < H\}, \tag{5.9}$$

and no-flow out of the remaining boundary,

$$\nabla u \cdot \mathbf{n} = 0 \text{ for } \mathbf{x} \in \partial\Omega_N, \quad \partial\Omega_N = \{(x, y, z) \in \partial\Omega : x > H\}. \tag{5.10}$$

The solution then admits a splitting

$$u = \frac{1}{4\pi} \sum_{i=1}^{n_a+n_v} (E_i(f)G + w) \tag{5.11}$$

where the extension is given by

$$E_i(f)(\mathbf{x}) = \gamma_i R_i \text{ for } \mathbf{x} \in \Omega, \tag{5.12}$$

and w solves the boundary value problem Laplace equation (with right-hand side $F = 0$) with boundary conditions

$$w_D = 4\pi u_D - \sum_{i=1}^{n_a+n_v} E_i(f)G_i \qquad \text{for } \mathbf{x} \in \partial\Omega_D, \tag{5.13}$$

$$\nabla w \cdot \mathbf{n} = -\sum_{i=1}^{n_a+n_v} \nabla E_i(f)G_i \cdot \mathbf{n} \qquad \text{for } \mathbf{x} \in \partial\Omega_N. \tag{5.14}$$

We see that for the choice of piecewise constant linear mass flux from each line segment, the singularity subtraction technique reduces the line source problem to a boundary value problem.

The results from using the SSB-FE method to solve this model problem are shown in Figure 6. Figure 6a shows the source intensity f_i prescribed for each edge in the graph and the resulting pressure solution u. The flux, found by a projection of $-\nabla u$, is also shown, from which we see that the solution satisfies the no-flow boundary condition imposed on $\partial\Omega_N$. As was discussed in Section 3, the line sources in the right-hand side of (5.7a)–(5.7c) induce a logarithmic type singularity in the pressure profile around each line segment. Figure 6b shows a contour plot of the pressure, with a close-up view given of one region. The singular parts of the solution, *i.e.*, the $E_i(f)G_i$-terms, were here discretized by interpolation onto a fine mesh. In this close-up view the logarithmic profile of the solution is indeed visible, showing that the SSB-FE method is capable of producing good discrete approximations of the pressure. The logarithmic behaviour of the solution is especially pronounced around line segments representing arteries; this is to be expected as the arteries were prescribed a comparatively high mass flux.

Lastly, let us consider the robustness of the solution with respect to removing branches of the network. This serves as a proxy for more detailed studies regarding imperfect data acquisition and image segmentation, as well as for assessing changes in the actual arterial or venous network associated with diseases such as stroke. In particular, we ask the question as to how sensitive the solution (here represented by the L^2 norm of the error) is to a loss of a certain fraction of the edges of the graph.

Recall from Section 4 that the modelling error associated with neglecting line segments $i = n_0, ..., n_a + n_v$ is given by

$$\|u - u_{n_0}\|_{L^2(\Omega)} \lesssim \sum_{i=n_0}^{n_a+n_v} \|E_i(f)G_i\|_{L^2(\Omega)} + \underbrace{\|F_i\|_{L^2(\Omega)}}_{=0} + \|w_D\|_{L^2(\Omega)} \tag{5.15}$$

$$\lesssim \sum_{i=n_0}^{n_a+n_v} \|E_i(f)G_i\|_{L^2(\Omega)} + \|E_i(f)G_i\|_{H^{\frac{1}{2}}(\partial\Omega)} \tag{5.16}$$

$$= \sum_{i=n_0}^{n_a+n_v} \gamma_i R_i \left(\|G_i\|_{L^2(\Omega)} + \|G_i\|_{H^{\frac{1}{2}}(\Omega)} \right), \tag{5.17}$$

where $F_i = 0$ as the extensions $E_i(f)$ were chosen as constant functions. We can then define a relative modelling error bounded by

$$\frac{\|u - u_{n_0}\|_{L^2(\Omega)}}{\|u\|_{L^2(\Omega)}} = \sum_{i=n_0}^{n_a+n_v} \gamma_i R_i \left(\|G_i\|_{L^2(\Omega)} + \|G_i\|_{H^{\frac{1}{2}}(\Omega)} \right). \tag{5.18}$$

This suggests that the modelling error associated with neglecting line segment i depends the vessel radius R_i as well as logarithmic term G_i, where the exact interplay between the two is not known. For this reason, we consider now four different enumerations of the edge segments. The two first enumerations were based on sorting monotonically decreasing by edge length L_i and parametrized radius r_i, respectively. The third is formed

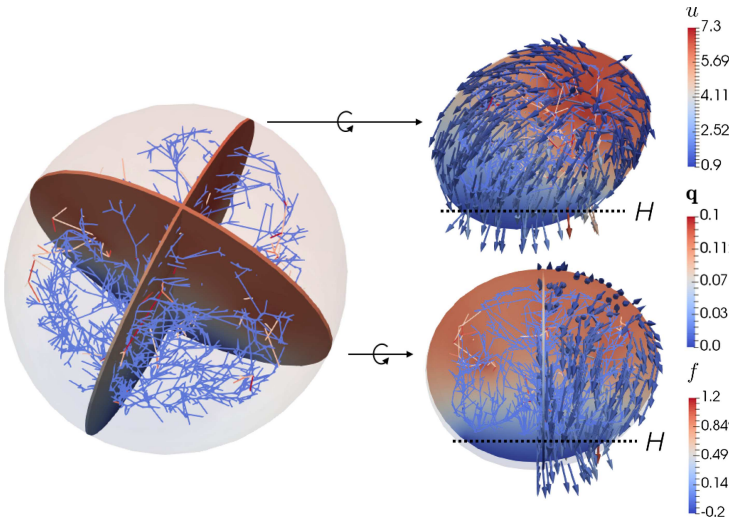

FIGURE 6. Pressure and flux found when using the SSB-FEM to solve (5.7a)–(5.7c) on a dataset describing the vascular system of the brain, with boundary conditions and source intensities set as specified in (5.8)–(5.10). The correction function w was solved using linear elements ($k = 1$) and the singular parts of the solution interpolated using quartic elements ($k = 4$). (a) (Left) perspective view of the brain, with two cross section views showing the pressure in the plane dividing the left/right hemisphere and front/rear hemisphere, respectively. (Right top) side view and (right bottom) rear view of these two cross sections. No-flow was imposed in the region above H, while a a Dirichlet condition for the pressure was imposed in the region below H. (b) Contour plot of the pressure. The singular parts of the solution were interpolated using $k = 4$; this was found necessary in order to resolve the logarithmic nature of the solution around the individual blood vessels.

by sorting monotonically decreasing with respect to $R_i\sqrt{L_i}$. This was motivated by considering the L^2 norm of G in the cylindrical domain $U_{R,H} = \{(r, \theta, z) : 0 < r < R,\, 0 < \theta < 2\pi,\, -H < z < H\}$ when G corresponds to the line segment $\Lambda_i = \{(r, \theta, z) \in \Omega_{R,H} : -L < z < L\}$. We then have the approximation

$$G = \ln\left(\frac{\sqrt{r^2 + (z+L)^2} - (z+L)}{\sqrt{r^2 + (z-L)^2} - (z-L)}\right) = \ln\left(\frac{\sqrt{1 + (\frac{r}{z+L})^2} - 1}{\sqrt{1 + (\frac{r}{z-L})^2} - 1}\right) \tag{5.19}$$

$$\approx \ln\left(\frac{r^2}{2(z-L)^2}\right) - \ln\left(\frac{r^2}{2(z+L)^2}\right) = \frac{1}{2}\left(\ln(z+L) - \ln(z-L)\right), \tag{5.20}$$

where we have used the binomial expansion $\sqrt{1+x} = 1 + 1/2x$. From this approximation, the L^2-norm of G can be calculated explicitly, and we find that it scales $\|G\|_{L^2(U_{R,H})} \sim \sqrt{L}$.

The fourth and final enumeration was made by numerically evaluating the L^2-norm of G_i in the domain Ω, and sorting monotonically decreasing by the approximation M_i of the full modelling error:

$$M_i = \gamma_i R_i \|G_i\|_{L^2(\Omega)}. \tag{5.21}$$

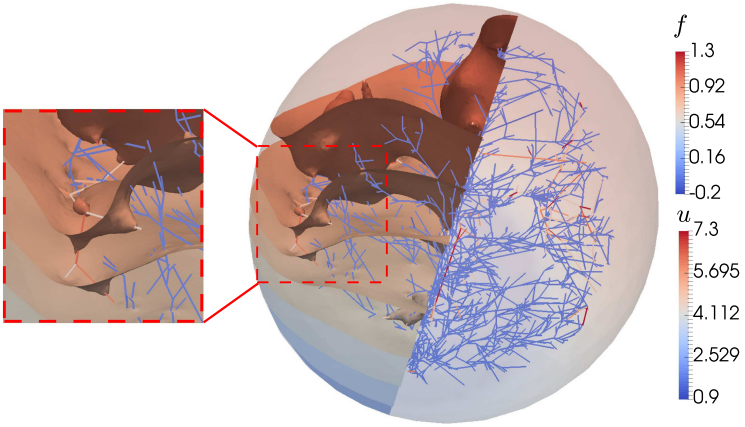

FIGURE 6. (Continued.)

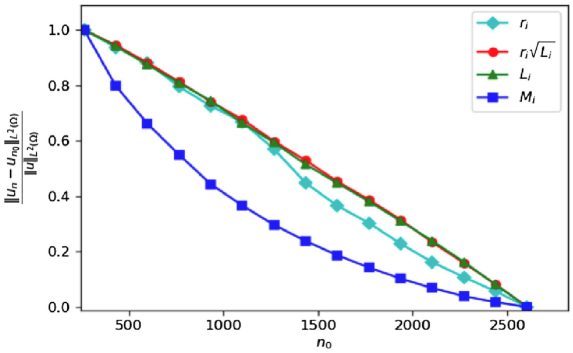

FIGURE 7. The model reduction error found when the graphs Λ_a and Λ_v were sorted montonically decreasing by vessel radius r_i, vessel length L_i, and the model reduction error M_i.

Figure 7 shows the actual (computed) error associated by removing a fraction of the edges based on the four enumerations given above. We see that there is essentially no correlation between the model error and segment length or radius (as reflected in nearly straight lines in the figure). This suggests that the modelling error in (5.17) is difficult to quantify in terms of the model parameters, even for the simple test case presented here. The L^2-norm of each G_i-term depends on the line segment length as well as its location within the domain. For this reason, the approximation shown in (5.20) is not helpful as $\|G_i\|_{L^2(\Omega)}$ can depend strongly on the location of Λ_i relative to the domain. The enumeration using the model reduction error estimate, M_i, is the most successful of the four; Figure 7 shows that the reduction error decreases near quadratically to zero when the dataset is sorted using this parameter. This suggest that, to assess the impact of removing a line segment Λ_i, it is appropriate to calculate the norm $\|G_i\|_{L^2(\Omega)}$ numerically.

Although this study is beholden to several academic simplifications, observations of this nature have several practical implications. Firstly, imaging technology based on finite resolution will primarily omit edges with small radius. Figure 7 implies that it is not appropriate to assume that these edges can be neglected, as a smaller edge radius was not seen to imply negligible impact. For applications, it may therefore be desirable to consider data sets which are augmented from the registered data with synthetic vessels of finer radius. Secondly, these results also give an understanding of the associated risks of failure of blood flow to the brain. Indeed, if the L^2-error of pressure is taken as a proxy for the change in oxygen perfusion in the brain, we again see that the term M_i provides an indicator for the most sensitive edges of the arterial and venous systems. While these observations are encouraging, we emphasize that a more detailed study is required in order to claim medical relevance. Such a study will need to include (among other things) a realistic geometry for not just of the arterial and venous network, but also the brain tissue; a coupling between the source terms of the edges with transport on the edge network (coupled 1D–3D); a time dependent right-hand side to account for the pulsating nature of the macro-vascular system, as the assumption of stationary flow is generally only valid for micro-circulation (see *e.g.*, the model in [39]); as well as an assessment of the non-linearities associated with non-Newtonian fluid flow.

6. Conclusions

We studied an elliptic equation having line sources in a 3D domain. The line sources act as Dirac measure defined on a line causing the solutions to be singular on the line itself. Central to this work is the result that the solution admits a split into a singular and a regular part. This allows us to study the nature of the solution as well as to develop a numerical algorithm for solving the problem. Mathematically, we see that the solution has anisotropic regularity, it is smooth along the line source and the line singularity acts as a Dirac point measure in a 2D domain. Our numerical approach solves for the regular part only and therefore obtains optimal convergence rates. We illustrate our approach for several numerical examples including a data set describing the vascular system of a human brain. Our solution approach is mesh-independent and can be adapted to a variety of discretizations.

Acknowledgements. This work was partially supported by the Research Council of Norway, project number 250223, and Deutsche Forschungsgemeinschaft, grant number WO-671/11-1. The authors thank J. Reichenbach and A. Deistung for bringing our attention to the data used in Section 5.3 [42], and E. Hanson and E. Hodneland for providing us with the data segmentation and tree extraction.

References

[1] I. Aavatsmark and R. Klausen, Well index in reservoir simulation for slanted and slightly curved wells in 3D grids. *SPE J.* **8** (2003) 41–48.
[2] R.A. Adams and J.J. Fournier, Sobolev Spaces. Academic Press, Cambridge, MA **140** (2003).
[3] T. Apel, O. Benedix, D. Sirch and B. Vexler, A priori mesh grading for an elliptic problem with dirac right-hand side. *SIAM J. Numer. Anal.* **49** (2011) 992–1005.
[4] T. Bærland, M. Kuchta and K.-A. Mardal, Multigrid Methods for Discrete Fractional Sobolev Spaces (2018).
[5] S. Balay, W.D. Gropp, L.C. McInnes and B.F. Smith, Efficient management of parallelism in object oriented numerical software libraries (1997) 163–202.
[6] S. Balay, S. Abhyankar, M.F. Adams, J. Brown, P. Brune, K. Buschelman, L. Dalcin, V. Eijkhout, W.D. Gropp, D. Kaushik, M.G. Knepley, L.C. McInnes, K. Rupp, B.F. Smith, S. Zampini, H. Zhang and H. Zhang, PETSc users manual. *Technical Report ANL-95/11 – Revision 3.8*, Argonne National Laboratory (2017).
[7] S. Bertoluzza, A. Decoene, L. Lacouture and S. Martin, Local error estimates of the finite element method for an elliptic problem with a dirac source term. *Numer. Methods Partial Differ. Equ.* **34** (2018) 97–120.
[8] W.M. Boon, J.M. Nordbotten and J.E. Vatne, Functional Analysis and Exterior Calculus on Mixed-Dimensional Geometries. Preprint arXiv:1710.00556 (2017).
[9] L. Cattaneo and P. Zunino, A computational model of drug delivery through microcirculation to compare different tumor treatments. *Int. J. Numer. Methods Biomed. Eng.* **30** (2014) 1347–1371.
[10] L.D. Dalcin, R.R. Paz, P.A. Kler and A. Cosimo, Parallel distributed computing using Python. New Computational Methods and Software Tools. *Adv. Water Res.* **34** (2011) 1124–1139.
[11] C. D'Angelo, Finite element approximation of elliptic problems with dirac measure terms in weighted spaces: Applications to one- and three-dimensional coupled problems. *SIAM J. Numer. Anal.* **50** (2012) 194–215.

[12] C. D'Angelo and A. Quarteroni, On the coupling of 1D and 3D diffusion-reaction equations: Application to tissue perfusion problems. *Math. Models Methods Appl. Sci.* **18** (2008) 1481–1504.
[13] F. Drechsler, C. Wolters, T. Dierkes, H. Si and L. Grasedyck, A full subtraction approach for finite element method based source analysis using constrained delaunay tetrahedralisation. *NeuroImage* **46** (2009) 1055–1065.
[14] L.C. Evans, Partial Differential Equations. American Mathematical Society, Providence, RI (2010).
[15] R.E. Ewing, R.D. Lazarov, S.L. Lyons, D.V. Papavassiliou, J. Pasciak and G. Qin, Numerical well model for non-darcy flow through isotropic porous media. *Comput. Geosci.* **3** (1999) 185–204.
[16] A. Ferroni, L. Formaggia and A. Fumagalli, Numerical analysis of Darcy problem on surfaces. *ESAIM: M2AN* **50** (2016) 1615–1630.
[17] V. Girault, K. Kumar and M.F. Wheeler, Convergence of iterative coupling of geomechanics with flow in a fractured poroelastic medium. *Comput. Geosci.* **20** (2016) 997–1011.
[18] I.G. Gjerde, K. Kumar and J.M. Nordbotten, A singularity removal method for coupled 1D–3D flow models. Preprint arXiv:1812.03055 (2018).
[19] I.G. Gjerde, K. Kumar and J.M. Nordbotten, Well modelling by means of coupled 1D–3D flow models. In: *ECMOR XVI – 16th European Conference on the Mathematics of Oil Recovery* (2018).
[20] L. Grinberg, E. Cheever, T. Anor, J.R. Madsen and G.E. Karniadakis, Modeling blood flow circulation in intracranial arterial networks: a comparative 3D/1D simulation study. *Ann. Biomed. Eng.* **39** (2011) 297–309.
[21] V.A. Kondratiev and O. Oleinik, Russian mathematical surveys boundary-value problems for partial differential equations in non-smooth domains. *Russ. Math. Surv* **38** (1983).
[22] T. Köppl and B. Wohlmuth, Optimal a priori error estimates for an elliptic problem with dirac right-hand side. *SIAM J. Numer. Anal.* **52** (2014) 1753–1769.
[23] T. Köppl, E. Vidotto and B. Wohlmuth, A local error estimate for the poisson equation with a line source term. Numerical Mathematics and Advanced Applications ENUMATH 2015. In Vol. 112 of *Lecture Notes in Computational Science and Engineering*. Springer, Cham (2016) 421–429.
[24] T. Köppl, E. Vidotto, B. Wohlmuth and P. Zunino, Mathematical modeling, analysis and numerical approximation of second-order elliptic problems with inclusions. *Math. Models Methods Appl. Sci.* **28** (2018) 953–978.
[25] V.A. Koslov, V.G. Mazya and J. Rossman, Elliptic boundary value problems in domains with point singularities. In Vol. 52 of *Mathematical Surveys and Monographs* (1997).
[26] M. Kuchta, M. Nordaas, J.C.G. Verschaeve, M. Mortensen and K.-A. Mardal, Preconditioners for saddle point systems with trace constraints coupling 2D and 1D domains. *SIAM J. Sci. Comput.* **38** (2016) B962–B987.
[27] A. Kufner, em Weighted Sobolev Spaces. John Wiley and Sons, Hoboken, NJ (1993).
[28] K.-A. Lie, S. Krogstad, I.S. Ligaarden, J.R. Natvig, H.M. Nilsen, and B. Skaflestad, Open-source matlab implementation of consistent discretisations on complex grids. *Comput. Geosci.* **16** (2012) 297–322.
[29] A. Llau, L. Jason, F. Dufour and J. Baroth, Finite element modelling of 1D steel components in reinforced and prestressed concrete structures. *Eng. Struct.* **127** (2016) 769–783.
[30] A. Logg, K.-A. Mardal and G.N. Wells, Automated Solution of Differential Equations by the Finite Element Method. Springer, Berlin (2012).
[31] V. Martin, J. Jaffré and J.E. Roberts, Modeling fractures and barriers as interfaces for flow in porous media. *SIAM J. Sci. Comput.* **26** (2005) 1667–1691.
[32] S.S. Mundal, E. Keilegavlen and I. Aavatsmark, Simulation of anisotropic heterogeneous near-well flow using mpfa methods on flexible grids. *Comput. Geosci.* **14** (2010) 509–525.
[33] M. Nabil and P. Zunino, A computational study of cancer hyperthermia based on vascular magnetic nanoconstructs. *R. Soc. Open Sci.* **3** (2016).
[34] D.W. Peaceman, Interpretation of well-block pressures in numerical reservoir simulation. *Soc. Pet. Eng. J.* **18** (1978) 183–194.
[35] L. Possenti, G. Casagrande, S.D. Gregorio, P. Zunino and M. Constantino, Numerical simulations of the microvascular fluid balance with a non-linear model of the lymphatic system. MOX-Report No. 35 (2018).
[36] F. Rathgeber, D.A. Ham, L. Mitchell, M. Lange, F. Luporini, A.T.T. McRae, G.-T. Bercea, G.R. Markall and P.H.J. Kelly, Firedrake: automating the finite element method by composing abstractions. *ACM Trans. Math. Softw.* **43** (2016) 24:1–24:27.
[37] J. Reichold, M. Stampanoni, A.L. Keller, A. Buck, P. Jenny and B. Weber, Vascular graph model to simulate the cerebral blood flow in realistic vascular networks. *J. Cerebral Blood Flow Metab.* **29** (2009) 1429–1443.
[38] R. Scott, Finite element convergence for singular data. *Numer. Math.* **21** (1973) 317–327.
[39] T. Secomb, R. Hsu, N. Beamer and B. Coull, Theoretical simulation of oxygen transport to brain by networks of microvessels: effects of oxygen supply and demand on tissue hypoxia. *Microcirculation* **7** (2010) 237–247.
[40] O. Strack, Analytical Groundwater Mechanics. Cambridge University Press, Cambridge (2017).
[41] T. Strouboulis, I. Babuška and K. Copps, The design and analysis of the generalized finite element method. *Comput. Methods Appl. Mech. Eng.* **181** (2000) 43–69.
[42] C.L. Tardif, A. Schäfer, R. Trampel, A. Villringer, R. Turner and P.-L. Bazin, Open science cbs neuroimaging repository: Sharing ultra-high-field mr images of the brain. Sharing the wealth: Brain Imaging Repositories in 2015. *NeuroImage* **124** (2016) 1143–1148.
[43] C.J. Weiss, Finite-element analysis for model parameters distributed on a hierarchy of geometric simplices. *Geophysics* **82** (2017) E155–E167.
[44] C.H. Wolters, H. Köstler, C. Möller, J. Härdtlein, L. Grasedyck and W. Hackbusch, Numerical mathematics of the subtraction method for the modeling of a current dipole in EEG source reconstruction using finite element head models. *SIAM J. Sci. Comput.* **30** (2007) 24–45.

Paper B

A Mixed Approach to the Poisson Problem with Line Sources

Ingeborg G. Gjerde, Kundan Kumar, Jan M. Nordbottenn

SIAM Journal of Numerical Analysis. Submitted

arXiv:1910.11785

Paper C

Well Modelling by Means of Coupled 1D-3D Flow Models

Ingeborg G. Gjerde, Kundan Kumar, Jan M. Nordbotten

ECMOR XVI - 16th European Conference on the Mathematics of Oil & Recovery
doi:10.3997/2214-4609.201802117

Paper D

A Singularity Removal Method for Coupled 1D-3D Flow Models

Ingeborg G. Gjerde, Kundan Kumar, Jan M. Nordbotten

Computational Geosciences. In press
doi:10.3997/2214-4609.201802117

A Singularity Removal Method for Coupled 1D-3D Flow Models

Ingeborg G. Gjerde · Kundan Kumar · Jan M. Nordbotten

Abstract In reservoir simulations, the radius of a well is inevitably going to be small compared to the horizontal length scale of the reservoir. For this reason, wells are typically modelled as lower-dimensional sources. In this work, we consider a coupled 1D-3D flow model, in which the well is modelled as a line source in the reservoir domain and endowed with its own 1D flow equation. The flow between well and reservoir can then be modelled in a fully coupled manner by applying a linear filtration law.

The line source induces a logarithmic type singularity in the reservoir pressure that is difficult to resolve numerically. We present here a singularity removal method for the model equations, resulting in a reformulated coupled 1D-3D flow model in which all variables are smooth. The singularity removal is based on a solution splitting of the reservoir pressure, where it is decomposed into two terms: an explicitly given, lower regularity term capturing the solution singularity and some smooth background pressure. The singularities can then be removed from the system by subtracting them from the governing equations. Finally, the coupled 1D-3D flow equations can be reformulated so they are given in terms of the well pressure and the background reservoir pressure. As these variables are both smooth (i.e. non-singular), the reformulated model has the advantage that it can be approximated using any standard numerical method. The reformulation itself resembles a Peaceman well correction performed at the continuous level.

Keywords Singularities · Green's functions · finite elements · Improved well modelling

1 Introduction

Accurate well models are of critical importance for reservoir simulations. The well constitutes the driving force for reservoir flow, in addition to being the main access point of

I. G. Gjerde
Department of Mathematics, University of Bergen
E-mail: ingeborg.gjerde@uib.no

K. Kumar
Department of Mathematics, University of Karlstad
E-mail: kundan.kumar@karlstad.se
Department of Mathematics, University of Bergen

J. M. Nordbotten
Department of Mathematics, University of Bergen
E-mail: jan.nordbotten@uib.no

information about its state. The major challenge of well modelling is that of scale disparity; a well has a radius of ~ 10 cm, while the reservoir might extend several kilometres in the horizontal plane. From a computational viewpoint, this makes it exceedingly expensive to resolve the well as a 3D object in the grid representing the reservoir. For this reason, wells are typically modelled using either zero-dimensional (0D) point sources or (1D) line sources.

In this work, we take as a starting point the coupled 1D-3D flow model

$$\mathbf{q} + \frac{\kappa}{\mu}\nabla p = 0 \qquad \text{in } \Omega, \tag{1a}$$

$$\nabla \cdot \mathbf{q} = \beta\,(\hat{p} - \bar{p})\,\delta_\Lambda \qquad \text{in } \Omega, \tag{1b}$$

$$\hat{q} + \frac{\hat{\kappa}}{\mu}\frac{\mathrm{d}\hat{p}}{\mathrm{d}s} = 0 \qquad \text{in } \Lambda, \tag{1c}$$

$$\frac{\mathrm{d}\hat{q}}{\mathrm{d}s} = -\,\hat{\beta}\,(\hat{p} - \bar{p}) \qquad \text{in } \Lambda, \tag{1d}$$

where $\Omega \subset \mathbb{R}^3$ denotes the reservoir domain and $\Lambda = \cup_{w=1}^{\text{wells}} \Lambda_w \subset \mathbb{R}^1$ a collection of line segments each representing a well. The 1D domain is parametrized by its arc-length s. The parameters κ, $\hat{\kappa}$ and μ denote reservoir permeability, well permeability and fluid viscosity, respectively, and are assumed to be positive and constant. The variables p and $\mathbf{q}$ denote fluid pressure and flux in the reservoir, $\hat{p}$ and $\hat{q}$ fluid pressure and flux in the well, and $\bar{p}$ the reservoir pressure averaged over the surface of the borehole $r = R$:

$$\bar{p}(z, R) = \frac{1}{2\pi R}\int_0^{2\pi} p(R, z, \theta)\mathrm{d}\theta, \tag{2}$$

as is illustrated in Figure 1.

Physically, equations (1a)-(1b) describe a Darcy-type flow in the reservoir domain Ω, and equations (1c)-(1d) a Poiseuille-type flow in the well. The latter is a 1D flow equation, where the radial and angular components have been neglected. For a description of this model reduction method for the well flow, we refer to the work of Cerroni et al. in [11]. The mass flux q between reservoir and well is modelled using a linear filtration law,

$$q = \beta(\hat{p} - \bar{p}), \tag{3}$$

which states that the connection flow between them is proportional to their pressure difference. The proportionality coefficients $\beta, \hat{\beta} \in C^1(\Lambda_w)$ are assumed piecewise continuous and allowed to vary along the well. The wells are considered as concentrated line sources δ_Λ in the reservoir equation (1a)-(1b), with the line sources defined in the following manner:

$$\int_\Omega f\delta_\Lambda\,\phi\,\mathrm{d}\Omega = \sum_{w=1}^{\text{wells}}\int_{\Lambda_w} f(s_w)\phi(s_w)\mathrm{d}s_w \tag{4}$$

for all $\phi \in C^0(\Omega)$, with s_w denoting the arc-length of line segment Λ_w.

Elliptic equations with line sources of the type (4) have been used in a variety of applications, e.g., the modelling of 1D steel components in concrete structures [29] or the interference of metallic pipelines and bore-casings in electromagnetic modelling of reservoirs [38]. A coupled 1D-3D heat transfer problem was considered in the context of geothermal energy in [5], where it was used to model heat exchange between (3D) soil and a (1D) pipe. Coupled 1D-3D flow models have also been studied in the context of biological applications, such as the efficiency of cancer treatment by hyperthermia [31], the efficiency of drug delivery through microcirculation [10, 35], and the study of blood flow in the vascularized tissue of the brain [21, 36]. In this work, we restrict ourselves to considering its application in the context of reservoir modelling.

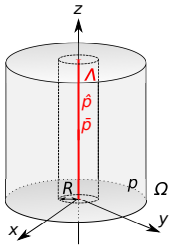

Fig. 1: A 1D domain Λ embedded in a 3D domain Ω representing the reservoir. The reservoir domain Ω is allowed to be arbitrarily shaped. The well is considered to be a thin cylinder of radius $R \ll \text{size}(\Omega)$. For this reason, the radial and angular components of the well pressure $\hat{p}$ are ignored, so that it can be described as a 1D variable $\hat{p} = \hat{p}(s)$.

The main challenge with the coupled 1D-3D flow problem is that the line source induces the reservoir pressure to be singular, thereby making its analysis and approximation non-standard. Typically, reservoir simulations are performed using finite volume methods. The discretized form of the coupling in (1a)-(1d) is then given by

$$q = \beta(\hat{p} - p_K), \tag{5}$$

where p_K denotes the average pressure in the grid block containing the well. Due to the singularity, p_K will not be representative of the reservoir pressure at the bore-hole; this is typically accounted for by multiplying β with a well index J. A correction of this type was first developed by Peaceman in [33], where he considered the two-point flux approximation method on uniform, square grids when the well is aligned with one of its axes. Via an analytic solution valid for simplified cases, he gave a well index depending on the equivalent radius of the well, i.e., the radius at which the reservoir pressure equals the well block pressure. The equivalent radius depends, among other factors, on the discretization scheme, placement of the well relative to the mesh, and reservoir permeability. The problem of finding appropriate well indexes has been treated in a multitude of works; Peaceman himself treated an extension of his method to non-square grid-blocks and anisotropic permeability [34]. The extension to more generalized grids was treated by e.g. Aaavatsmark in [1–3], to more generalized flow models by e.g. Ewing in [18], and to more generalized discretization schemes by e.g. Chen et al. in [12]. Many authors have contributed to the extension to generalized well placements, we mention here the work of King et. al in [24], Aavatsmark in [4], and of special relevance to our work, that of Wolfsteiner et al. in [39] and Babu et al. in [7].

In this work, we take a different approach, in which the singularities are explicitly removed from the governing equations. We start by showing that the reservoir pressure p admits a splitting

$$p = \sum_{w=1}^{\text{wells}} E\left(\beta(\hat{p} - \bar{p})\right) \Psi_w G_w + v, \tag{6}$$

where G_w is a given logarithmic function that captures the near-well behaviour of the reservoir pressure, E is an extension operator $E\colon H^2(\Lambda) \to H^2(\Omega)$, Ψ_w some smooth cut-off function, and $v \in H^2(\Omega)$ some higher-regularity remainder term. The key point here is that the singular nature of the solution is explicitly captured by the logarithmic terms G_w. With the splitting (6) in hand, we can therefore remove the singular terms from the system by straightforward subtraction. Finally, we reformulated coupled 1D-3D

flow model can then be reformulated so it is given with respect to the high-regularity variables $\hat{p}$ and v. The main contribution of this article is the reformulation of the coupled 1D-3D flow model into equations (34a)-(34d), for which the solution is smooth (non-singular). On a practical level, this means the solution can be approximated using any standard numerical method.

The technique of removing singularities is commonly known for point sources; we refer here to [17, p. 14] for a more in depth explanation. It has previously been studied in the context of reservoir models by e.g. Hales, who used it to improve well modelling for 2D reservoir models [22]. A splitting of the type (6) was introduced by Ding in [16] for the point source problem, where it was used to formulate grid refinement strategies. We are, to the best of our knowledge, the first to formulate a singularity removal method for the coupled 1D-3D flow problem. Central to this method is the construction of a function G_w capturing the solution singularity; we use here a function G_w found by integrating the Green's function for the reservoir equations (1a)-(1b) over the line Λ; we refer here to our earlier work in [20, Section 3.2]. This use of Green's functions to construct analytical and semi-analytical well models has a rich history. Of special relevance to our work, we mention that of Wolfsteiner et al. and Babu et al. in [7, 39], in which the Green's function was used to construct analytical solutions with which to calculate the well index J. More recently, Nordbotten et al. used Green's functions to construct analytical models to estimate leakage of CO_2 stored in geological formations [32].

The singularity removal, and subsequent reformulation of the model in terms of the smooth variables v and $\hat{p}$, is similar to the Peaceman well correction in that it leads to an alteration of the inflow parameter β. We discuss this in more detail in Section 7. It differs, however, in that it works on the continuous level. It is therefore easily adapted to different discretization methods, generalized well placements within the domain and different types of boundary conditions. Moreover, since our method gives an explicit representation of the logarithmic nature of the solution, it allows us to accurately represent the reservoir pressure in the whole domain (including in the near-vicinity of the well).

In our presentation of the method, we limit ourselves to considering a linear reservoir equation with constant, scalar-valued permeabilities and Poiseuille flow in the well. The latter restriction is not critical to the methodology; the well equation could for example be taken non-linear as long as the well pressure remains sufficiently regular. To be more precise, the method requires $\hat{p}$ to be piecewise C^1 on Λ. As for the reservoir equation, the reservoir pressure could be replaced with a potential expression ϕ so that the effect of gravity can be included. The singularity removal and reformulation can be extended to handle spatially varying, scalar-valued permeabilities as shown in [20]. For an extension to tensor-valued permeabilities and non-linear reservoir equations, we suggest using the solution splitting in (6) to formulate a multiscale finite volume method such as in [40], or a generalized finite element method [37], where the analytic functions capturing the solution singularity are used to enrich the set of basis functions.

For the discretization and numerical experiments, we consider herein the Galerkin Finite Element (FE) method. The FE approximation of the line source problem was studied by D'Angelo in [13] by means of weighted Sobolev spaces, using similar techniques as those known for e.g. corner-point problems [8]. D'Angelo proved that the approximation of the coupled 1D-3D flow problem (1a)-(1b) converges sub-optimally unless the mesh is sufficiently refined around the well. The sub-optimal convergence rates were found to be local to the line source by Köppl et al. in [28], meaning that they only pollute the pressure approximation inside the well block. However, this means the approximation of the coupled 1D-3D flow problem will suffer until the mesh parameter h is smaller than the well radius R. In practice, one therefore needs a very fine mesh around the well for the FE approximation of (1a)-(1d) to converge. This makes the

problem computationally expensive to solve. Different strategies have been proposed to remedy this, e.g., Kuchta et al. studied suitable preconditioners in [27]. Holter et al. then applied this preconditioner to simulate flow through the microcirculature found in a mouse brain [23]. An alternative coupling scheme was introduced by Köppl et al. in [25], where the source term was taken to live on the boundary of the inclusions. The result is a 1D-(2D)-3D method where the approximation properties have been improved, at the expense of having to resolve the 2D boundary of the well.

The article is structured as follows. We start in Section 2 by defining the relevant function spaces for the problem. In Section 3, we introduce in more detail the coupled 1D-3D flow model we take as a starting point. In Section 4, we show that the reservoir pressure p admits a splitting into lower-regularity terms that capture the solution singularities, and a higher-regularity remainder term v. With the splitting in hand, the singularities can then be subtracted from the governing equations. The result is the reformulated coupled 1D-3D flow model (34a)-(34d), posed in terms of the smooth variables $\hat{p}$ and v. As the solutions then enjoy significantly improved regularity, this system can be approximated using standard numerical methods. The variational formulation and FE discretization of the reformulated problem are given in Sections 5 and 6, respectively, and require only standard function spaces. In Section 7, we discuss how this discretization of the reformulated model resembles a Peaceman well correction. We then conclude the article with two numerical experiments, where we test the Galerkin FE method of both the standard and reformulated coupled 1D-3D flow model. We show that the singularity removal recovers optimal convergence rates on uniform meshes, i.e., without needing to refine the mesh around the well. Moreover, in a manner similar to altering the well index, it makes the approximation robust with respect to the ratio R/h.

2 Background and notation

The purpose of this section is to introduce the appropriate function spaces for the coupled 1D-3D flow model. Let $H^k(\Omega)$ be the Sobolev space,

$$H^k(\Omega) = \{u \in L^2(\Omega) : D^\beta u \in L^2(\Omega) \text{ for } |\beta| \leq k\},$$

with β denoting a multi-index and D^β the corresponding weak distributional derivative of u. $H^k(\Omega)$ is a Hilbert space endowed with inner product

$$(u, v)_{H^k(\Omega)} = \sum_{|\beta| \leq k} \int_\Omega D^\beta u \, D^\beta v \, \mathrm{d}\Omega.$$

We use a subscript to denote the subspace of H^k with zero trace on the boundary, H^k_0, i.e.,

$$H^k_0(\Omega) = \{u \in H^k(\Omega) : u|_{\partial\Omega} = 0\}.$$

As we will see, the reservoir solution p in (1a)-(1d) fails to belong to $H^1(\Omega)$ due to singular behaviour on Λ. For this reason, we consider also a weighted Sobolev space. To define it, let $-1 < \alpha < 1$, and take $L^2_\alpha(\Omega)$ to denote the weighted Hilbert space consisting of measurable functions u such that

$$\int_\Omega u^2 r^{2\alpha} \mathrm{d}\Omega < \infty,$$

where r denotes the distance of a point to Λ, i.e., $r(\mathbf{x}) = \mathrm{dist}(\mathbf{x}, \Lambda)$. This space is equipped with the inner product

$$(u, v)_{L^2_\alpha(\Omega)} = \int_\Omega r^{2\alpha} uv \, \mathrm{d}\Omega.$$

For $\alpha > 0$, the weight r^α has the power to dampen out singular behaviour in the function being normed; for $\alpha < 0$, the weight function can induce or worsen already singular behaviour. We therefore have the relation $L^2_{-\alpha}(\Omega) \subset L^2(\Omega) \subset L^2_\alpha(\Omega)$ for $\alpha > 0$. Letting now $H^1_\alpha(\Omega)$ be the Sobolev space

$$H^1_\alpha(\Omega) = \{u \in L^2_\alpha(\Omega) : D^\beta u \in L^2_\alpha(\Omega) \text{ for } |\beta| \leq k\},$$

we will later find that the reservoir pressure solving (1a)-(1d) belongs to $H^1_\alpha(\Omega)$ for $\alpha > 0$.

A practical use of this space is found, for example, considering the logarithmic grading (refinement) that is often performed on a mesh around the well. The well introduces a logarithmic type singularity in the reservoir pressure that cannot be resolved using linear elements. Consequently, the convergence rate of standard numerical methods degrade using uniform meshes. Optimal convergence can be retrieved by a specific refinement of the mesh around the well [6, 13, 16]. The exact convergence rates and mesh grading requirements are closely related to the weighted Sobolev space wherein the solution exists; in fact, the graded mesh will be uniform with respect to the weight function r^α.

3 Mathematical model

Here, we introduce in more detail the coupled 1D-3D equation we take as a starting point. Let $\Omega \subset \mathbb{R}^3$ denote a bounded domain describing a reservoir, with smooth boundary $\partial\Omega$. We consider here steady-state, incompressible Darcy flow

$$\mathbf{q} = -\frac{\kappa}{\mu}\nabla p, \tag{7}$$

where $\mathbf{q}$ and p denote reservoir flow and pressure, μ the fluid viscosity, and κ a given positive and scalar permeability. We consider also a collection of wells, each considered to be a thin tube with fixed radius R and centreline Λ_w. The centreline is parametrized by the arc length s_w. We denote by $\boldsymbol{\tau}_{s_w}$ its normalized tangent vector. As the radius of the tube is small, we assume the radial and angular components of the well pressure can be neglected, meaning $\hat{p}|_{\Lambda_w} = \hat{p}(s_w)$. The well flow domain Λ will then consist of a collection of line segments, $\Lambda = \cup_{w=1}^{\text{wells}} \Lambda_w$. We consider on this domain Poiseuille-type flow,

$$\hat{\mathbf{q}}_w = -\frac{R^2}{8\mu}\frac{\mathrm{d}\hat{p}}{\mathrm{d}s_w}\boldsymbol{\tau}_{s_w}, \tag{8a}$$

$$\frac{\mathrm{d}\hat{\mathbf{q}}_w}{\mathrm{d}s_w} = -\frac{q}{\pi R^2}, \tag{8b}$$

with $\hat{\mathbf{q}}_w$ and $\hat{p}_w$ denoting flow and pressure in the well and q the linear mass flux into or out of the well. $\frac{\mathrm{d}}{\mathrm{d}s_w}$ denotes the derivative with respect to the tangent line, or equivalently, the projection of ∇ along $\boldsymbol{\tau}$, i.e., $\frac{\mathrm{d}}{\mathrm{d}s_w} = \nabla \cdot \boldsymbol{\tau}_{s_w}$. As the fluid flux in the well has a fixed direction, it can be given as a scalar function $\hat{q}_w$, characterized by the property $\hat{\mathbf{q}}_w = \hat{q}_w \boldsymbol{\tau}_w$. Note that the assumption of Poiseuille flow is not critical; (8a) could for example contain certain non-linearities.

Letting now $\Lambda = \cup_{w=1}^{\text{wells}} \Lambda_w$ denote the collection of line segments Λ_w, the well pressure and flux can be written as 1D variables $\hat{p}, \hat{q} \colon \Lambda \to \mathbb{R}$. The well and reservoir flow can then be coupled together using a linear filtration law, which states that the mass flux q between them is proportional to their pressure difference:

$$q = 2\pi\lambda R f(\hat{p}, \bar{p}) \quad \text{where } f(\hat{p}, \bar{p}) = \hat{p} - \bar{p}. \tag{9}$$

The mass flux is given as the rate of transfer per unit length, and the variable $\lambda \in C^2(\Lambda)$ denotes the permeability of the borehole lateral surface. It accounts for the fact that the well may not be in perfect contact with the reservoir, leading to a pressure drop across the borehole. Letting Δp_{skin} denote this pressure drop, this can be expressed by the following relation: $q = 2\pi R\lambda \Delta p_{\text{skin}}$.

The pressure difference $f(\hat{p}, \bar{p})$ between well and reservoir uses an averaged value $\bar{p}(z; R)$ for the reservoir pressure given in (2). This can be interpreted physically as the reservoir pressure averaged around the borehole. The flow in well and reservoir can be then modelled, in a fully coupled manner, by the set of equations

$$\mathbf{q} + \frac{\kappa}{\mu}\nabla p = 0 \qquad \text{in } \Omega, \tag{10a}$$

$$\nabla \cdot \mathbf{q} = \beta f(\hat{p}, \bar{p})\delta_\Lambda \qquad \text{in } \Omega, \tag{10b}$$

$$p = p_D \qquad \text{on } \partial\Omega, \tag{10c}$$

$$\hat{q} + \frac{\hat{\kappa}}{\mu}\frac{\mathrm{d}\hat{p}}{\mathrm{d}s} = 0 \qquad \text{in } \Lambda, \tag{10d}$$

$$\frac{\mathrm{d}}{\mathrm{d}s}\hat{q} = -\hat{\beta} f(\hat{p}, \bar{p}) \qquad \text{in } \Lambda, \tag{10e}$$

$$\hat{p} = \hat{p}_D \qquad \text{on } \partial\Lambda, \tag{10f}$$

where $\hat{\kappa} = R^2/8$, $\beta = 2\pi R\lambda$, $\hat{\beta} = \beta/\pi R^2$. The functions $p_D \in C^2(\bar{\Omega})$ and $\hat{p}_D(\bar{\Lambda})$ denote given boundary data. The connection flow from well to reservoir is modelled by means of a generalized Dirac delta function δ_Λ, which we understand in the sense of (4). Finally, this system can be reduced to its conformal form by eliminating the 1D and 3D fluxes:

$$\nabla \cdot \left(-\frac{\kappa}{\mu}\nabla p\right) = \beta f(\hat{p}, \bar{p})\delta_\Lambda \qquad \text{in } \Omega, \tag{11a}$$

$$p = p_D \qquad \text{on } \partial\Omega, \tag{11b}$$

$$\frac{\mathrm{d}}{\mathrm{d}s}\left(-\frac{\hat{\kappa}}{\mu}\frac{\mathrm{d}}{\mathrm{d}s}\hat{p}\right) = -\hat{\beta} f(\hat{p}, \bar{p}) \qquad \text{in } \Lambda, \tag{11c}$$

$$\hat{p} = \hat{p}_D \qquad \text{on } \partial\Lambda, \tag{11d}$$

with $f(\hat{p}, \bar{p}) = \hat{p} - \bar{p}$.

4 Splitting Properties of the Solution

In this section, we will show that the line source in the right-hand side of (11a) introduces a particular structure to the solution of the coupled 1D-3D flow problem. We do this by means of a splitting technique, in which the reservoir pressure is split into a low regularity term that explicitly captures the singularity, and a regular component v being the solution of a suitable elliptic equation. To start with, we discuss in detail the splitting when Λ is assumed a single line segment aligned with the z-axis, $\frac{\kappa}{\mu} = 1$ and the well outflow q is a given function $f \in C_0^1(\Lambda)$. The splitting is then especially simple; this case therefore serves to illustrate the splitting method itself. We then generalize it in two steps, handling first an arbitrary line segment and $\frac{\kappa}{\mu} \neq 1$, and finally the coupling between reservoir and well. Finally, we use the splitting to reformulate the coupled 1D-3D flow problem into the system (34a)-(34d), wherein the singularity has been removed and all variables are smooth.

4.1 Elliptic equations with a single line source

In this section, we consider the elliptic equation

$$-\Delta p = f\delta_\Lambda \tag{12}$$

when Λ and Ω are as illustrated in Figure 1, and $f = f(z) \in C_0^1(\Lambda)$ is a *given*, smooth line source intensity (assumed zero at the endpoints of Λ). The solution p then admits a splitting into an explicit, low-regularity term $f(z)\Psi(r)G(r)$, and an implicit, high-regularity term v:

$$p = f(z)\Psi(r)G(r) + v(r,z). \tag{13}$$

Here, $G(r)$ captures the singular part of the solution, and is given by

$$G(r) = -\frac{1}{2\pi}\ln(r), \tag{14}$$

and $\Psi(r)$ denotes some smooth cut-off function satisfying

$$\Psi(r) = 1 \qquad \text{for } 0 \le r < R_\epsilon, \tag{15a}$$
$$\Psi(r) \in (0,1) \qquad \text{for } R_\epsilon < r < R_c, \tag{15b}$$
$$\Psi(r) = 0 \qquad \text{for } r > R_c. \tag{15c}$$

Assuming the cut-off radius R_c is chosen small enough to satisfy $\Psi(r) = 0$ on $\partial\Omega$, the regular component v can then be defined as the solution of

$$-\Delta v = F \qquad \text{in } \Omega, \tag{16a}$$
$$v = p_D \qquad \text{on } \partial\Omega, \tag{16b}$$

where

$$F = f''(z)G(r). \tag{17}$$

To see that p given by (13) indeed solves (12), let us first note that $G = -1/2\pi \ln(r)$ was so chosen because it satisfies $-\Delta G = \delta_\Lambda$. To be more precise, G is the fundamental solution of the Laplace equation in 2D, and thus has the property

$$-\int_\Omega \Delta G(r)\phi \,\mathrm{d}\Omega = \int_\Lambda \phi \,\mathrm{d}\Lambda \quad \forall \phi \in C^0(\Omega). \tag{18}$$

Considering then the Laplacian of p given by (13), a straightforward calculation shows that all but one term vanish by construction, i.e.,

$$-\Delta p = \int_\Omega f(z)\Psi(r)\Delta G(r)\phi \,\mathrm{d}\Omega. \tag{19}$$

By (18), we then find that

$$-\Delta p = \int_\Lambda f\phi \,\mathrm{d}\Lambda \quad \forall \phi \in C^0(\Omega),$$

and it follows that the p constructed in (13) indeed solves (12) in a suitably weak sense.

Formally speaking, the splitting works by introducing first the logarithmic term G for which the Laplacian returns the line source with the required intensity f. The higher-regularity term v is then used to correct the solution so it solves the original problem. The existence of such a function v follows from standard elliptic theory. As $\ln(r) \in L^2(\Omega)$, and $f''(z) \in L^2(\Lambda)$ by assumption, one can show that the entire right-hand side F in (16a) belongs to $L^2(\Omega)$ [20, Section 3.1]. Consequently, there exists $v \in H^2(\Omega)$ solving

(16a)-(16b). The full solution p, meanwhile, fails to belong to $H^1(\Omega)$. This can be shown by straightforward calculation, as one has $\ln(r) \in L^2(\Omega)$ but $\nabla \ln(r) \notin L^2(\Omega)$. Instead, one has p belonging to the weighted Sobolev space $H^1_\alpha(\Omega)$ for any $\alpha > 0$. It follows that v is indeed the higher-regularity term in the splitting (13). Formally, this means that v is smoother and better behaved than the full solution p. This observation will be central to the numerical method considered in Section 6.

4.2 Elliptic equations with an arbitrary line source

In this section, we consider the elliptic problem

$$\nabla \cdot \left(-\frac{\kappa}{\mu} \nabla p \right) = f \delta_\Lambda, \tag{20}$$

when the right-hand side is a line source δ_Λ located on a single line segment Λ with endpoints $\mathbf{a}, \mathbf{b} \in \Omega$. The line Λ can be described by the parametrization $\mathbf{y} = \mathbf{a} + \boldsymbol{\tau} s \quad \text{for } s \in (0, L)$, where $L = \|\mathbf{b} - \mathbf{a}\|$ denotes the Euclidean norm and $\boldsymbol{\tau} = (\mathbf{b} - \mathbf{a})/L$ is the normalized tangent vector of Λ. Letting again $f = f(s) \in C^1(\Lambda)$ be a given line source intensity, the solution p then admits a splitting into an explicit, low-regularity term $E(f)G(r)$, and a high-regularity component v:

$$p = E(f)\Psi G + v. \tag{21}$$

The function G is now given by

$$G(\mathbf{x}) = \frac{1}{4\pi} \frac{\mu}{\kappa} \ln \left(\frac{r_b + L + \boldsymbol{\tau} \cdot (\mathbf{a} - \mathbf{x})}{r_a + \boldsymbol{\tau} \cdot (\mathbf{a} - \mathbf{x})} \right), \tag{22}$$

with $r_b(\mathbf{x}) = \|\mathbf{x} - \mathbf{b}\|$ and $r_a(\mathbf{x}) = \|\mathbf{x} - \mathbf{a}\|$. This function was constructed by integrating the 3D Green's function for (11a) (when posed in $\mathbb{R}^2$) over the line segment Λ. It thus satisfies the property $\nabla \cdot (-\frac{\kappa}{\mu} \nabla G) = \delta_\Lambda$ [20, Section 3.2]. Next, E denotes an extension operator $E \colon H^2(\Lambda) \to H^2(\Omega)$ extending f so that it can be evaluated in the entire domain Ω. Assuming again that the cut-off function Ψ satisfies $\Psi = 0$ on $\partial\Omega$, the regular component v is then defined as the solution of

$$-\Delta v = F \qquad \text{in } \Omega, \tag{23a}$$

$$v = p_D \qquad \text{on } \partial\Omega, \tag{23b}$$

where

$$F = G\Delta\big(E(f)\Psi\big) + 2\nabla\big(E(f)\Psi\big) \cdot \nabla G. \tag{24}$$

To see that the constructed p indeed solves the right problem, let us start by inserting it into (20). construction, all terms disappear except $E(f)\Psi\Delta G$. Integrating this term over the domain, we find that

$$\begin{aligned} -\Delta p &= -\int_\Omega E(f)\Psi \Delta G \phi \, \mathrm{d}\Omega \\ &= \int_\Lambda f \phi \, \mathrm{d}\Lambda, \end{aligned} \tag{25}$$

for all $\forall \phi \in C^0(\Omega)$, where we used the property that $E(f) = f$ on Λ. It follows that the p constructed in (13) indeed solves (12) in a suitably weak sense.

By a similar argument as the one given in [20, Section 3.2], one finds that F given by (24) belongs to $L^{2-\epsilon}(\Omega)$ for arbitrarily small $\epsilon > 0$. It follows that there exists

$v \in H^{2-\epsilon}(\Omega)$ solving (23a)-(23b). Moreover, a straightforward calculation shows that G again fails to belong to $H^1(\Omega)$. In fact, one has $G \in H^{1-\epsilon}(\Omega)$. It follows that v constitutes the higher-regularity component of the solution split (21), meaning that v is smoother and better behaved than the full solution p.

4.3 The coupled 1D-3D flow problem

Let us now consider the coupled 1D-3D flow problem (11a)-(11d). To start with, let us again consider a single line segment Λ with endpoints $\mathbf{a}, \mathbf{b} \in \Omega$. From the discussion in the preceding section, it is natural to assume p solving (11a)-(11d) admits a solution splitting of the type:

$$p = \Psi E(\beta f) G + v, \tag{26}$$

with G being as in (22), Ψ being some smooth cut-off function, f being the previously introduced pressure difference $f = \hat{p} - \bar{p}$, and v defined as the solution of

$$\begin{aligned} -\Delta v &= F(\hat{p}, \bar{p}; \beta) && \text{in } \Omega, && \text{(27a)} \\ v &= p_D. && \text{on } \partial\Omega, && \text{(27b)} \end{aligned}$$

with

$$F = G\Delta\big(E(\beta f)\Psi\big) + 2\nabla\big(E(\beta f)\Psi\big) \cdot \nabla G. \tag{28}$$

Unlike in Sections 4.1 and 4.2, $f = f(\hat{p}, \bar{p})$ is now implicitly given from $\hat{p}$ and $\bar{p}$ solving the coupled 1D-3D flow problem. To reformulate (11a)-(11d) in terms of $\hat{p}$ and v, the right-hand side therefore needs to be reformulated. To this end, let us first treat the pressure difference $\hat{p} - \bar{p}$. By the splitting (26) and the definition of the averaging in (2), calculations reveal that

$$\begin{aligned} \bar{p} &= \beta\,(\hat{p} - \bar{p})\,\bar{G} + \bar{v}, \\ \Rightarrow \bar{p} &= \frac{\beta\bar{G}\hat{p} + \bar{v}}{1 + \beta\bar{G}}, \\ \Rightarrow \hat{p} - \bar{p} &= \frac{\hat{p} - \bar{v}}{1 + \beta\bar{G}}. \end{aligned} \tag{29}$$

Here we used the simplifications $\overline{E(f)} = f|_\Lambda$ and $\overline{\Psi} \approx 1|_\Lambda$. This is motivated by the fact that the well radius R is assumed negligible. From this, we can state the reformulated coupled 1D-3D flow model:

$$\begin{aligned} -\Delta v &= F(\hat{p}, \bar{v}; \beta^*) && \text{in } \Omega, && \text{(30a)} \\ v &= p_D && \text{on } \partial\Omega, && \text{(30b)} \\ -\frac{\mathrm{d}^2\hat{p}}{\mathrm{d}s^2} &= \hat{\beta}^*(\hat{p} - \bar{v}) && \text{in } \Lambda, && \text{(30c)} \\ \hat{p} &= \hat{p}_D && \text{on } \partial\Lambda, && \text{(30d)} \end{aligned}$$

where

$$\begin{aligned} F = G\Delta\,&(E(\beta^*(\hat{p} - \bar{v}))\Psi) \\ &+ 2\nabla(E(\beta^*(\hat{p} - \bar{v}))\Psi) \cdot \nabla G, \end{aligned} \tag{31}$$

β^* is given by

$$\beta^* = \frac{\beta}{1 + \beta G(R)}, \tag{32}$$

and $\hat{\beta}^* = \beta^*/\pi R^2$.

The extension to multiple wells follows naturally by applying the superposition principle. Considering now $\Lambda = \cup_{w=1}^{\text{wells}} \Lambda_w$, with each line segment Λ_w having endpoints $(\mathbf{a}_w, \mathbf{b}_w) \in \Omega$, we can formulate a solution splitting

$$p = \sum_{w=1}^{\text{wells}} E\big(\beta^*(\hat{p} - \bar{v})\big)\Psi_w G_w + v, \tag{33}$$

where $E\colon H^2(\Lambda) \to H^2(\Omega)$ is the same extension operator as before,G_w is given by (22) with $\mathbf{a} = \mathbf{a}_w$ and $\mathbf{b} = \mathbf{b}_w$, Ψ_w is some smooth cut-off function with respect to line segment Λ_w, and v solves

$$\begin{aligned}
-\Delta v &= F(\hat{p}, \bar{v}; \beta^*) && \text{in } \Omega, && (34a)\\
v &= p_D && \text{on } \partial\Omega, && (34b)\\
-\frac{\mathrm{d}^2\hat{p}}{\mathrm{d}s^2} &= -\hat{\beta}^*(\hat{p} - \bar{v}) && \text{in } \Lambda, && (34c)\\
\hat{p} &= \hat{p}_D && \text{on } \partial\Lambda, && (34d)
\end{aligned}$$

with right-hand side

$$\begin{aligned}
F = \sum_{w=1}^{\text{wells}} & G_w \Delta\big(E(\beta^*(\hat{p} - \bar{v}))\Psi_w\big) \\
& + 2\nabla\big(E(\beta^*(\hat{p} - \bar{v}))\Psi_w\big) \cdot \nabla G_w,
\end{aligned} \tag{35}$$

and

$$\beta^* = \frac{\beta}{1 + \sum_{w=1}^{\text{wells}} \beta \overline{G_w \Psi_w}}, \quad \hat{\beta}^* = \frac{\beta^*}{\pi R^2}. \tag{36}$$

The system (34a)-(34d) constitutes a reformulation of the coupled 1D-3D flow model in terms of the smooth variables v and $\hat{p}$. For an example of what the splitting might look like, the reader is invited to examine Figure 2. As the singularities have here been removed from the system, it enjoys significantly improved regularity compared to the standard formulation (11a)-(11d).

5 Weak formulation

In this section, we state a weak formulation of the reformulated coupled 1D-3D flow problem (34a)-(34d). As the variables in this formulation are all smooth functions, this can be done using standard Sobolev spaces. For the sake of completeness, we give also a weak formulation of the standard coupled 1D-3D flow problem (11a)-(11d). The reservoir pressure p therein contains a singularity; for this reason, its weak formulation requires the use of weighted Sobolev spaces.

Consider first the reformulated coupled 1D-3D flow problem. Let $\mathbf{V}$ denote the product space $\mathbf{V} = V \times \hat{V}$, where

$$V = \{u \in H^1(\Omega)\colon u|_{\partial\Omega} = p_D\}, \tag{37}$$

$$\hat{V} = \{\hat{u} \in H^1(\Lambda)\colon u|_{\partial\Lambda} = \hat{p}_D\}, \tag{38}$$

normed by

$$\|(v, \hat{p})\|_{\mathbf{V}}^2 = \|v\|_{H^1(\Omega)}^2 + \|\hat{p}\|_{H^1(\Lambda)}^2. \tag{39}$$

Multiplying (34a) and (34c) with test functions $\phi \in H_0^1(\Omega)$ and $\hat{\phi} \in H_0^1(\Lambda)$, respectively, integrating over their respective domains, and performing an integration by parts, we arrive at the following variational formulation:

Find $(v, \hat{p}) \in \mathbf{V}$ such that

$$a\left((v,\hat{p}),(\phi,\hat{\phi})\right) = 0 \tag{40}$$

for all $(\phi, \hat{\phi}) \in \mathbf{V}_0$, where

$$\begin{aligned} a\left((v,\hat{p}),\phi,\hat{\phi})\right) = (\nabla v, \nabla\phi)_\Omega + \left(\frac{\mathrm{d}}{\mathrm{d}s}\hat{p}, \frac{\mathrm{d}}{\mathrm{d}s}\hat{\phi}\right)_\Lambda \\ + (F_1(\beta^*(\hat{p}-\bar{v})), \nabla\phi)_\Omega \\ - (F_2(\beta^*(\hat{p}-\bar{v})), \phi)_\Omega \\ + (\hat{\beta}^*(\hat{p}-\bar{v})), \hat{\phi})_\Lambda, \end{aligned} \tag{41}$$

and

$$F_1(\hat{\phi}) = \sum_{w=1}^{\text{wells}} \nabla\Big(\Psi_w E\big(\hat{\phi}\big)\Big) G_w, \tag{42a}$$

$$F_2(\hat{\phi}) = \sum_{w=1}^{\text{wells}} \nabla\Big(\Psi_w E\big(\hat{\phi}\big)\Big) \cdot \nabla G_w. \tag{42b}$$

The full reservoir pressure can then be constructed from v and $\hat{p}$ by the relation

$$p = \sum_{w=1}^{\text{wells}} E\big(\beta^*\left(\hat{p}-\bar{v}\right)\big) G_w + v. \tag{43}$$

Next, let us consider the standard coupled 1D-3D flow model, and give its variational formulation as it was proposed in [14]. Let $\mathbf{V}_\alpha$ denote the weighted product space $\mathbf{V}_\alpha = V_\alpha \times \hat{V}$, where

$$V_\alpha = \{u \in H^1_\alpha(\Omega) \colon u|_{\partial\Omega} = p_D\}, \tag{44}$$

$$\hat{V} = \{\hat{u} \in H^1(\Lambda) \colon \hat{u}|_{\partial\Lambda} = \hat{p}_D\}, \tag{45}$$

normed by

$$\|(p,\hat{p})\|^2_{\mathbf{V}_\alpha} = \|p\|^2_{H^1_\alpha(\Omega)} + \|\hat{p}\|^2_{H^1(\Lambda)}. \tag{46}$$

Multiplying (11a) and (11c) with test functions $v \in H^1_{-\alpha,0}(\Omega)$ and $\hat{v} \in H^1_0(\Lambda)$, respectively, integrating over their domain of support, and performing an integration by parts, we arrive at the variational formulation:

Find $(p, \hat{p}) \in \mathbf{V}_\alpha$ such that

$$a\left((p,\hat{p}),(\phi,\hat{\phi})\right) = 0 \tag{47}$$

for all $(\phi, \hat{\phi}) \in \mathbf{V}_{-\alpha,0}$, where

$$\begin{aligned} a\left((p,\hat{p}),(\phi,\hat{\phi})\right) = (\nabla p, \nabla\phi)_\Omega + \left(\frac{\mathrm{d}}{\mathrm{d}s}\hat{p}, \frac{\mathrm{d}}{\mathrm{d}s}\hat{\phi}\right)_\Lambda \\ - \left(\beta\left(\hat{p}-\bar{p}\right), \phi\right)_\Lambda \\ + (\hat{\beta}(\hat{p}-\bar{p})), \hat{\phi})_\Lambda, \end{aligned} \tag{48}$$

and the test space $\mathbf{V}_{-\alpha,0}$ is the space of functions $(\phi, \hat{\phi}) \in \mathbf{V}_{-\alpha,0}$ with zero trace on the boundary. Notice here that the test and trial spaces are chosen with opposite weight functions; this is what ensures the continuity and coercivity of the bilinear form (48). For a proof of the well-posedness of this formulation, the reader is referred to [13, 14].

6 Numerical Discretization

In this section, we show the block matrix resulting from a finite element discretization of weak formulation of the reformulated coupled 1D-3D problem. As the pressure difference $f(\hat{p}, \bar{v}) = \hat{p} - \bar{v}$ now uses the regular part of the pressure, $v \in H^2(\Omega)$, we introduce here also the simplification $\bar{v}_h = v_h|_\Lambda$; i.e., we take the trace of v_h on Λ rather than the average over the cylinder. This is motivated by the fact that R is assumed negligible compared to the mesh size h, and v is regular, meaning $\bar{v} \approx v|_\Lambda$. The result is a "true" coupled 1D-3D flow model, in that it considers only 1D and 3D variables, with no averaging performed over a 2D cylinder. The same approximation is not possible for the standard coupled 1D-3D flow model as the reservoir pressure is there undefined on Λ.

We will now give the discretized form of the variational formulation (40). For simplicity, let us assume Ω is a polyhedron that readily admits a partitioning $\mathcal{T}_{T,h}$ into simplicial elements T:

$$\bar{\Omega} = \bigcup_{T \in \mathcal{T}_{T,h}} T.$$

The simplicial partitioning $\mathcal{T}_{T,h}$ forms a mesh, assumed conforming, which can then be characterized by the mesh size $h = \max_{T \in \mathcal{T}_{T,h}} h_T$. Next, we associate this mesh with the usual (3D) Lagrange space of order 1, V_u^h, given by

$$V_u^h = \{v_h \in C_u^0(\Omega),\, v_h|_T \in \mathbb{P}_1 \text{ where } T \in \mathcal{T}_{T,h}\}.$$

Here, $\mathbb{P}^1$ denotes the space of polynomials of degree 1, and $C_u^0(\Omega)$ the space of continuous elements that equal the interpolation of u on the boundary, i.e.,

$$C_u^0(\Omega) = \{p \in C^0(\Omega) \colon p|_{\partial\Omega} = \mathcal{I}_h u\}. \tag{49}$$

Next, we assume Λ admits a partitioning $\mathcal{T}_{I,h}$ into line segments I:

$$\bar{\Lambda} = \bigcup_{I \in \mathcal{T}_{I,h}} I,$$

assumed again to satisfy all the requirements of a conforming mesh, and associated with the mesh size $\hat{h} = \max_{I \in \mathcal{T}_{I,h}} h_I$. For the discretization of $\hat{V}$, we use the (1D) Lagrange space of order 1,

$$\hat{V}_{\hat{p}}^h = \{v_h \in C_{\hat{u}}^0(\Lambda),\, \hat{v}|_I \in \hat{\mathbb{P}}_1 \text{ where } I \in \mathcal{T}_{I,h}\},$$

with $C_{\hat{u}}^0(\Lambda)$ interpreted as in (49).

Considering first the reformulated system (40), let

$$v = \sum_{k=1}^{N} v_k \phi_k, \qquad \hat{p} = \sum_{l=1}^{\hat{N}} \hat{p}_l \hat{\phi}_l, \tag{50}$$

where $\{\phi_1, \phi_2, ..., \phi_N\}$ and $\{\hat{\phi}_1, \hat{\phi}_2, ..., \hat{\phi}_{\hat{N}}\}$ are linear hat functions spanning V^h and $\hat{V}^h$, respectively. Note next that v_h is a linear function used to approximate the high regularity term $v \in H^2(\Omega)$. For $R \ll h$, its average $\bar{v}_h$ can be well approximated by simply taking the trace $v|_\Lambda$. The pressure difference $\hat{p} - \bar{v}$ is then given by

$$\begin{aligned} \hat{p} - \bar{v} &= \sum_{l=1}^{\hat{N}} \hat{p}_l \hat{\phi}_l - \sum_{k=1}^{N} v_k \bar{\phi}_k \\ &= \sum_{l=1}^{\hat{N}} \hat{\phi}_l \left(\hat{p}_l - \sum_{k=1}^{N} T_{k,l} v_k \right). \end{aligned} \tag{51}$$

Here, $T\colon V^h \to \hat{V}^h$ is the discrete trace matrix, characterized by the property $\phi_k|_\Lambda = \sum_{l=1}^{\hat{N}} T_{k,l}\hat{\phi}_l$.

Testing (40) with $v = \phi_i$ for $i = 1, ..., N$ and $\hat{v} = \hat{\phi}_j$ for $j = 1, ..., \hat{N}$, we arrive at the following discrete system:

$$\begin{bmatrix} A - CT^T & C \\ -\hat{M}T^T & \hat{A} + \hat{M} \end{bmatrix} \begin{bmatrix} v \\ \hat{p} \end{bmatrix} = 0. \tag{52}$$

where A and $\hat{A}$ are the standard stiffness matrices

$$A_{i,k} = (\nabla\phi_k, \nabla\phi_i), \tag{53}$$

$$\hat{A}_{j,l} = (\frac{\mathrm{d}}{\mathrm{d}s}\hat{\phi}_l, \frac{\mathrm{d}}{\mathrm{d}s}\hat{\phi}_j). \tag{54}$$

$\hat{M}$ denotes the standard 1D mass matrix,

$$\hat{M}_{j,l} = (\hat{\beta}^*\hat{\phi}_j, \hat{\phi}_l)_\Lambda \tag{55}$$

and C denotes the coupling block,

$$C_{i,l} = \sum_{w=1}^{\text{wells}} \left(F_1(\beta^*\hat{\phi}_l), \nabla\phi_i\right)_\Omega - \left(F_2(\beta^*\hat{\phi}_l), \phi_i\right)_\Omega. \tag{56}$$

We will refer to this system as the Singularity Removal Based FE method. After solving (52), a discretization of the full reservoir pressure p_h can be reconstructed using

$$p_h = \sum_{w=1}^{\text{wells}} \beta^*(\hat{p}_h - \bar{v}_h|_\Lambda)\mathcal{I}_h^k G + v_h, \tag{57}$$

where $\mathcal{I}_h^k$ denotes the interpolation onto the Lagrange space of order k. As the interpolation of $G(r)$ is fairly cheap, the approximation property of p_h can here be improved by choosing the interpolation degree k high.

A more straightforward method can be found by discretizing (47) directly; this is the finite element formulation analysed in e.g. [13]. As we will compare the performance of this method against the Singularity Removal Based FE method, we give here its discretization for the sake of completeness. Setting

$$p = \sum_{k=1}^{N} p_k\phi_k \qquad \hat{p} = \sum_{l=1}^{\hat{N}} \hat{p}_l\hat{\phi}_l, \tag{58}$$

The pressure difference $\hat{p} - \bar{p}$ is then given by

$$\begin{aligned} f &= \hat{p} - \bar{p} \\ &= \sum_{l=1}^{\hat{N}} \hat{p}_l\hat{\phi}_l - \sum_{k=1}^{N} p_k\bar{\phi}_k \\ &= \sum_{l=1}^{\hat{N}} \hat{p}_l\hat{\phi}_l - \sum_{k=1}^{N}\sum_{m=1}^{\hat{M}} \Pi_{m,k}p_k\hat{\psi}_m, \end{aligned} \tag{59}$$

where Π is the discrete averaging matrix $\Pi : V^h \to X^h$ and $\{\hat{\psi}_1, \hat{\psi}_2, ..., \hat{\psi}_{\hat{M}}\}$ are the basis functions spanning $\hat{X}^h$.

Testing now (47) with $v = \phi_i$ for $i = 1, ..., N$ and $\hat{v} = \hat{\phi}_j$ for $j = 1, ..., \hat{N}$, we arrive at the following block system for the discretization of (47):

$$\begin{bmatrix} A + \beta T^T N \Pi & -\beta T^T \hat{M} \\ -\beta N \Pi & \hat{A} + \beta \hat{M} \end{bmatrix} \begin{bmatrix} p \\ \hat{p} \end{bmatrix} = 0. \tag{60}$$

Here, N denotes the mass matrix given by

$$N_{m,l} = (\hat{\psi}_m, \hat{\phi}_l), \tag{61}$$

for $\hat{\psi}_m$ belonging to the discontinuous Galerkin space of order 0:

$$\hat{X}^h = \{v_h \in L^2(\Gamma),\, v_h|_I \in \mathbb{P}_0 \text{ where } I \in \mathcal{T}_{I,h}\}.$$

We will refer to this system as the standard FE method.

7 Relation to the Peaceman well model

In this section, we show that the reformulated coupled 1D-3D flow model (34a)-(34d) under certain conditions reduces to the Peaceman well correction. We start by giving a brief summary of the methodology Peaceman introduced in his seminal work [33]. We then return to our reformulated model, and show that with $G(r)$ chosen so that its support is the equivalent radius of the Peaceman well correction, the reformulation results in a well index that equals the one derived by Peaceman.

In reservoir simulations, the mass flux between well and aquifer, q, is usually modelled in a manner analogous to that in (11a):

$$q = J(p_w - p_K), \tag{62}$$

where p_w is the flowing pressure in the well, J its well index, and p_K the reservoir pressure averaged over the grid cell K. In Section 4, we showed how the line source that models the well introduces a logarithmic type singularity in the reservoir pressure. For wells with radius much smaller than the grid size h, i.e., $R \ll h$, p_K is therefore likely to constitute a poor representation of the reservoir pressure in the near vicinity of the well.

The Peaceman well model accounts for this by altering the well index J in (62) so that q better corresponds to the numerical approximation of the pressure difference between well and aquifer. Assuming radial flow, Darcy's law in a heterogeneous reservoir is given, per unit well length, by the relation

$$\frac{q}{2\pi r} = -\frac{\kappa}{\mu}\frac{\mathrm{d}p}{\mathrm{d}r}. \tag{63}$$

Integrating this equation to a radius r_e,

$$\frac{2\pi\kappa}{q\mu}\int_{p_w}^{p_e} \mathrm{d}p = -\int_R^{r_e} \mathrm{d}r, \tag{64}$$

we find that

$$q = \frac{2\pi\kappa}{\mu}\frac{p_w - p_e}{\ln(r_e/R)} \tag{65}$$

when $p_e = p(r_e)$. We also need to take into account the pressure drop Δp_{skin} across the skin of the well. To do so, let S be the skin-factor, defined by the relation

$$S = \frac{2\pi\kappa}{q\mu}\Delta p_{\text{skin}}. \tag{66}$$

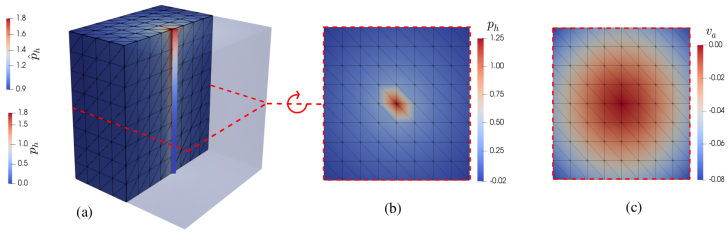

Fig. 2: (a) FE approximations of $\hat{p}_h$ and the reconstructed reservoir pressure p_h for $h = 1/8$. (b) Full reservoir pressure p_h and (c) background pressure v_h on the slice $\{(x, y, z) \in \Omega : z = 0.5\}$

Letting now r_e be the radius at which the reservoir pressure equals the averaged grid cell pressure p_K, Peaceman used the following relation between q and the pressure difference $p_w - p_K$ [33]:

$$q = \frac{2\pi\kappa}{\mu} \frac{p_w - p_K}{\ln(r_e/R) + S}. \tag{67}$$

To utilize this correction, one must first identify the equivalent radius r_e entering in (67). This radius generally depends on the discretization method, the location of the well within the grid, and the permeability of the rock around the well. Assuming for example square grid blocks and a well at the center of an interior grid block, Peaceman derived an equivalent radius $r_e = 0.2h$ for the two-point flux approximation [33].

The reformulation of the pressure difference f in terms of $\hat{p}$ and v bears a strong resemblance to the Peaceman well correction in (67). In a practical sense, the reformulation into (34a)-(34d) can be interpreted as a non-local well correction, which has a support in a region around the well which may significantly exceed the grid resolution. To see more clearly the similarity with the Peaceman well correction, let us now consider a single well. We have then

$$q = \frac{\beta}{1 + \frac{\mu}{\kappa}\beta\overline{G}}(\hat{p} - \bar{v}). \tag{68}$$

Next, we let now $\hat{p}$ be the flowing well pressure p_w. The term $G(r)$ contains the logarithmic component of the solution; in a manner analogous to the Peaceman well correction, we make it local to the cylinder of radius r_e by setting

$$G_{r_e}(r) = \begin{cases} -\frac{1}{2\pi}\frac{\mu}{\kappa}\ln(r/r_e) & \text{for } r \le r_e, \\ 0 & \text{otherwise.} \end{cases} \tag{69}$$

Note that this G is not smooth enough to work for the solution split (33), we use it here only for the sake of comparison. By the definition of the averaging (2), we have $\overline{G} = -\mu/2\pi\kappa \ln(R/r_e)$ Inserting it in (68) yields the relation

$$q = \frac{\beta}{1 - \beta\frac{\mu}{2\pi\kappa}\ln(\frac{R}{r_e})}(p_w - \bar{v}) \tag{70}$$

$$= \frac{2\pi\kappa}{\mu} \frac{p_w - \bar{v}}{\frac{2\pi\kappa}{\mu\beta} + \ln(\frac{r_e}{R})}. \tag{71}$$

Here, $2\pi\kappa/\mu\beta$ can be substituted by the skin factor of the well by recalling $q = \beta\Delta p_{\text{skin}}$. This results in an expression that equals the Peaceman well correction given in (67), i.e.,

$$q = \frac{2\pi\kappa}{\mu} \frac{p_w - \bar{v}}{\ln(\frac{r_e}{R}) + S}. \tag{72}$$

The regular component v can be interpreted as a sort of background pressure, or more precisely, the component of the reservoir pressure that can be approximated using linear functions. We see then that the singularity removal constitutes an alteration of β (which can be interpreted as a well index) so that the mass flux function q better corresponds to the *numerically* computed pressure difference between well and reservoir, i.e., $\hat{p} - \bar{v}$. For this reason, we expect that the singularity removal, in a manner similar to the Peaceman well correction, will improve the stability of the FE approximation with respect to the ratio R/h.

8 Numerical Results

In this section, we perform numerical experiments to test the approximation properties of the Singularity Subtraction Based FE method given by (52). For the implementation, we utilized the finite element framework FEniCS [30]. For the first test case, we consider a single well with smooth lateral well permeability β, and compare the results against those obtained using the standard FE given by (60). Our implementation of this method uses an earlier implementation from Kuchta [26], the same as was utilized for the results of Holter et al. in [23]. The Singularity Removal Based FE method was implemented by an extension of this code, using also the mixed-dimensional functionality of FEniCS developed and implemented by Daversin-Catty [15]. For the second test case, we consider a discontinuous lateral permeability β, and an extension operator that uses radial basis function interpolation. We show here that the reconstructed reservoir pressure p_h converges optimally when the Singularity Removal Based FE method is applied.

8.1 Convergence test for well with smooth lateral permeability

In this section, we take $\Omega = (0,1)^3$ and $\Lambda = \{(x,y,z) \in \Omega : x = y = 1/2\}$. We want to test the capability of each method in approximating the test problem

$$p_a = -\frac{1}{2\pi}(z^3+1)\ln(r) + v_a, \tag{73a}$$

$$v_a = -\frac{3}{4\pi}\left(zr^2\left(\ln(r)-1\right)\right), \tag{73b}$$

$$\hat{p}_a = \frac{1-\ln(R)}{2\pi}\left(z^3 + 1 - \frac{3}{2}R^2 z\right), \tag{73c}$$

with the following parameters:

$$\kappa = \hat{\kappa} = \mu = 1, \quad \beta = 2\pi, \quad \hat{\beta} = \frac{6z(1-\ln(R))}{z^3+1}. \tag{74}$$

The solution, along with the splitting terms, are shown in Figure 2.

In order to test the stability of the approximation when the well radius is small compared to mesh size h, we test using four different values for the well radius:

$$R \in \{\text{1.0e-1, 1.0e-2, 1.0e-3, 1.0e-4}\}. \tag{75}$$

Furthermore, we set $\Psi = 1$ and choose as the extension operator

$$E(f) = f(z) \text{ for all } (x,y,z) \in \Omega. \tag{76}$$

In this case, the reformulated FE method will approximate the analytic solution for v_a given in (73b), meaning we can compute its error directly using $\|v_a - v_h\|$.

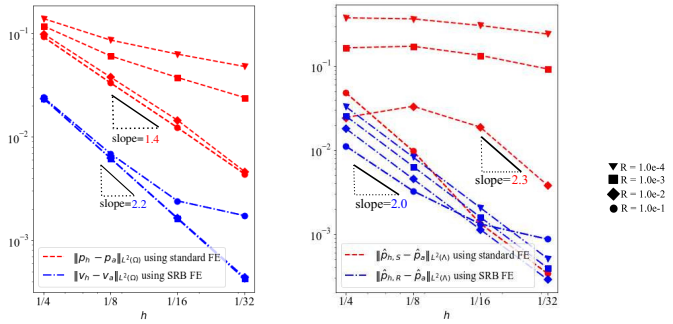

(a) Reservoir pressure approximations, $p - p_a$ and $v - v_a$.

(b) Well pressure approximation errors, $\hat{p}_h - \hat{p}_a$.

Fig. 3: Log-log plot of the approximation errors obtained using the standard FE method (red) and the Singularity Removal Based FE method (blue) as the mesh size h decreases. The approximations were tested for different well radius values R and is indicated with a marker, where the radius corresponding to each marker is shown to the right.

Figure 3 shows the approximation errors, measured in the L^2-norm, when the problem was solved using a sequence of increasingly fine meshes. The blue lines in Figure 3a show the approximation error of v_h, measured in the L^2-norm, i.e., $\|v_h - v_a\|_{L^2(\Omega)}$ with v_a being the analytic solution in (73b). For $R < h$, the errors are seen to be invariant with respect to R, and the approximation of v_h exhibits moderate superconvergence. To expand upon this, we expect for this approximation optimal convergence rates of order h^l with $l = 2.0$; we see here a slight super-convergence as $l = 2.2$. For $h > 1/8$ and $R = 0.1$, our assumption of $R < h$ is no longer valid, and we see a degradation of the convergence rates. To be more precise, we made in the construction of the block matrix (52) the simplification $\bar{v} = v|_\Lambda$, and this is not justified for $R \sim h$. Optimal convergence rates could be restored by taking the average of v_h rather than its trace.

The red lines in Figure 3a give the approximation errors for the full reservoir pressure using the standard FE method described by (60). We give here the approximation error of p_h in the L^2-norm, i.e., $\|p_h - p_a\|_{L^2(\Omega)}$. For the standard FE method, the convergence properties strongly depend on the well radius R, with decreasing R leading to a reduction in the convergence rate. The best convergence rates are seen when $R \sim h$, but even here, the convergence is sub-optimal compared to the Singularity Removal Based FE method. This can be explained by noting that the standard FE method explicitly resolves the line source in the problem; it was shown in [13] that this leads to a reduction in the convergence rate of p_h. We refer here to our comments in [20, p. 14-15] for a more in-depth explanation of this, and remark only that the line source problem is expected to converge with order $h^{1-\epsilon}$ for $\epsilon > 0$ arbitrarily small. Thus, the convergence order h^l with $l = 1.4$ surpasses the theoretical expectation when $R \sim h$.

The blue and red lines in Figure 3b give the approximation error of $\hat{p}_h$ using the Singularity Removal Based and standard FE method, respectively. The approximation error is also here measured in the L^2-norm, i.e., using $\|\hat{p}_h - \hat{p}_a\|_{L^2(\Lambda)}$. We see here that the singularity removal significantly improves the convergence properties of the problem for $R < h$. The convergence rates degrade when $R > h$. This is again due to the simplification $\bar{v} = v|_\Lambda$ used in the construction of the block matrix (52), and could be resolved by removing this simplification.

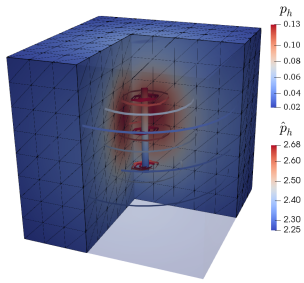

Fig. 4: SRB FE approximations of the reconstructed reservoir pressure p_h and well pressure $\hat{p}_h$. Isolines are plotted for p_h.

From 3b, is clear that the standard FE method has trouble approximating the solution when $R < h$. Moreover, the approximation error of $\hat{p}_h$ is seemingly more sensitive than p_h with respect to the ratio R/h. This can be understood by returning to the reservoir pressure splitting $p = \beta(\hat{p} - \bar{p})G + v$, where $G = -1/2\pi \ln(r)$, and noting that the error in p_h is due to three separate issues, namely, the error in the approximation of the pressure difference, i.e., $\|\hat{p}_h - \bar{p}_h - (\hat{p}_a - \bar{p}_a)\|_{L^2(\Lambda)}$, the error in approximating the logarithm, i.e., $\|\ln(r)_h - \ln(r)\|_{L^2(\Omega)}$, and the error in approximating v (which is comparatively small). The standard FE method has trouble resolving the logarithmic nature of the reservoir pressure around the well, leading to a large approximation error in $\bar{p}$. This further pollutes the approximations of both $\hat{p}$ and p. The effect is not as noticeable for p as its approximation error is dominated by the approximation error for $\ln(r)$. The well pressure $\hat{p}$, however, is in principle a smooth function, for which the FE approximation should be comparatively small. Its approximation error is therefore dominated by the term $\|\bar{p}_a - \bar{p}_h\|_{L^2(\Lambda)}$.

In summary, we see here that the standard FE method has difficulty resolving the pressure difference $\hat{p} - \bar{p}$ when $R < h$, due to the fact that $\bar{p}$ is then poorly approximated. This further pollutes the approximations of both the well and reservoir pressure. Explicitly subtracting the singularity in p, which results in the Singularity Removal Based FE described by (52), restores optimal convergence rates for the reservoir pressure p, and improves the robustness of the method with respect to a small well radius R.

8.2 Convergence test for well with discontinuous lateral permeability

Let $\Omega = (0, 1)^3$ and

$$\Lambda = \{(x, y, z) \in \Omega : x = y = \frac{1}{2},\ z \in (\frac{1}{4}, \frac{3}{4})\}. \tag{77}$$

In this section, we will test the ability of the Singularity Remov1l Based FE method in approximating the analytic test problem

$$p_a = zG + v_a, \tag{78a}$$
$$v_a = \frac{1}{4\pi}(r_b - r_a), \tag{78b}$$
$$\hat{p}_a = \sin(z) + 2, \tag{78c}$$

h	$\|p_e\|_{L^2(\Omega)}$	$\|p_e\|_{H^1(\Omega)}$	$\|\hat{p}_e\|_{L^2(\Lambda)}$	$\|\hat{p}_e\|_{H^1(\Lambda)}$
1/4	1.94e-02	1.88e-01	2.30e-3	2.51e-2
1/8	5.44-03	4.99e-02	6.27e-4	1.26e-2
1/16	1.25e-03	9.26e-02	1.55e-4	6.27e-2
1/32	2.77e-04	4.50e-02	7.80e-5	3.32e-2
l	2.0	1.0	2.0	1.0

Table 1: The reservoir pressure approximation error $p_e = \mathcal{I}_h(p_a) - p_h$ and well pressure approximation error $\hat{p}_e = \hat{p}_a - \hat{p}_h$ when p_h was reconstructed using (82) with $k = 1$. Both errors were found to converge with optimal order, i.e., with $l = 2$ in the L^2-norm and $l = 1$ in the H^1-norm.

when G is given as in Section 4.2:

$$G = \frac{1}{4\pi} \ln\Big(\frac{r_b - (z-b)}{r_a - (z-a)}\Big). \tag{79}$$

The problem parameters are then as follows:

$$\kappa = \hat{\kappa} = \mu = 1, \quad \beta = \frac{z}{\hat{p}_a - \bar{p}_a}, \quad \hat{\beta} = -\frac{\beta \sin(z)}{z}. \tag{80}$$

Physically, this can be interpreted as modelling a well that passes through the domain but is only in contact with the reservoir when $1/4 < z < 3/4$. This translates to a jump in the lateral permeability, with discontinuities at the points $(1/2, 1/2, 1/4)$ and $(1/2, 1/2, 3/4)$.

As the cut-off function, we use the Gaussian function

$$\Psi = \exp(-\frac{\text{dist}(\mathbf{x}, \Lambda)^2}{2c^2}) \tag{81}$$

with $c = 0.04$. For the extension operator E, we choose spline interpolation with radial basis functions as given in [9]. Given a discretized solution pair $(v_h, \hat{p}_h)$ to (52), we can then reconstruct the discretized full reservoir pressure by the relation

$$p_h = \beta^*(\hat{p}_h - \bar{w}_h)\mathcal{I}_h^k(\Psi G) + v_h, \tag{82}$$

where $\mathcal{I}_h^k$ denotes the interpolation operator onto the Lagrange elements of order k. Finally, the numerical error associated with v_h can be computed as

$$p_e = I_h^{k=1}(p_a) - p_h, \tag{83}$$

where p_a is interpolated onto the Lagrange elements with the same order as the solution v_h.

The results of applying the SRB-FE method to solve this problem are plotted in Figure 4 for $h = 1/8$. The errors and convergence rates are given for different mesh sizes in Table 1. As is evident from this table, the SRB-FE approximation of p_h and $\hat{p}_h$ both converge with optimal order. I.e., we find that

$$\|p_e\|_{L^2(\Omega)} \leq Ch^2 \|I_h^{k=1}(p_a)\|_{H^1(\Omega)}, \tag{84}$$

$$\|p_e\|_{H^1(\Omega)} \leq Ch^1 \|I_h^{k=1}(p_a)\|_{H^2(\Omega)}, \tag{85}$$

$$\|\hat{p}_e\|_{L^2(\Lambda)} \leq Ch^2 \|\hat{p}\|_{H^1(\Lambda)}, \tag{86}$$

$$\|\hat{p}_e\|_{H^1(\Lambda)} \leq Ch^1 \|\hat{p}\|_{H^2(\Lambda)}. \tag{87}$$

9 Conclusion

In this work, we have developed a singularity removal method for the coupled 1D-3D flow model. This type of model can be used to model the interaction of wells with a reservoir. The well is endowed with its own 1D flow equation, and modelled as a 1D line source in the reservoir domain. This line source introduces a logarithmic type singularity in the reservoir solution that negatively affects the approximation properties of the problem. We provide here a method for identifying and removing this singularity from the governing equations. The result is a reformulated coupled 1D-3D flow model in which all variables are smooth.

As the reformulated model is posed in terms of smooth variables, it has the advantage that it can be approximated using any standard numerical method. In this work, we have shown that the singularity removal restores optimal convergence rates for the Galerkin FE method. Moreover, it makes the approximation stable with respect to the ratio R/h between well radius and mesh size.

A natural development of this work consists of extending the singularity removal method to apply to (i) different control modes for the wells, (ii) tensor-valued permeability and (iii) a mixed formulation of the flow, where both pressure and flux are approximated. We believe these extensions would be particularly valuable in the context of subsurface flow applications, as it would allow one to capture the interaction between well and reservoir using coarse grids. The extension to different control modes for the wells, i.e., rate controlled or pressure controlled wells, is straightforward; it can be achieved by altering the boundary conditions for the well flow equations. As the singularity subtraction is performed at the continuous level, it is likewise straightforward to adapt the method to different discretization methods [19]. The extension to tensor-valued permeability is more challenging, and will be treated in future work.

Acknowledgements This work was partially supported by the Research Council of Norway, project number 250223. The participation of the first author at ECMOR XVI 2018 was funded by the Academia Agreement between the University of Bergen and Equinor.

The authors thank B. Wohlmuth for her help in formulating the original splitting approach. The authors also thank P. Zunino for the interesting discussions on coupled 1D-3D flow problems. Finally, the authors would like to thank M. Kuchta, K. E. Holter and C. Daversin-Catty for developing and sharing with us code for the implementation of mixed-dimensional models in FEniCS.

References

1. Aavatsmark, I.: Equivalent well-cell radius for hexagonal k-orthogonal grids in numerical reservoir simulation. Applied Mathematics Letters **61**, 122 – 128 (2016)
2. Aavatsmark, I.: Interpretation of well-cell pressures on hexagonal grids in numerical reservoir simulation. Computational Geosciences **20**(5), 1029–1042 (2016)
3. Aavatsmark, I.: Interpretation of well-cell pressures on stretched hexagonal grids in numerical reservoir simulation. Computational Geosciences **20**(5), 1043–1060 (2016)
4. Aavatsmark, I., Klausen, R.A.: Well index in reservoir simulation for slanted and slightly curved wells in 3d grids. SPE Journal pp. 41–48 (2003). DOI 10.2118/75275-PA
5. Al−Khoury, R., Bonnier, P.G., Brinkgreve, R.B.J.: Efficient finite element formulation for geothermal heating systems. part i: steady state. International Journal for Numerical Methods in Engineering **63**(7), 988–1013 (2005)
6. Apel, T., Benedix, O., Sirch, D., Vexler, B.: A priori mesh grading for an elliptic problem with dirac right-hand side. SIAM Journal on Numerical Analysis **49**(3), 992–1005 (2011)
7. Babu, D.K., Odeh, A.S., Al-Khalifa, A.J., McCann, R.C.: The relation between wellblock and wellbore pressures in numerical simulation of horizontal wells (1991)

8. Babuška, I., Rosenzweig, M.B.: A finite element scheme for domains with corners. Numerische Mathematik **20**(1), 1–21 (1972)
9. Broomhead, D.S., Lowe, D.: Multivariable Functional Interpolation and Adaptive Networks. Complex Systems 2 pp. 321–355 (1988)
10. Cattaneo, L., Zunino, P.: A computational model of drug delivery through microcirculation to compare different tumor treatments. International Journal for Numerical Methods in Biomedical Engineering **30**(11), 1347–1371 (2014)
11. Cerroni, D., Laurino, F., Zunino, P.: Mathematical analysis, finite element approximation and numerical solvers for the interaction of 3d reservoirs with 1d wells. GEM - International Journal on Geomathematics **10**(1), 4 (2019)
12. Chen, Z., Zhang, Y.: Well flow models for various numerical methods. International Journal of Numerical Analysis and Modeling **3**, 375–388 (2006)
13. D'Angelo, C.: Finite element approximation of elliptic problems with dirac measure terms in weighted spaces: Applications to one- and three-dimensional coupled problems. SIAM Journal on Numerical Analysis **50**(1), 194–215 (2012)
14. D'Angelo, C., Quarteroni, A.: On the coupling of 1d and 3d diffusion-reaction equations: Application to tissue perfusion problems. Mathematical Models and Methods in Applied Sciences **18**(08), 1481–1504 (2008)
15. Daversin-Catty, C.: `https://hub.docker.com/r/ceciledc/fenics_mixed_dimensional/`
16. Ding, Y., Jeannin, L.: A new methodology for singularity modelling in flow simulations in reservoir engineering. Computational Geosciences **5**(2), 93–119 (2001)
17. Ewing, R.E. (ed.): The mathematics of reservoir simulation, *Frontiers in Applied Mathematics*, vol. 1. Society for Industrial and Applied Mathematics (SIAM), Philadelphia, PA (1983)
18. Ewing, R.E., Lazarov, R.D., Lyons, S.L., Papavassiliou, D.V., Pasciak, J., Qin, G.: Numerical well model for non-darcy flow through isotropic porous media. Computational Geosciences **3**(3), 185–204 (1999)
19. Gjerde, I.G., Kumar, K., Nordbotten, J.M.: Well modelling by means of coupled 1d-3d flow models (2018). DOI 10.3997/2214-4609.201802117
20. Gjerde, I.G., Kumar, K., Nordbotten, J.M., Wohlmuth, B.: Splitting method for elliptic equations with line sources. ArXiv e-prints p. arXiv:1810.12979 (2018)
21. Grinberg, L., Cheever, E., Anor, T., Madsen, J.R., Karniadakis, G.E.: Modeling blood flow circulation in intracranial arterial networks: A comparative 3d/1d simulation study. Annals of Biomedical Engineering **39**(1), 297–309 (2011)
22. Hales, H.B.: An improved method for simulating reservoir pressures through the incorporation of analytical well functions (1977). DOI 10.2118/39065-MS
23. Holter, K.E., Kuchta, M., Mardal, K.A.: Sub-voxel perfusion modeling in terms of coupled 3d-1d problem. ArXiv e-prints (2018)
24. King, M.J., Mansfield, M.: Flow simulation of geologic models (1997). DOI doi:10.2118/39065-MS
25. Köppl, T., Vidotto, E., Wohlmuth, B.I., Zunino, P.: Mathematical modelling, analysis and numerical approximation of second order elliptic problems with inclusions. Numerical Mathematics and Advanced Applications ENUMATH 2015 (2017)
26. Kuchta, M.: `https://github.com/MiroK`, repo: fenicsii, branch: master
27. Kuchta, M., Mardal, K.A., Mortensen, M.: Preconditioning trace coupled $3d$-$1d$ systems using fractional Laplacian. ArXiv e-prints (2016)
28. Köppl, T., Vidotto, E., Wohlmuth, B.: A local error estimate for the poisson equation with a line source term. Numerical Mathematics and Advanced Applications ENUMATH pp. 421–429 (2015)
29. Llau, A., Jason, L., Dufour, F., Baroth, J.: Finite element modelling of 1d steel components in reinforced and prestressed concrete structures. Engineering Structures **127**(Supplement C), 769 – 783 (2016)
30. Logg, A., Mardal, K.A., Wells, G.N.: Automated Solution of Differential Equations by the Finite Element Method. Springer (2012). DOI 10.2118/75275-PA
31. Nabil, M., Zunino, P.: A computational study of cancer hyperthermia based on vascular magnetic nanoconstructs. Royal Society Open Science **3**(9) (2016)
32. Nordbotten, J.M., Kavetski, D., Celia, M.A., Bachu, S.: Model for co2 leakage including multiple geological layers and multiple leaky wells. Environmental Science & Technology **43**(3), 743–749 (2009). PMID: 19245011
33. Peaceman, D.W.: Interpretation of well-block pressures in numerical reservoir simulation. Society of Petroleum Engineers Journal **18**(03), 183–194 (1978)
34. Peaceman, D.W.: Interpretation of well-block pressures in numerical reservoir simulation with nonsquare grid blocks and anisotropic permeability. Society of Petroleum Engineers Journal **23**(3) (1983)
35. Possenti, L., Casagrande, G., Gregorio, S.D., Zunino, P., Constantino, M.: Numerical simulations of the microvascular fluid balance with a non-linear model of the lymphatic system. MOX-Report No. 35 (2018)
36. Reichold, J., Stampanoni, M., Keller, A.L., Buck, A., Jenny, P., Weber, B.: Vascular graph model to simulate the cerebral blood flow in realistic vascular networks. Journal of Cerebral Blood Flow & Metabolism **29**(8), 1429–1443 (2009)

37. Strouboulis, T., Babuška, I., Copps, K.: The design and analysis of the generalized finite element method. Comput. Methods Appl. Mech. Engrg. **181**(1-3), 43–69 (2000)
38. Weiss, C.J.: Finite-element analysis for model parameters distributed on a hierarchy of geometric simplices. GEOPHYSICS **82**(4), E155–E167 (2017)
39. Wolfsteiner, C., Durlofsky, L.J., Aziz, K.: Calculation of well index for nonconventional wells on arbitrary grids. Computational Geosciences **7**(1), 61–82 (2003)
40. Wolfsteiner, C., Lee, S., Tchelepi, H.: Well modeling in the multiscale finite volume method for subsurface flow simulation. Multiscale Modeling & Simulation **5**(3), 900–917 (2006)

Graphic design: Communication Division, UiB / Print: Skipnes Kommunikasjon AS

uib.no

ISBN: 9788230869796 (print)
9788230858028 (PDF)